Multivalent elastin-like glycopolypeptides: subtle chemical structure modifications with high impact on lectin binding affinity.

Marie Rosselin, Zoeisha S. Chinoy, Lourdes Monica Bravo-Anaya, Sébastien Lecommandoux and Elisabeth Garanger*

Univ. Bordeaux, CNRS, Bordeaux INP, LCPO, UMR 5629, Pessac, F-33600, France.

KEYWORDS:

Elastin-like polypeptides (ELPs), saccharides, glycoconjugates, chemoselective modifications, macromolecular click chemistry, lectins.

ABSTRACT:

A library of synthetic elastin-like glycopolypeptides was synthesized and screened by microscale thermophoresis to identify key structural parameters affecting lectin binding efficacy. While polypeptide backbone' size and glycovalency were found to have little influence, the presence of a linker at the anomeric position of galactose and absence of positive charge on the polypeptide residue holding the sugar unit were found critical for the binding to RCA120.

MAIN TEXT:

Found in most organisms and involved in many different cellular processes, glycoproteins constitute a wide family of natural biomacromolecules composed of glycans covalently attached to proteins. Glycoproteins play crucial roles in major biological phenomena such as infection, cellular recognition and signal transduction.[1, 2] Carbohydrates in glycoproteins interact with a specific class of proteins, termed lectins, through weak monomeric interactions, the high binding affinity between a specific glycoprotein and a lectin being insured by the architecture of the protein and by the presentation of the carbohydrate ligands in a multivalent manner, a phenomenon termed as the "glycoside cluster effect".[3, 4] Considerable efforts have been made to synthesize glycoprotein mimics as powerful tools for glycobiology or as lead compounds for therapeutic applications. A wide variety of scaffolds have been explored to access multivalent glycoarchitectures,[5] dendrimers and polymers being the widest families of synthetic compounds explored so far. Polymer chemistry affords myriads of possibilities in terms of glycopolymer design: different architectures can be engineered, chain lengths, sugar numbers and sugar density can also be tuned to increase the potency of glycopolymers towards specific lectins.[6] Because any polymer backbone may not closely mimic the chemical structure of glycoproteins, particular attention was paid to glycopolymers composed of polypeptide backbones decorated with pendant carbohydrates, so designated as glycopolypeptides, as simplified analogues of glycoproteins.[7-10] Glycopolypeptides obtained by polymerization techniques are accessible at large scales[7, 11, 12] and impressive advances have been made towards well-defined glycopolypeptides. Inherent macromolecular dispersity arising from polymerization techniques has also encouraged the development of unimolecular multivalent glycoconjugates. To access multivalent glycopeptides with precise compositions, scientists have explored a wide range of chemical strategies ranging from solid-phase synthesis of glycopeptides,[13, 14] ligation techniques[15, 16] or enzymatic syntheses.[5, 17] Despite significant progresses, limitations still remain regarding the high complexity of these macromolecular structures and low amount of materials accessible. We believe recombinant DNA and genetic engineering are unique opportunities to access high precision polypeptides with an exact control over monomer sequence and chain length at reasonable scales, while chemoselective modification reactions can be employed to anchor sugar units and access monodisperse glycopolypeptides. Using this dual biotechnological/chemical approach, we recently reported the design of a thermosensitive glycopolypeptide based on a recombinant elastin-like polypeptide (ELP) scaffold.[18] In this study, a recombinant ELP composed of 40 [-VPGXG-] pentapeptide repeat units (X=V/M 3:1) was produced in 100 mg/L culture yield and chemoselectively modified at each methionine residue to anchor galactose units and access a monodisperse multivalent ELP(Gal) conjugate. Thermal properties of the ELP were subsequently advantageously used to precipitate and isolate a target lectin (*Ricinus communis agglutinin*, RCA_{120}) from a complex mixture of proteins. Using a similar approach, the group of B. D. Olsen also described the synthesis of ELP-based glycopolypeptides with dense brushes of glycans to mimic natural glycoproteins with dense glycosylation such as mucins and aggrecans.[19] These were synthesized from a recombinant ELP containing non-natural amino acid surrogates, namely homopropargylglycine (HPG) residues, that were subsequently chemically modified *via* copper(I)-catalyzed alkyne−azide cycloaddition with different types of mono-, di- or trisaccharides. Despite a relatively low production yield (ca. 10 mg/L culture) explained by the global amino acid substitution approach, a high number and density of alkyne groups (ca. 38 per 264 residue-long chain) was obtained. The present work aimed at synthesizing different chemical structures of ELP(Gal) bioconjugates and comparing their binding affinity to a target lectin (RCA_{120}) in order to establish structure-affinity relationships. Three main parameters were, in particular, investigated, namely *i*) the polypeptide chain length and therefore the number of carbohydrate motifs, keeping the sugar density constant, *ii*) the presence or absence of a positive charge on the methionine residue's side chain bearing the sugar unit, and *iii*) the presence of an additional small *n*-propyl linker to augment the flexibility and accessibility of the carbohydrate. Binding affinities of the different glycoconjugates to RCA_{120} were studied using microscale thermophoresis (MST). While carbohydrate-protein interactions are usually studied using isothermal calorimetry or surface plasmon resonance spectroscopy, we have preferred MST that avoids any artifact from the immobilization of one of the binding partners and uses very small quantities of materials. This technique is based on the phenomenon of thermophoresis (also called Soret effect or thermodiffusion) by which molecules drift along temperature gradients.[20] Binding affinities of the different glycopolypeptides were measured from the change in the thermophoretic behavior resulting from the binding to the lectin.[21, 22]

A library of fifteen elastin-like glycopolypeptides was therefore designed and synthesized from two recombinant ELP backbones, namely ELP[M_1V_3-*20*] and ELP[M_1V_3-*40*] containing either 20 or 40 (-VPGXG-) repeat units (X=V,M 3:1), respectively. (Figure 1) Chemoselective modifications were applied at methionine residues to access ELP-based glycoconjugates with a total of six (series of compounds **1** and **3**) or eleven (series of compounds **2** and **4**) saccharide units.

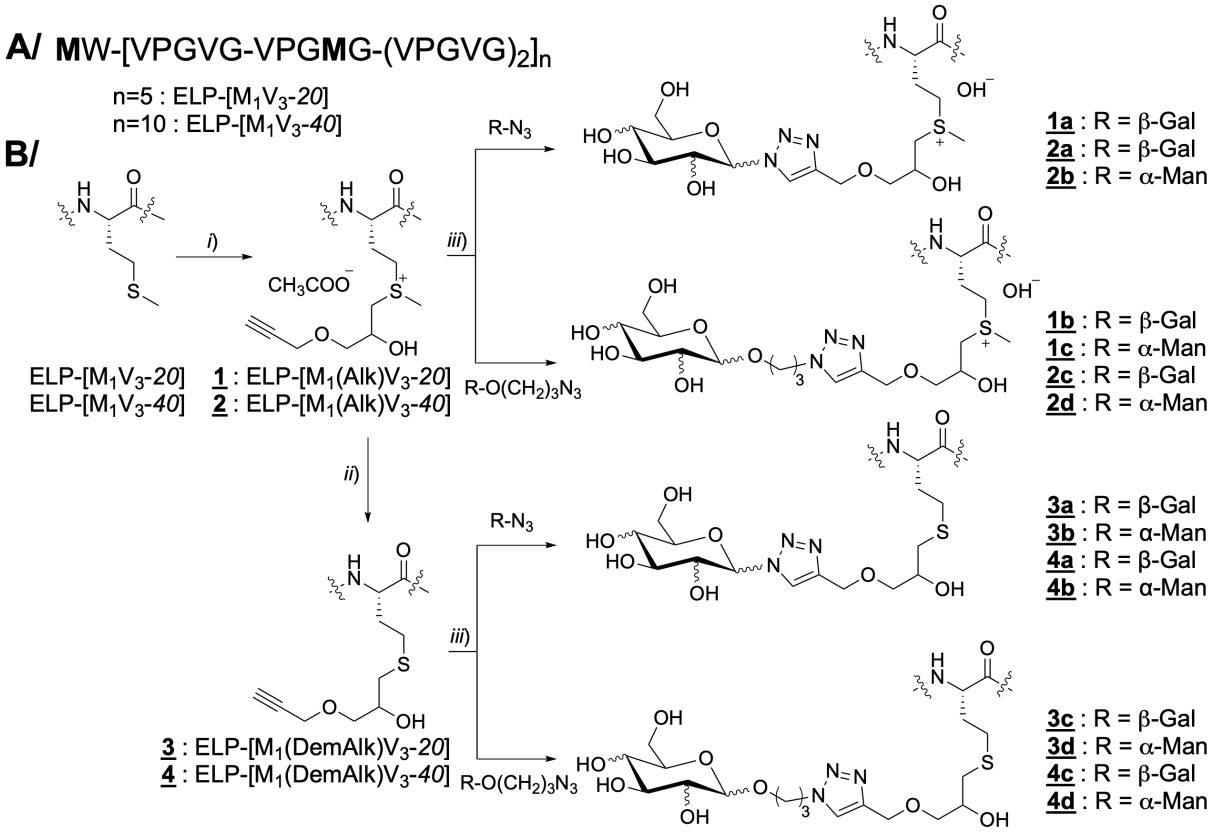

Figure 1. A/ Protein sequence of of ELP-[M_1V_3-*n*] (*n*=20, 40). B/ Scheme of chemical modifications applied at methionine residues to access the library of glycoconjugates. Conditions: (i) AcOH/HFIP mixture (9/1, v/v), glycidyl propargyl ether (10 equiv. per Met; (ii) 75% EtOH (aq); ammonium pyrrolidinedithiocarbamate (APDC) (5 equiv per Met); (iii) Milli-Q water, azido-carbohydrate (1.5 equiv. per alkyne), Cu(II)SO_4 (0.26 equiv. per alkyne), sodium ascorbate (1.3 equiv. per alkyne) and pentamethyldiethylenetriamine (PMDETA) (0.26 equiv. per alkyne).

In a first step, ELP[M_1V_3-*20*] and ELP[M_1V_3-*40*] (exact protein sequence provided in Figure 1A) were chemoselectively alkylated at the side chain of methionine residues using glycidyl propargyl ether following previously established procedures.[23, 24] After purification, derivatives **1** and **2** were obtained in good yield (isolated yields ranging from 79% to 86%) and high purity with >95% functionalization degrees, corresponding to the percentage of functionalized Met as determined by ^{1}H NMR spectroscopy. (Figures S18 and S44-45) Half batches of thioalkylated-ELPs **1** and **2** were subsequently demethylated to obtain their uncharged thioether analogues, numbered **3** and **4**, in 98% and 88% yield, respectively. (Figures S28-29 and S56-57) Huisgen's copper-catalyzed azide-alkyne cycloaddition reaction (CuAAC) was ultimately used to conjugate the sugar units onto these four alkyne-bearing ELP scaffolds. Compounds **1**-**4** were quantitatively modified with β-D-galactopyranosyl azide (β-Gal-N_3) to obtain compounds **1a**, **2a**, **3a** and **4a**, while α-D-mannopyranosyl azide (α-Man-N_3) was used to access control compounds **2b**, **3b** and **4b**. In order to reduce steric hindrance and increase the flexibility of the linkage to the sugar unit, Gal and Man derivatives containing an azido *n*-propyl linker at the anomeric carbon were synthesized (details available in supplementary materials) and subsequently reacted with alkyne-containing ELPs **1**-**4**. 3-Azidopropyl-β-D-galactopyranoside (β-Gal-*link*-N_3) afforded compounds **1b**, **2c**, **3c** and **4c**, while 3-azidopropyl-α-D-mannopyranoside (α-Man-*link*-N_3) was used to access the respective control compounds **1c**, **2d**, **3d** and **4d**. All glycopolypeptides were obtained with excellent functionalization degrees (>94%) as summarized in Table 1. Isolated yields are also provided in Table 1. ^{1}H and HSQC NMR spectra of all derivatives are provided in the supplementary information (Table S1, Figures S19−S69). The molecular weight shifts after each step of synthesis were followed by size-exclusion chromatography measurements in aqueous solvent using two detectors (RI and SEC-MALS). (Figures S70−S71) In most cases, expected shifts were observed according to the chemical modifications achieved on the ELP scaffold. The strongest shifts were observed after the thioalkylation reaction (Figure 1B, step *i*) affording derivatives **1** and **2** from ELP-[M_1V_3-*20*] and ELP-[M_1V_3-*40*], respectively. Similar retention times were observed for demethylated derivatives **3** and **4** as compared to the pristine ELP backbones ELP-[M_1V_3-*20*] and ELP-[M_1V_3-*40*], respectively, despite their higher molar mass. This suggests that these uncharged compounds have similar hydrodynamic volumes, while charged sulfonium derivatives **1** and **2** likely have larger hydrodynamic volumes due to electrostatic repulsions resulting in shorter retention times. Also, as observed in a previous study,[18] the presence of a small peak attributed to dimer species was noticed after demethylation and click reactions. The characteristics of all glycopolypeptides synthesized are summarized in table 1.

The library of synthetic glycopolypeptides was subsequently submitted to binding affinity assays against RCA_{120}. RCA_{120} is a dimeric lectin (120 kDa) consisting of two monomeric

Table 1. Summary of the characteristics of glycopolypeptides.

Cpd. #	ELP backbone	Monosaccharide	Molar mass[1]	% Function.[2]	Yield[3]
1a	ELP-[$M_1(Alk)V_3$-*20*] **1**	β-Gal-N_3	10,535	95	73 %
1b		β-Gal-*link*-N_3	11,045	94	69 %
1c		α-Man-*link*-N_3		94	70 %
2a	ELP-[$M_1(Alk)V_3$-*40*] **2**	β-Gal-N_3	20,723	94	71 %
2b		α-Man-N_3		99	81 %
2c		β-Gal-*link*-N_3	21,825	94	73 %
2d		α-Man-*link*-N_3		95	77 %
3a	ELP-[M_1(*Dem*Alk)V_3-*20*] **3**	β-Gal-N_3	10,505	100	80 %
3b		α-Man-N_3		100	74 %
3c		β-Gal-*link*-N_3	10,853	100	75 %
3d		α-Man-*link*-N_3		100	78 %
4a	ELP-[M_1(*Dem*Alk)V_3-*40*] **4**	β-Gal-N_3	20,372	100	76 %
4b		α-Man-N_3		100	74 %
4c		β-Gal-*link*-N_3	21,011	100	79 %
4d		α-Man-*link*-N_3		100	79 %

[1] Theoretical molar mass ($g.mol^{-1}$); [2] Calcd. by ^1H NMR; [3] CuAAC reaction yield.

chains connected by a disulfide bridge.[25] RCA_{120} specifically binds to galactose and interacts more strongly with branched cluster glycosides presenting β-D-galactose at the non-reducing end.[26] In a previous work, we have demonstrated the selective binding of ELP-[M_1V_3-*40*] decorated with galactose units (corresponding to compound **4a** of the present work) using dynamic light scattering.[18] Due to the presence of two binding sites in the native form of RCA_{120}, ELP(Gal) and RCA_{120} were shown to form structures similar to disordered fractal aggregates at 37°C, which could be precipitated and isolated from a complex mixture of proteins by taking advantage of the thermoresponsive properties of the multivalent glycopolypeptide.[18] However, these techniques did not provide any quantitative information on the affinity between the multivalent glycopolypeptide and RCA_{120}. In the present study, we have carried out a systematic study of the library of ligands synthesized using microscale thermophoresis (MST) in order to compare their affinity and dissociation constant (K_D) with RCA_{120}. The binding affinity was measured at 22 °C to ensure full solubility of ELP-glycoconjugates and prevent temperature-triggered aggregation phenomena that could interfere with the fluorescence measurements during MST experiments. Small temperature gradients were applied upon the application of an infrared laser (MST-on), and the movements of the lectin (labeled with a near-infrared dye) in the presence of increasing amounts of glycopolypeptides were measured by fluorescence (MST-off). We have chosen to label the target rather than the ligands in order to insure comparable fluorescence intensities and systematically study the series of glycopolypeptides against RCA_{120}. For all ELP-glycoconjugates, serial 2-fold dilutions were prepared in Tris buffer (pH 7.6) containing 0.05 % tween 20 and 20 mM $MgCl_2$, the highest concentration being 1 mM for the series of ELP-[M_1V_3-*20*] derivatives (series **1** and **3**) and 0.5 mM for the series of ELP-[M_1V_3-40] derivatives (series **2** and **4**) corresponding to their respective limit of solubility (around 10 $mg.mL^{-1}$). Labeled-RCA_{120} was added to all solutions in order to reach a final lectin concentration of 5 nM. For all ligands, MST experiments were triplicated to have a confidence value and a precise estimation of the dissociation constant. These results are summarized in Table 2. The high dissociation constants (K_D > 10^{-4} $mol.L^{-1}$) found for all negative control compounds, *i.e.* ELP-derivatives decorated with Man (**1c**, **2b**, **2d**, **3b**, **3d**, **4b**, **4d**), were assigned to non-specific interactions since similar results were obtained for the pristine ELP-[M_1V_3-*20*] and ELP-[M_1V_3-*40*]. (Figure S57) In contrast, almost all glycopolypeptides presenting galactose epitopes displayed a significant binding affinity with a dissociation constant ranging from 10^{-5} to 10^{-7} $mol.L^{-1}$. (Figure 2 and Table 2) Two Gal-presenting glycopolypeptides - compounds **1a** and **2a** - obtained from ELP-[$M_1(Alk)V_3$-*20*] **1** and ELP-[$M_1(Alk)V_3$-*40*] **2**, respectively, and β-Gal-N_3 showed no specific affinity to RCA_{120} with dissociation constant in the same range as the control compounds (> $7.1 \cdot 10^{-4}$ and > $3.4 \cdot 10^{-4}$ M, respectively). Regarding the K_D measured for the other glycopolypeptides, we concluded that the simultaneous presence of a positive charge from the sulfonium group bearing the galactose unit and absence of linker at the anomeric position were detrimental to the binding to RCA_{120} whatever the number of β-Gal units presents (6 or 11).

The addition of a flexible *n*-propyl linker at the anomeric position of β-Gal, separating the binding epitope from the constrained triazole ring, was found highly favorable for the interaction with RCA_{120}. Indeed, glycopolypeptide **1b** showed a dissociation constant one hundred times lower than **1a**, and a similar effect was observed between compounds **2c** and **2a** presenting 11 galactose units. (Figure 2 and Table 2) The benefit of the presence of the *n*-propyl linker was also evidenced with uncharged glycopolypeptides, compound **3c** having a 20-time lower K_D than **3a**, and **4c** a 6-time lower K_D than **4a**. These results clearly highlighted the significant benefit of the short alkyl linker on the binding affinity to the lectin, as a result of higher flexibility and less steric hindrance of the sugar as compared to glycopolypeptides presenting a constrained triazole at the anomeric position of the sugar. This

observation echoes similar ones reported in the literature highlighting the importance of linkers at the anomeric position of carbohydrate epitopes.[27] Conversely, the presence of the positive charge from the sulfonium group proved deleterious to the binding affinity to RCA_{120}. Indeed, the dissociation constants of neutral glycopolypeptides were found to be systematically lower than those of their corresponding positively charged analogues (*i.e.*, comparing **3a** with **1a**, **4a** and **2a**, **3c** and **1b**, **4c** and **2c**). We assume that the presence of positively charged residues (*i.e.*, Arg) close to the binding sites of galactose in RCA_{120} could explain an unfavorable approach of the ligand due to electrostatic repulsions.[28, 29] Finally, the simultaneous presence of the *n*-propyl linker and absence of positive charge provided the glycopolypeptides with the highest affinity to RCA_{120}. Indeed, compounds **3c** and **4c** displayed 30-fold lower dissociation constants than sulfonium derivatives **1b** and **2c**, respectively, and lower K_D than uncharged glycopolypeptides devoid of linker **3a** and **4a**. With dissociation constants of respectively $3.1 \cdot 10^{-7}$ M and $2.4 \cdot 10^{-7}$ M, glycopolypeptides **3c**

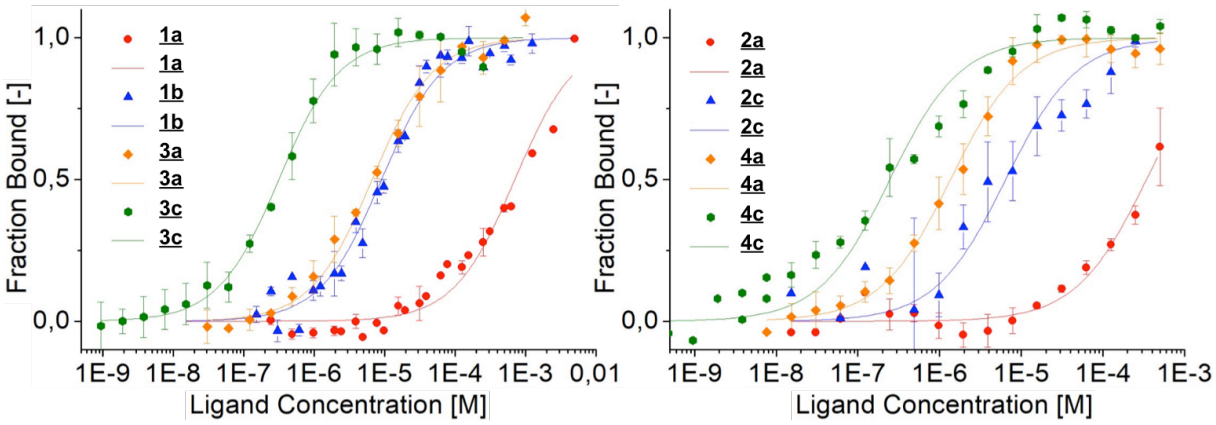

Figure 2. Thermophoretic analysis of interactions between RCA_{120} and multivalent galactose-presenting glycopolypeptides in Tris at 22°C. ELP[M_1V_3-20] series (left) and ELP[M_1V_3-40] series (right). Dots correspond to experimental data points, lines to fitted data.

Table 2. Dissociation constants (K_D) of glycopolypeptide/RCA_{120} complexes.

ELP scaffold	Cpd. #	Monosaccharide	K_D (mol.L^{-1})
ELP[M_1V_3-*20*]	**1a**	β-Gal	$> 7.1 \pm 1.4 \times 10^{-4}$
	1b	β-Gal-*link*	$9.1 \pm 1.2 \times 10^{-6}$
	1c	α-Man-*link*	$> 9.2 \pm 1.6 \times 10^{-4}$
	3a	β-Gal	$6.7 \pm 0.7 \times 10^{-6}$
	3b	α-Man	$> 1,2 \pm 0.2 \times 10^{-3}$
	3c	β-Gal-*link*	$3.1 \pm 0.4 \times 10^{-7}$
	3d	α-Man-link	$> 2.5 \pm 0.9 \times 10^{-3}$
ELP[M_1V_3-*40*]	**2a**	β-Gal	$> 3.4 \pm 1.4 \times 10^{-4}$
	2b	α-Man	$> 1.4 \pm 1.0 \times 10^{-3}$
	2c	β-Gal-*link*	$6.5 \pm 2.5 \times 10^{-6}$
	2d	α-Man-*link*	$> 1.0 \pm 0.3 \times 10^{-3}$
	4a	β-Gal	$1.4 \pm 0.1 \times 10^{-6}$
	4b	α-Man	$> 7.6 \pm 2.1 \times 10^{-4}$
	4c	β-Gal-*link*	$2.4 \pm 0.5 \times 10^{-7}$
	4d	α-Man-*link*	$> 4.0 \pm 1.4 \times 10^{-4}$

and **4c** displayed the highest binding affinity to RCA_{120} of the compounds in the library. It is worth noting that the same trend of affinity was observed for both ELP[M_1V_3-*20*] and ELP[M_1V_3-*40*] series. However, to reveal the impact of multivalency on lectin binding affinity, the results were reported as a function of sugar (galactose) concentration. Attention was particularly focused on the glycopolypeptides showing the highest affinity for RCA_{120}, namely **3a** and **3c** for ELP[M_1V_3-*20*] series, and **4a** and **4c** for ELP[M_1V_3-*40*] series. (Figure 3) With a molar mass around 10 kDa, ELP[M_1V_3-*20*]-based glycopolyeptides are decorated with six galactose units, whereas the backbone of ELP[M_1V_3-*40*] with double size displays eleven Gal motifs per chain. Similar trends were

obtained when the fraction bound was reported as a function of glycopolypeptide concentration or as function of galactose concentration. Only a small effect of multivalency was noticed. Enhanced affinities of ELP[M_1V_3-*40*] glycopolypeptides relative to ELP[M_1V_3-*20*] glycopolypeptides for RCA_{120} lectin are consistent with an increase in the probability of binding due to multiple binding sites in the longest construction. The multivalency effect was however found more pronounced for glycopolypeptides devoid of linker (**3a** and **4a**), than for glycopolypeptides with linker (**3c** and **4c**). Altogether, these results evidence that different parameters can be exploited to increase the binding affinity properties of multivalent glycopolypeptides, not only the number or density of sugars as mostly reported in the literature, but also the way they are connected to the scaffold.

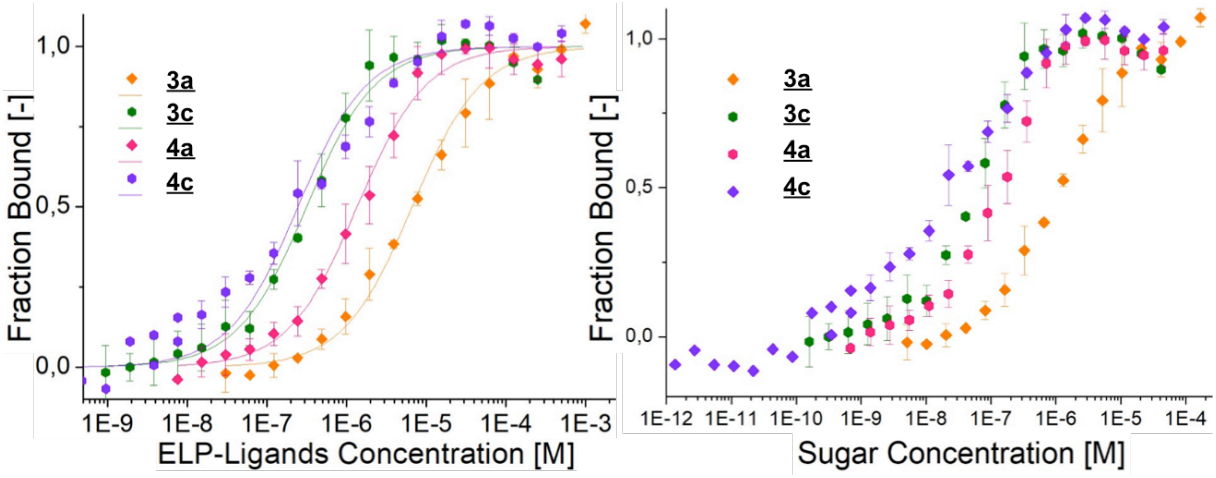

Figure 3. Thermophoretic analysis of interactions between lectin RCA_{120} and ligands in Tris at 22°C as function of glycopolypeptide molar concentration (left) and as function of galactose molar concentration (right). Dots correspond to experimental data points, lines to fitted data.

ASSOCIATED CONTENT

Supporting Information

Electronic Supplementary Information (ESI) available: Experimental procedures, NMR spectra, SEC chromatograms, and additional thermophoretic analyses. See DOI: 10.1021/x0xx00000x

AUTHOR INFORMATION

Corresponding Author

*Elisabeth Garanger - Univ. Bordeaux, CNRS, Bordeaux INP, LCPO, UMR 5629, Pessac, F-33600, France. E-mail: garanger@enscbp.fr

Author Contributions

The manuscript was written through contributions of all authors. All authors have given approval to the final version of the manuscript.

Notes

There are no conflicts to declare.

ACKNOWLEDGMENT

This work was supported by the French National Research Agency (ANR-15-CE07-0002) and the Cancéropole Grand Sud-Ouest (Emergence 2018-E18). L.M.B.-A. acknowledges the fellowship grant provided by CONACYT (CVU 350759). The support of Guillaume Goudounet for ELP production is particularly acknowledged. Authors wish to address special thanks to J.J. Bono and V. Gasciolli from the Laboratoire des Interactions Plantes Micro-organismes (LIPM, UMR CNRS-INRA 2594/441) for the access to the Monolith NT.115 equipement. CNRS, Univ. Bordeaux, and Bordeaux INP are also gratefully acknowledged.

REFERENCES

1. Gruber, P. J.; Glimelius, K.; Eriksson, T.; Frederick, S. E. Interactions of galactose-binding lectins with plant protoplasts. *Protoplasma* **1984**, *121*, 34-41.
2. Shylaja, M.; Seshadri, H. S. Glycoproteins: An overview. *Biochem. Educ.* **1989**, *17*, 170-178.
3. Lee, Y. C.; Lee, R. T. Carbohydrate-Protein Interactions: Basis of Glycobiology. *Acc. Chem. Res.* **1995**, *28*, 321-327.
4. Lundquist, J. J.; Toone, E. J. The Cluster Glycoside Effect. *Chem. Rev.* **2002**, *102*, 555-578.
5. Renaudet, O.; Roy, R. Multivalent scaffolds in glycoscience: an overview. *Chem. Soc. Rev.* **2013**, *42*, 4515-4517.
6. Becer, C. R. The glycopolymer code: synthesis of glycopolymers and multivalent carbohydrate-lectin interactions. *Macromol. Rapid Commun.* **2012**, *33*, 742-752.
7. Bonduelle, C.; Lecommandoux, S. Synthetic glycopolypeptides as biomimetic analogues of natural glycoproteins. *Biomacromolecules* **2013**, *14*, 2973-2983.
8. Buskas, T.; Ingale, S.; Boons, G. J. Glycopeptides as versatile tools for glycobiology. *Glycobiology* **2006**, *16*, 113r-136r.
9. Specker, D.; Wittmann, V., Synthesis and Application of Glycopeptide and Glycoprotein Mimetics. In *Glycopeptides and Glycoproteins: Synthesis, Structure, and Application*, Wittmann, V., Ed. Springer Berlin Heidelberg: Berlin, Heidelberg, **2007**; pp 65-107.

10. Westerlind, U. Synthetic glycopeptides and glycoproteins with applications in biological research. *Beilstein J. Org. Chem.* **2012**, *8*, 804-818.
11. Kramer, J. R.; Deming, T. J. Recent advances in glycopolypeptide synthesis. *Polym. Chem.* **2014**, *5*, 671-682.
12. Krannig, K. S.; Schlaad, H. Emerging bioinspired polymers: glycopolypeptides. *Soft Matter* **2014**, *10*, 4228-4235.
13. Kunz, H. Synthesis of Glycopeptides, Partial Structures of Biological Recognition Components [New Synthetic Methods (67)]. *Angew. Chem. Int. Ed.* **1987**, *26*, 294-308.
14. Zhang, J.; Liu, D.; Saikam, V.; Gadi, M. R.; Gibbons, C.; Fu, X.; Song, H.; Yu, J.; Kondengaden, S. M.; Wang, P. G.; Wen, L. Machine-Driven Chemoenzymatic Synthesis of Glycopeptide. *Angew. Chem. Int. Ed.* **2020**.
15. Payne, R. J.; Wong, C. H. Advances in chemical ligation strategies for the synthesis of glycopeptides and glycoproteins. *Chem. Commun.* **2010**, *46*, 21-43.
16. Thapa, P.; Zhang, R.-Y.; Menon, V.; Bingham, J.-P. Native Chemical Ligation: A Boon to Peptide Chemistry. *Molecules* **2014**, *19*, 14461-14483.
17. Bennett, C. S.; Wong, C. H. Chemoenzymatic approaches to glycoprotein synthesis. *Chem. Soc. Rev.* **2007**, *36*, 1227-1238.
18. Anaya, L. M. B.; Petitdemange, R.; Rosselin, M.; Ibarboure, E.; Garbay, B.; Garanger, E.; Deming, T. J.; Lecommandoux, S. Design of Thermoresponsive Elastin-Like Glycopolypeptides for Selective Lectin Binding and Sorting. *Biomacromolecules* **2020**.
19. Seifried, B. M.; Qi, W.; Yang, Y. J.; Mai, D. J.; Puryear, W. B.; Runstadler, J. A.; Chen, G.; Olsen, B. D. Glycoprotein Mimics with Tunable Functionalization through Global Amino Acid Substitution and Copper Click Chemistry. *Bioconjugate Chem.* **2020**, *31*, 554-566.
20. Duhr, S.; Braun, D. Why molecules move along a temperature gradient. *Proc. Natl. Acad. Sci. U. S. A.* **2006**, *103*, 19678-19682.
21. Jerabek-Willemsen, M.; André, T.; Wanner, R.; Roth, H. M.; Duhr, S.; Baaske, P.; Breitsprecher, D. MicroScale Thermophoresis: Interaction analysis and beyond. *J. Mol. Struct.* **2014**, *1077*, 101-113.
22. Jerabek-Willemsen, M.; Wienken, C. J.; Braun, D.; Baaske, P.; Duhr, S. Molecular interaction studies using microscale thermophoresis. *Assay Drug Dev. Technol.* **2011**, *9*, 342-353.
23. Petitdemange, R.; Garanger, E.; Bataille, L.; Bathany, K.; Garbay, B.; Deming, T. J.; Lecommandoux, S. Tuning Thermoresponsive Properties of Cationic Elastin-like Polypeptides by Varying Counterions and Side-Chains. *Bioconjugate Chem.* **2017**, *28*, 1403-1412.
24. Rosselin, M.; Xiao, Y.; Belhomme, L.; Lecommandoux, S.; Garanger, E. Expanding the Toolbox of Chemoselective Modifications of Protein-Like Polymers at Methionine Residues. *ACS Macro Lett.* **2019**, *8*, 1648-1653.
25. Olsnes, S.; Saltvedt, E.; Pihl, A. Isolation and comparison of galactose-binding lectins from Abrus precatorius and Ricinus communis. *J. Biol. Chem.* **1974**, *249*, 803-810.
26. Bhattacharyya, L.; Brewer, C. F. Binding and precipitation of lectins from Erythrina indica and Ricinus communis (Agglutinin I) with synthetic cluster glycosides. *Arch. Biochem. Biophys.* **1988**, *262*, 605-608.
27. Yilmaz, G.; Uzunova, V.; Hartweg, M.; Beyer, V.; Napier, R.; Becer, C. R. The effect of linker length on ConA and DC-SIGN binding of S-glucosyl functionalized poly(2-oxazoline)s. *Polym. Chem.* **2018**, *9*, 611-618.
28. Rutenber, E.; Katzin, B. J.; Ernst, S.; Collins, E. J.; Mlsna, D.; Ready, M. P.; Robertus, J. D. Crystallographic refinement of ricin to 2.5 A. *Proteins* **1991**, *10*, 240-250.
29. Protein Data Bank (PDB) Crystallographic refinement of ricin to 2.5 Angstroms. (PDB: 2AAI)

Supporting Information

Multivalent elastin-like glycopolypeptides: subtle chemical structure modifications with high impact on lectin binding affinity

Marie Rosselin, Zoeisha S. Chinoy, Lourdes Mónica Bravo Anaya, Sébastien Lecommandoux and Elisabeth Garanger*

Univ. Bordeaux, CNRS, Bordeaux INP, LCPO, UMR 5629, Pessac, F-33600, France.

EXPERIMENTAL SECTION

Materials.

All reagents and solvents were purchased from commercial sources. Glycidyl propargyl ether, glacial acetic acid, hexafluoroisopropanol (HFIP), acetic anhydride, anhydrous 1,2-dichloroethane, pyridine, boron trifluoride diethyl etherate, *N*,*N*,*N*′,*N*′′,*N*′′-pentamethyldiethylenetriamine (PMDETA) and Trizma® were obtained from Sigma-Aldrich (FR). Anhydrous CH_2Cl_2 was obtained using PureSolv MD-5 solvent purification system from Innovative Technology. Ultrapure water (18 MΩ-cm) was obtained by using a Millipore Milli-Q Biocel A10 purification unit. Cuprisorb^{TM} was from Seachem (USA). Ethanol (96.0 %, EtOH), methanol (98.5 %, MeOH), acetonitrile (99.9 %, ACN) and $CuSO_4.5H_2O$ were obtained from VWR international. NaCl (99 %) was purchased from Alfa Aesar (FR). β-D-galactopyranosyl azide (β-Gal-N_3), α-D-mannopyranosyl azide (α-Man-N_3), β-D-galactopyranosyl pentaacetate, and D-mannose were obtained from Carbosynth (UK). Ammonium acetate, ammonium pyrrolidinedithiocarbamate (APDC) and sodium ascorbate were obtained from Fisher Scientific (FR). Unconjugated Ricinus Communis Agglutinin I (RCA_{120}) from Vector Labs was purchased from Eurobio Scientific (FR). Amicon® ultra-15 centrifugal filter tubes (3,000 MWCO) were obtained from Merck Millipore (FR). Tris buffer was prepared with 0.05 M Trizma-HCl and 0.15 M NaCl in ultrapure water, and the pH of the solution was adjusted to 7.6 with 0.1 M NaOH.

Synthetic procedures.

Synthesis of 3-azidopropyl-β-D-galactopyranoside (β-Gal-*link*-N_3) and 3-azidopropyl-α-D-mannopyranoside (α-Man-*link*-N_3).

1,2,3,4,6-Penta-*O*-acetyl-D-mannopyranose. Acetic anhydride (10 mL) was added to a solution of mannose (2 g, 11.1 mmol) in pyridine (15 mL) and the resulting reaction mixture

was left to stir for 18 h. The solution was diluted with ethyl acetate (EtOAc), washed with a saturated solution of $NaHCO_3$ and a solution of $CuSO_4$, dried over $MgSO_4$, filtered and the filtrate was concentrated *in vacuo*. The resulting residue was purified by flash chromatography on silica gel (petroleum ether:EtOAc, 6:4, v:v) to afford 1,2,3,4,6-Penta-*O*-acetyl-D-mannopyranose (4.3 g, β:α = 4:1, quantitative yield) as an oil . ^{1}H NMR (400 MHz; $CDCl_3$): δ 2.00-2.16 (m, 15H, 5 × OAc), 3.80 (ddd, *J* = 9.9, 5.4, 2.4 Hz, 0.19H, H-5α), 4.03-4.16 (m, 2H, H-5β, H-6a), 4.26-4.30 (m, 1H, H-6b), 5.13 (dd, *J* = 10.0, 3.3 Hz, 0.18H, H-2α), 5.25-5.27 (m, 0.87H, H-2β), 5.29-5.38 (m, 1.82H, H-3α, H-4αβ), 5.48 (dd, *J* = 3.3, 1.1 Hz, 0.19H, H-3β), 5.86 (d, *J* = 1.2 Hz, 0.19H, H-1α), 6.09 (d, *J* = 1.7 Hz, 0.81H, H-1β). ^{13}C NMR assigned from HSQC (100 MHz, $CDCl_3$): δ 20.39 (5×), 61.80, 65.36, 67.95, 68.27, 68.59 (C-3β), 70.54 (C-3α), 70.54 (C-5β), 73.12 (C-5α), 90.27 (C-1). (Figures S1-S3)

3-Azidopropyl (2,3,4,6-tetra-*O*-acetyl-α-D-mannopyranoside. To a cooled (0 °C) solution of 3-azido-1-propanol (520 μL, 5.63 mmol) and 1,2,3,4,6-penta-*O*-acetyl-D-mannopyranose (733 mg, 1.88 mmol) in anhydrous CH_2Cl_2 (5 mL), boron trifluoride diethyl etherate (1.16 mL, 9.4 mmol) was added and the reaction left to stir, while warming to room temperature, for 18 h. The reaction mixture was diluted with CH_2Cl_2 and washed with a saturated solution of $NaHCO_3$, and then water till the pH was neutral, filtered through celite, The organic layers were combined, dried over $MgSO_4$, filtered and concentrated *in vacuo.* The resulting residue was purified by flash chromatography on silica gel (petroleum ether:EtOAc, 6:4, v:v), to give 3-azidopropyl (2,3,4,6-tetra-*O*-acetyl-α-D-mannopyranoside (331 mg, 41%) as an oil. ^{1}H NMR (400 MHz; $CDCl_3$): δ 1.87-1.93 (m, 2H, L2-CH_2), 2.00 (s, 3H, OAc), 2.05 (s, 3H, OAc), 2.11 (s, 3H, OAc), 2.16 (s, 3H, OAc), 3.43 (t, *J* = 6.5 Hz, 2H, L3-CH_2), 3.49-3.56 (m, 1H, L1-C*H*H), 3.79-3.85 (m, 1H, L1-CH*H*), 3.97 (ddd, *J* = 9.3, 5.5, 2.5 Hz, 1H, H-5), 4.12 (dd, *J* = 12.2, 2.5 Hz, 1H, H-6a), 4.28 (dd, *J* = 12.2, 5.4 Hz, 1H, H-6b), 4.82 (d, *J* = 1.7 Hz, 1H, H-1), 5.24 (dt, *J* = 3.4, 1.8 Hz, 1H, H-2), 5.28-5.34 (m, 2H, H-3, H-4). ^{13}C NMR assigned from HSQC (100 MHz, $CDCl_3$): δ 20.39 (5×), 28.48, 47.89, 62.45, 64.71, 66.01, 68.59 (C-5), 68.59 (C-2), 69.24, 97.39. MALDI-MS: $[M+Na]^+$ $C_{17}H_{25}N_3NaO_{10}$, calcd 454.14, obsd 454.46. (Figures S4-S6)

3-Azidopropyl-α-D-mannopyranoside. 3-Azidopropyl (2,3,4,6-tetra-*O*-acetyl-α-D-mannopyranoside (204 mg) was dissolved in 20 mM NaOMe (8 mL), and the reaction left to stir at room temperature for 4 h. The reaction was neutralized with Dowex 50WX8 H^+ resin, filtered, concentrated and azeotropically dried with toluene (4 × 5 mL) to afford the product 3-azidopropyl-α-D-mannopyranoside (130 mg, quantitative yield). ^{1}H NMR (400 MHz; D_2O):

δ 1.90-1.94 (m, 2H, L2-CH_2), 3.46 (td, *J* = 6.6, 2.1 Hz, 2H, L3-CH_2), 3.58-3.66 (m, 3H, H-4, H-5, L1-C*H*H), 3.74-3.85 (m, 3H, H-6a, H-3, L1-CH*H*), 3.90 (dd, *J* = 12.1, 1.8 Hz, 1H, H-6b), 3.96 (dd, *J* = 3.4, 1.8 Hz, 1H, H-2), 4.87 (d, *J* = 1.8 Hz, 1H, H-1). ^{13}C NMR assigned from HSQC (100 MHz, D_2O): δ 27.83, 48.21, 60.83, 64.71, 66.65, 69.89, 70.54, 72.80, 99.65. MALDI-MS: $[M+Na]^+$ $C_9H_{17}N_3NaO_6$, calcd 286.10, obsd 286.31. (Figures S7-S9)

3-Azidopropyl (2,3,4,6-tetra-*O*-acetyl-β-D-galactopyranoside. To a cooled (0 °C) solution of 3-azido-1-propanol (720 μL, 7.84 mmol) and β-D-galactopyranosyl pentaacetate (1.02 g, 2.61 mmol) in anhydrous 1,2-dichloroethane (8 mL), boron trifluoride diethyl etherate (640 μL, 5.22 mmol) was added and the reaction left to stir, while warming to room temperature, for 18 h. The reaction mixture was diluted with CH_2Cl_2 and washed with a saturated solution of $NaHCO_3$, and then water till the pH was neutral, filtered through celite, The organic layers were combined, dried over $MgSO_4$, filtered and concentrated *in vacuo.* The resulting residue was purified by flash chromatography on silica gel (petroleum ether:EtOAc, 7:3, v:v), to give 3-azidopropyl (2,3,4,6-tetra-*O*-acetyl-β-D-galactopyranoside (380 mg, 34%) as an oil. ^{1}H-NMR (400 MHz; $CDCl_3$): δ 1.75-1.84 (m, 2H, L2-CH_2), 1.92 (s, 3H, OAc), 1.99 (d, *J* = 6.8 Hz, 6H, 2 × OAc), 2.09 (s, 3H, OAc), 3.29-3.33 (m, 2H, L3-CH_2), 3.50-3.57 (m, 1H, L1-CH*H*), 3.83-3.92 (m, 2H, H-5, L2-C*H*H), 4.04-4.14 (m, 2H, H-6a, H-6b), 4.40 (d, *J* = 7.9 Hz, 1H, H-1), 4.95 (dd, *J* = 10.5, 3.4 Hz, 1H, H-3), 5.13 (dd, *J* = 10.5, 7.9 Hz, 1H, H-2), 5.33 (dd, *J* = 3.4, 1.0 Hz, 1H, H-4). ^{13}C NMR assigned from HSQC (100 MHz, D_2O): δ 20.71 (×4), 28.80, 47.57, 61.15, 66.33 (×2), 68.59, 70.54, 70.86, 101.27. MALDI-MS: $[M+Na]^+$ $C_{17}H_{25}N_3NaO_{10}$, calcd 454.14, obsd 454.35. (Figures S10-S12)

3-Azidopropyl-β-D-galactopyranoside. 3-azidopropyl (2,3,4,6-tetra-*O*-acetyl-β-D-galactopyranoside (241 mg) was dissolved in 20 mM NaOMe (10 mL), and the reaction left to stir at room temperature for 3 h. The reaction was neutralized with Dowex 50WX8 H^+ resin, filtered, concentrated and azeotropically dried with toluene (4 × 5 mL) to afford 3-azidopropyl-β-D-galactopyranoside (152 mg, quantitative yield) as an oil. ^{1}H-NMR (400 MHz; D_2O): δ 1.92 (quintet, *J* = 6.5 Hz, 2H, L2-CH_2), 3.54-3.46 (m, 3H, L3-CH_2, H-2), 3.65 (dd, *J* = 9.9, 3.5 Hz, 1H, H-2), 3.70 (ddd, *J* = 7.8, 4.4, 0.9 Hz, 1H, H-5), 3.80-3.73 (m, 3H, L1-CH*H*, H-6a, H-6b), 3.93 (dd, *J* = 3.4, 0.7 Hz, 1H, H-4), 4.01 (dt, *J* = 10.4, 6.2 Hz, 1H, L1-C*H*H), 4.40 (d, *J* = 7.9 Hz, 1H, H-1). ^{13}C NMR assigned from HSQC (100 MHz, D_2O): δ 27.83, 47.57, 60.83, 66.98, 68.27, 70.54, 72.48, 75.07, 102.89. MALDI-MS: $[M+Na]^+$ $C_9H_{17}N_3NaO_6$, calcd 286.10, obsd 286.31. (Figures S13-S15)

Synthesis of glycopolypeptides.

ELP[M_1V_3-20] and ELP[M_1V_3-40] (Figure 1A) were produced recombinantly in *Esherichia coli* bacteria and purified by *inverse transition cycling* (1999_ Nat.Biotechnol_Meyer_ A. Purification of Recombinant Proteins by Fusion with Thermally-Responsive Polypeptides) following established procedures. (2010_Chem.Biol._Basle,_ Protein Chemical Modification on Endogenous Amino Acids, Biomacromol Rosine 2017, 2017_Bioconjugate_Petitdemange) These two ELPs were chemoselectively thioalkylated with glycidyl propargyl ether (Figure 1B, step *i*), and part of the purified products were demethylated (Figure 1B, step *ii*) in 75% EtOH(aq) with ammonium pyrrolidinedithiocarbamate (APDC) as described in a previous contribution (2017_Bioconjugate_Petitdemange, ACS MacroLetters Rosselin). Both series of sulfonium- and thioether-containing derivatives were subsequently functionalized by copper catalyzed azide-alkyne cycloaddition (CuAAC) using β-D-galactopyranosyl azide (β-Gal-N_3), α-D-mannopyranosyl azide (α□Man-N_3), 3-azidopropyl-β-D-galactopyranoside (β-Gal-*link*-N_3) or 3-azidopropyl-α-D-mannopyranoside (α□Man-*link*-N_3) to give compounds **1a-c**, **2a-d**, **3a-d** and **4a-d**. (Figure 1B, step *iii*)

General procedure for ELP thioalkylation: synthesis of ELP[M(Alk)$_1$V$_3$-*20*] (1) and ELP[M(Alk)$_1$V$_3$-*40*] (2).

ELP[M_1V_3-*n*] (*n*= 20 or 40) was dissolved in AcOH/HFIP mixture (9/1, v/v) at 20 mg/mL. The solution was degassed with Ar and glycidyl propargyl ether was added to the mixture (10 equiv. per Met residue). After 24 h stirring, a second portion of glycidyl propargyl ether (10 equiv. per Met residue) was added and the reaction was stirred for a total of 48 h at room temperature and under Ar atmosphere. The reaction mixture was transferred into a 3,000 MWCO Amicon® ultra-15 centrifugal filter tube, washed with 40 mL ultrapure water and freeze-dried. Derivatives **1** and **2** were characterized by NMR spectroscopy. (Figures S18 and S44-45, respectively).

General procedure for ELP demethylation: synthesis of ELP[M(*Dem*Alk)$_1$V$_3$-*20*] (3) and ELP[M(*Dem*Alk)$_1$V$_3$-*20*] (4).

To a solution of ELP[M(Alk)$_1$V$_3$-*n*] (*n*= 20 or 40) in 75% EtOH(aq) was added ammonium pyrrolidinedithiocarbamate (APDC) (5.0 equiv per Met residue). The solution was stirred under Ar for 24 h at room temperature. The reaction mixture was transferred to a 1 kDa MWCO dialysis tubing and dialyzed against 50 % MeOH(aq) during 24 h with 3 solvent

changes, followed by 8 h dialysis against ultrapure water with 3 changes. The solution was then lyophilized. Derivatives **3** and **4** were characterized by NMR spectroscopy. (Figures S28-29, and S56-57, respectively).

General procedure for CuAAC in water: synthesis of glycopolypeptides 1a-c, 2a-d, 3a-d, 4a-d.

To a solution of ELP[M(Alk)$_1$V$_3$-*n*] or ELP[M(*Dem*Alk)$_1$V$_3$-*n*] (*n*= 20 or 40) derivative in degassed water (5 mg/mL) under Ar Atmosphere, the desired azido-containing monosaccharide derivative (1.5 equiv. per alkyne) was added. A solution of Cu(I) was prepared by addition of sodium ascorbate (1.3 equiv. per alkyne) to a degassed solution of Cu(II)SO_4 (0.26 equiv. per alkyne) and pentamethyldiethylenetriamine (0.26 equiv. per alkyne) in Milli-Q water. The fresh Cu(I) solution was then transferred to the reaction mixture with a syringe. The reaction was stirred under Ar at room temperature for 72 h. Cuprisorb was added to remove copper by shaking overnight. Few drops of an aqueous solution of EDTA (0.15 M) were added and the solution was purified by ultracentrifugation with Amicon® 3000 MWCO ultra-centrifugal filter tube against Milli-Q water (40 mL). The remaining mixture was lyophilized. All products were characterized by NMR. (Spectra provided in SI) Yields and functionalization degrees are provided in Table 1.

NMR Spectrometry Analysis. ^{1}H NMR analyses were performed in D_2O at 298 K on a Bruker AVANCE III HD 400 apparatus equipped with a 5 mm Bruker multinuclear z-gradient direct probe operating at 400.2 MHz. The solvent signal was used as the reference signal (δ = 4.79 ppm). HSQC analyses were performed on a Bruker AVANCE NEO 400 spectrometer operating at 100.7 MHz, equipped with a 5 mm Bruker multinuclear z-gradient direct cryoprobe-head operating at 298 K. Data processing was performed using Bruker Topspin Software.

Size-exclusion Chromatography (SEC). Measurements in aqueous solvent were performed on an Ultimate 3000 system from Thermoscientific equipped with diode array detector DAD. The system also includes a multi-angles light scattering detector MALS and differential refractive index detector dRI from Wyatt technology. Glycopolypeptides were separated on two TOSOH successive columns (one G4000PWXL (7.8*300) column with exclusion limits from 2000 Da to 300,000 Da and one G3000PWXL (7.8*300) column with exclusion limit below 40,000 Da). Measurements were performed at a flow rate of 0.6 mL/min and columns temperature was held at 26°C. Aqueous solvent composed by acetic acid (AcOH) 0.3 M,

ammonium acetate 0.2 M and ACN (6.5/3.5, v/v) was used as the eluent. Ethylene glycol was used as flow marker.

Micro-Scale Thermophoresis (MST).

MST experiments were conducted in triplicate on a Monolith NT.115 system (NanoTemper Technologies) using Auto Red laser power and medium MST power with temperature set at 22°C. The buffer containing RCA_{120} was exchanged for Tris buffer (pH 7.6) and RCA_{120} was fluorescently labeled using a Monolith protein labeling kit "RED-NHS 2nd generation" (amine reactive) provided by NanoTemper (DE). Tris buffer (pH 7.6) containing 0.05 % of Tween®-20 and 20 mM $MgCl_2$ was used for all binding assays.

Lectin binding tests. All compounds were screened in the same conditions. Glycopolypeptides were previously solubilized in Tris buffer at 4 °C at the maximum concentration corresponding to their respective limit of solubility (around 10 $mg.mL^{-1}$), *i.e.* 1 mM for the series of ELP-[M_1V_3-*20*] derivatives (series **1** and **3**) and 0.5 mM for the series of ELP-[M_1V_3-*40*] derivatives (series **2** and **4**). Serial 2-fold dilutions were prepared with RCA_{120} (5 nM) in Tris buffer. Thermophoresis was measured using "Auto Red laser power" and medium "MST power". MO Analysis software (NanoTemper Technologies, DE) was used to analyze data and calculate dissociation constants. For each sample, experimental data points were plotted on a graph representing the normalized fluorescence intensity as function of glycopolypeptide molar concentration. Experimental data were fitted with a sigmoidal curve model and the dissociation constant (K_D) was extracted (inflection point of fitted curve). Results are summarized in Table 2.

Table S1. List of NMR spectra provided for all compounds.

Figure #	Compound	NMR analysis
S1	1,2,3,4,6-penta-*O*-acetyl-D-mannopyranose	^{1}H
S2		COSY
S3		HSQC
S4	3-azidopropyl (2,3,4,6-tetra-*O*-acetyl-α-D-mannopyranoside	^{1}H
S5		COSY
S6		HSQC
S7	3-azidopropyl-α-D-mannopyranoside	^{1}H
S8		COSY
S9		HSQC
S10	3-azidopropyl (2,3,4,6-tetra-*O*-acetyl-β-D-galactopyranoside	^{1}H
S11		COSY
S12		HSQC
S13	3-Azidopropyl-β-D-galactopyranoside	^{1}H
S14		COSY
S15		HSQC
S16	ELP[M_1V_3-20]	^{1}H
S17		HSQC
S18	**1**	^{1}H
S19	**1a**	^{1}H
S20		^{1}H (zoom)
S21		HSQC
S22	**1b**	^{1}H
S23		^{1}H (zoom)
S24		HSQC
S25	**1c**	^{1}H
S26		^{1}H (zoom)
S27		HSQC
S28	**3**	^{1}H
S29		HSQC
S30	**3a**	^{1}H
S31		^{1}H (zoom)
S32		HSQC
S33	**3b**	^{1}H
S34		^{1}H (zoom)
S35		HSQC
S36	**3c**	^{1}H
S37		^{1}H (zoom)
S38		HSQC
S39	**3d**	^{1}H
S40		^{1}H (zoom)
S41		HSQC
S42	ELP[M_1V_3-40]	^{1}H
S43		HSQC
S44	**2**	^{1}H
S45		HSQC
S46	**2a**	^{1}H
S47		^{1}H (zoom)
S48		HSQC
S49	**2b**	^{1}H
S50		^{1}H (zoom)
S51	**2c**	^{1}H
S52		HSQC
S53	**2d**	^{1}H
S54		^{1}H (zoom)
S55		HSQC

S56	**4**	^{1}H
S57		HSQC
S58	**4a**	^{1}H
S59		^{1}H (zoom)
S60		HSQC
S61	**4b**	^{1}H
S62		^{1}H (zoom)
S63		HSQC
S64	**4c**	^{1}H
S65		^{1}H (zoom)
S66		HSQC
S67	**4d**	^{1}H
S68		^{1}H (zoom)
S69		HSQC

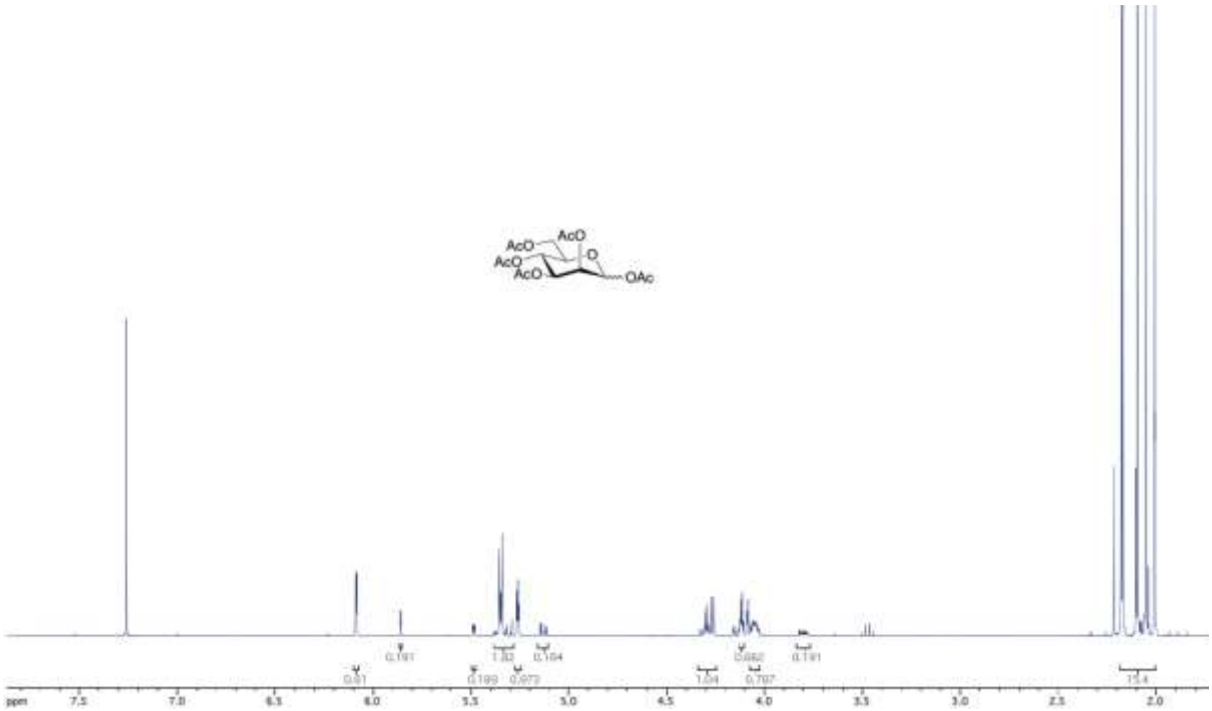

Figure S1. ^{1}H NMR spectrum of 1,2,3,4,6-penta-*O*-acetyl-D-mannopyranose in $CDCl_3$.

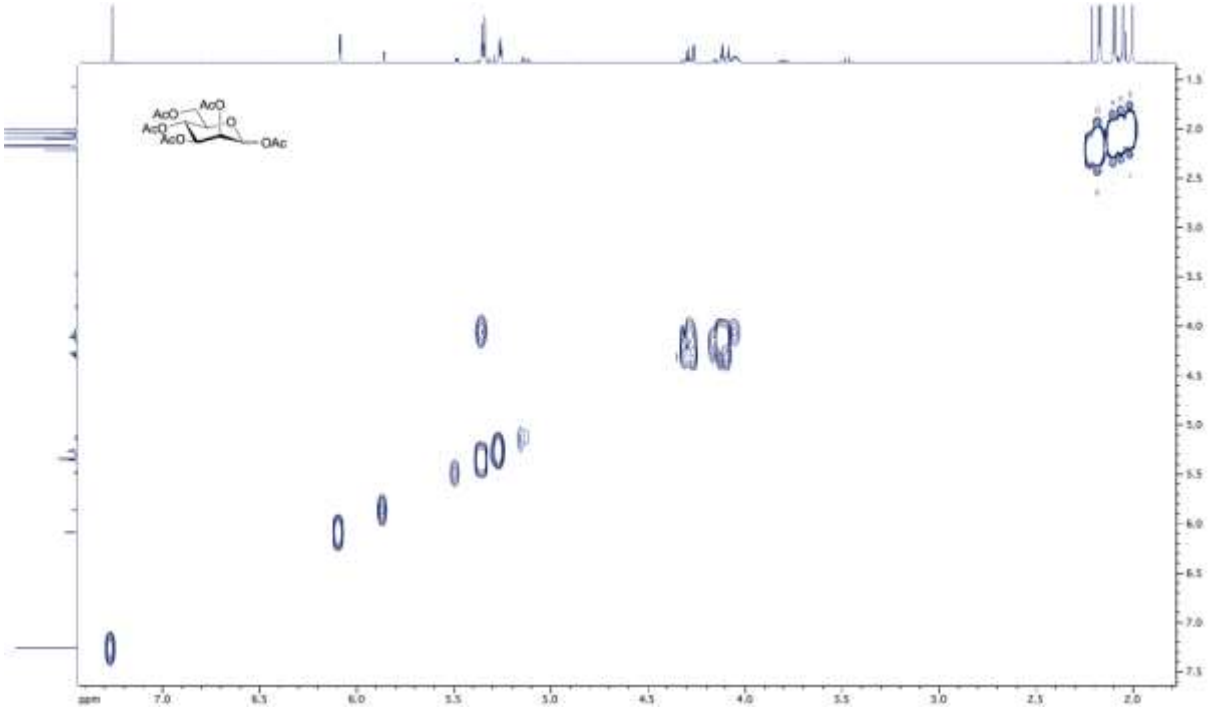

Figure S2. COSY NMR spectrum of compound 1,2,3,4,6-penta-*O*-acetyl-D-mannopyranose in $CDCl_3$.

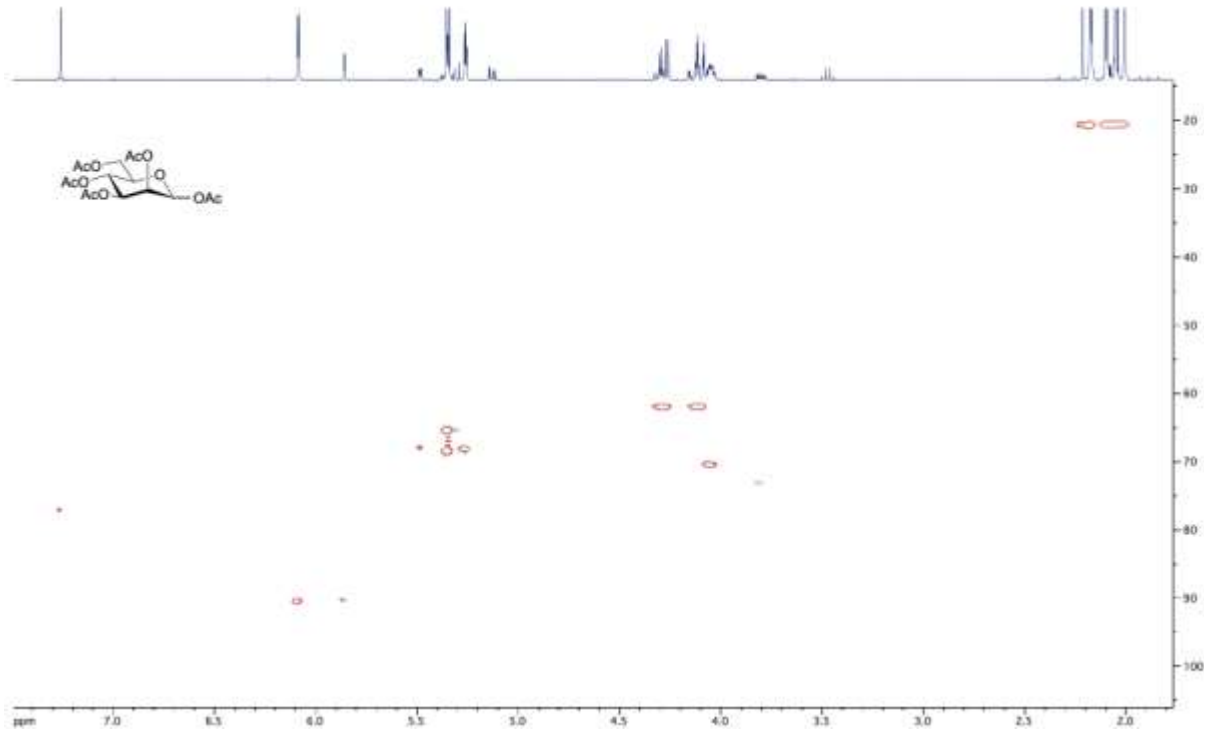

Figure S3. HSQC NMR spectrum of 1,2,3,4,6-penta-*O*-acetyl-D-mannopyranose in $CDCl_3$.

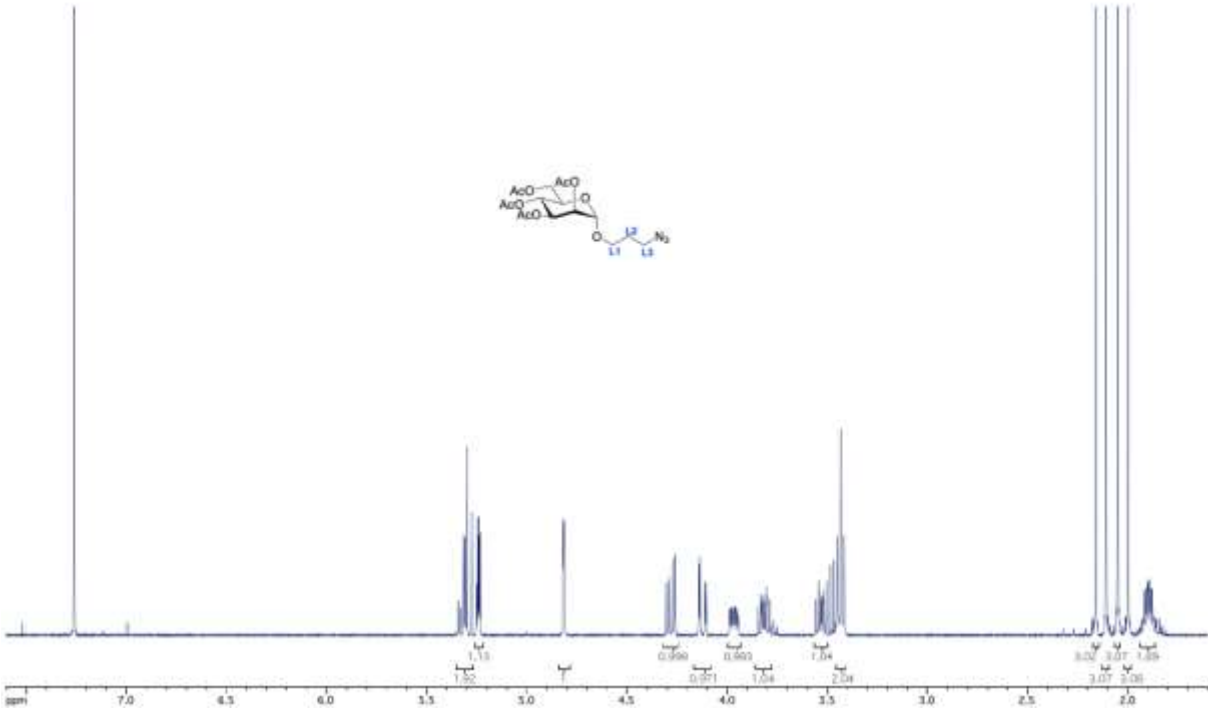

Figure S4. ^{1}H NMR spectrum of 3-azidopropyl (2,3,4,6-tetra-*O*-acetyl-α-D-mannopyranoside in $CDCl_3$.

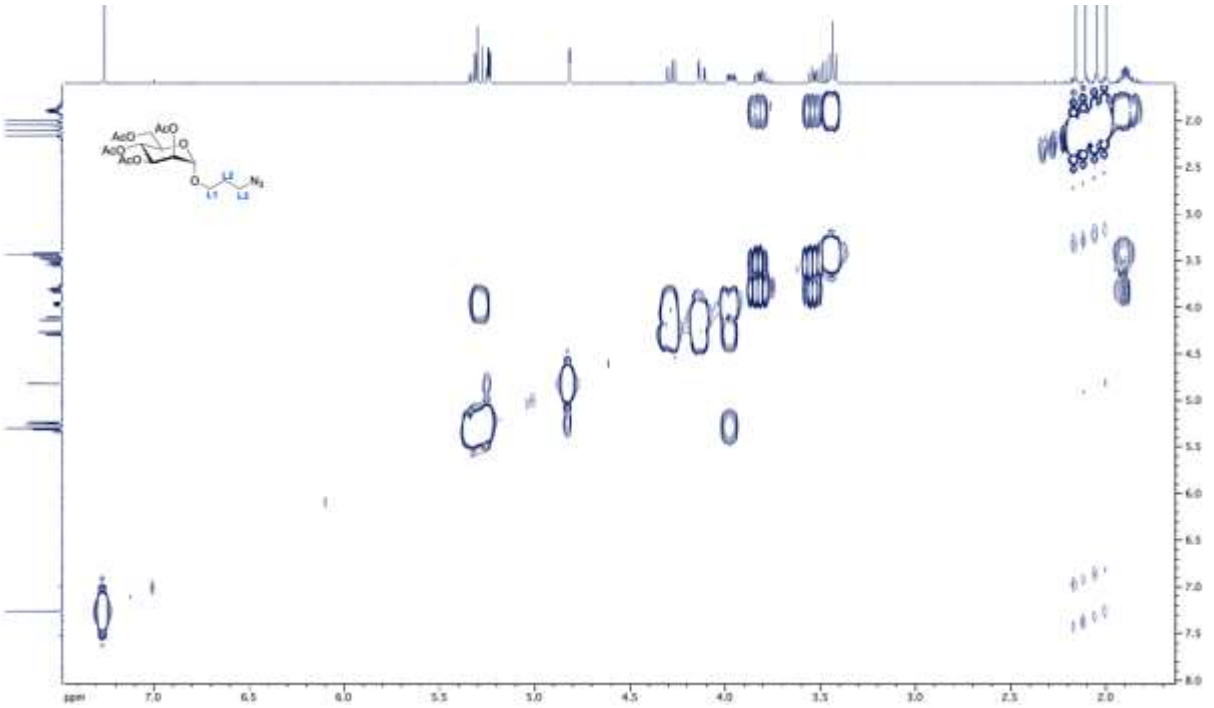

Figure S5. COSY NMR spectrum of 3-azidopropyl (2,3,4,6-tetra-*O*-acetyl-α-D-mannopyranoside in $CDCl_3$.

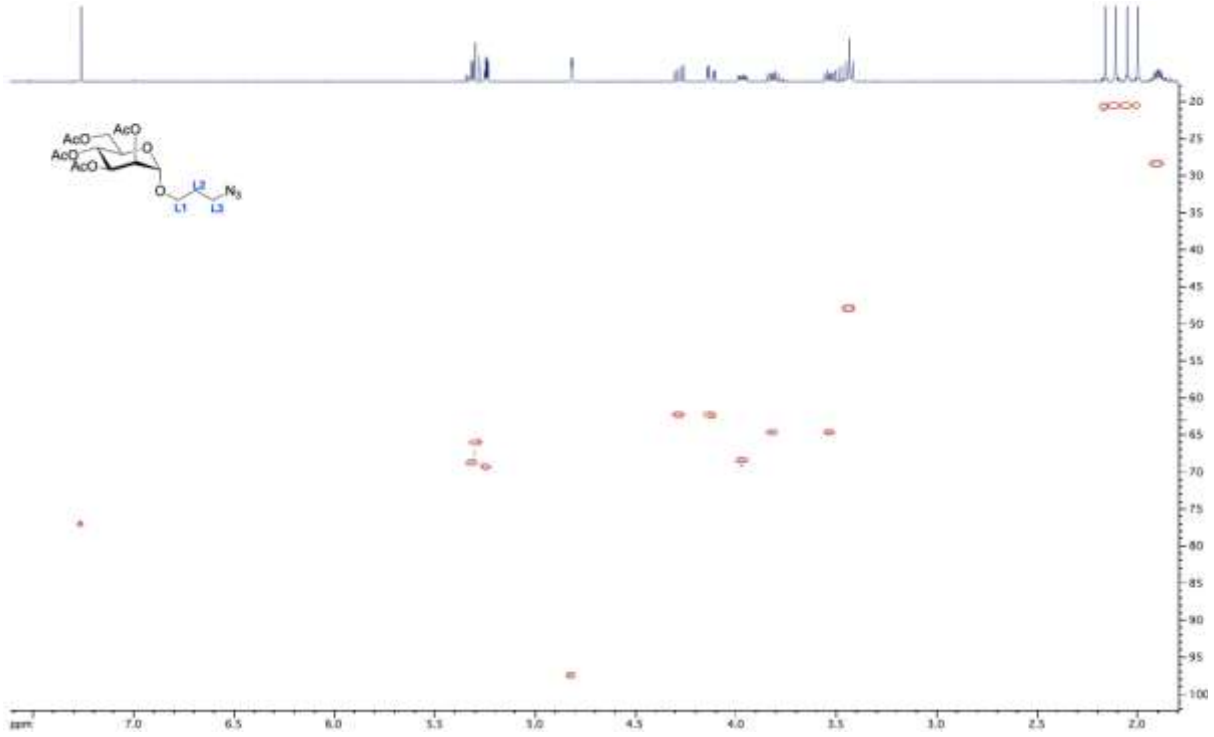

Figure S6. HSQC NMR spectrum of 3-azidopropyl (2,3,4,6-tetra-*O*-acetyl-α-D-mannopyranoside in $CDCl_3$.

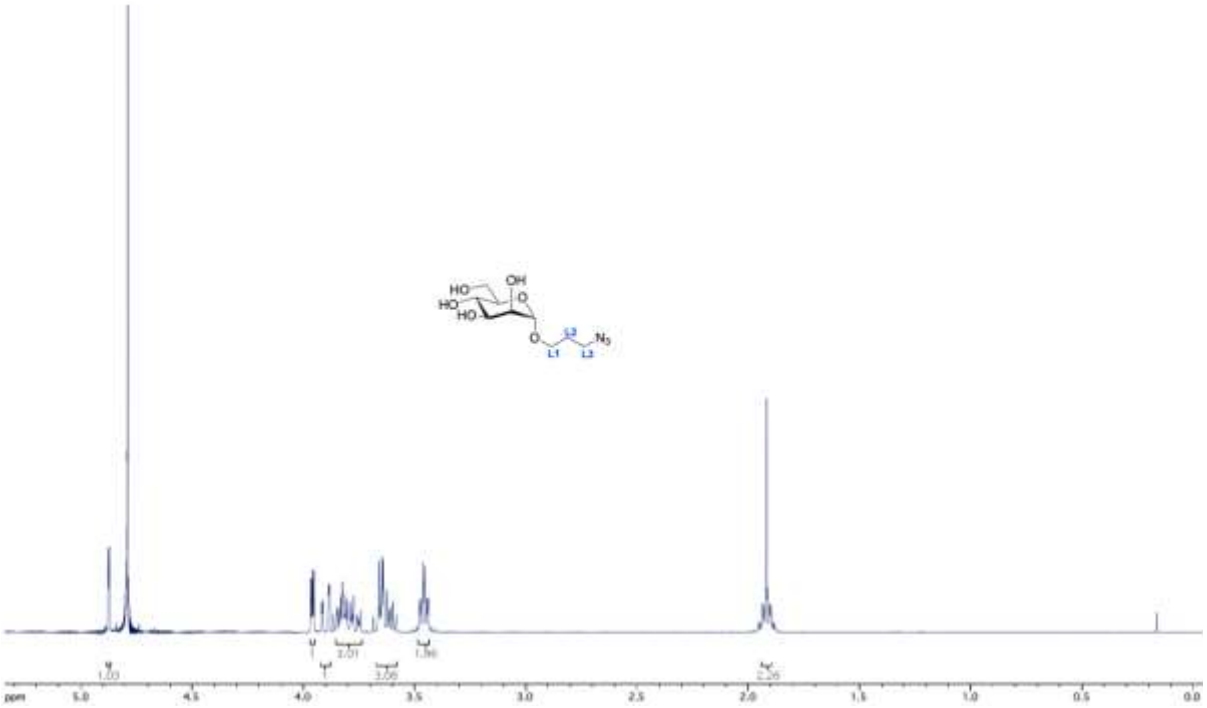

Figure S7. ^{1}H NMR spectrum of 3-azidopropyl-α-D-mannopyranoside in D_2O.

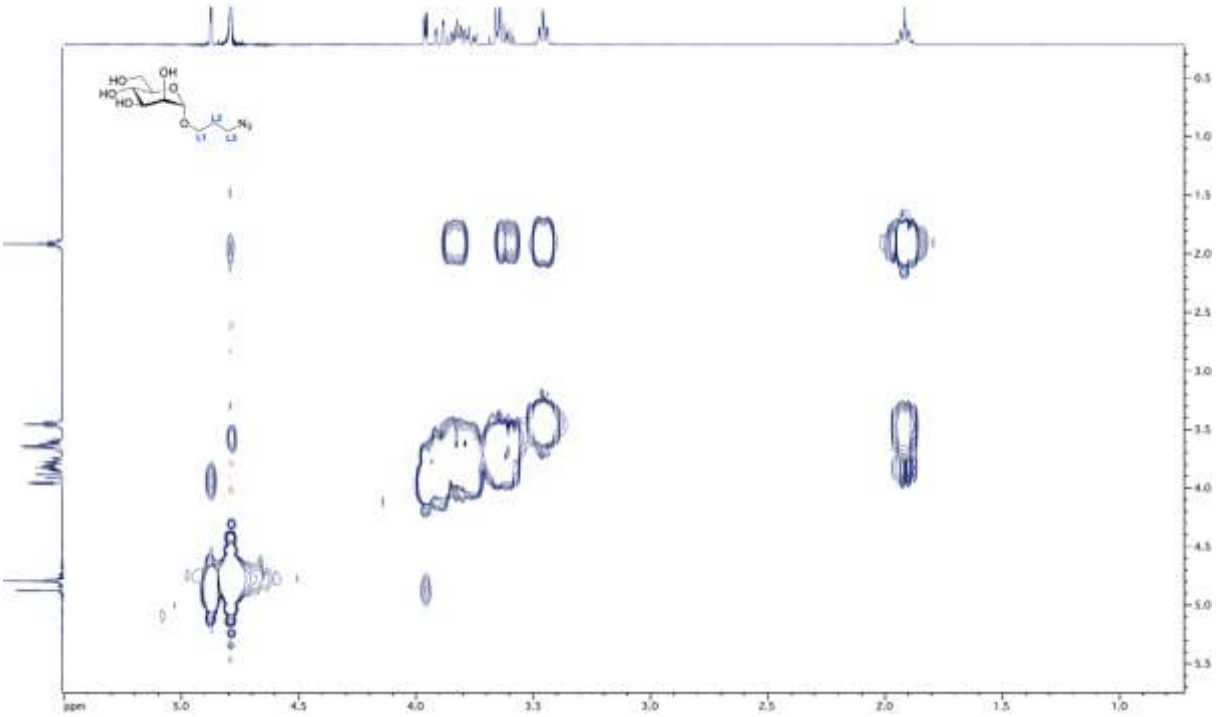

Figure S8. COSY NMR spectrum of 3-azidopropyl-α-D-mannopyranoside in D_2O.

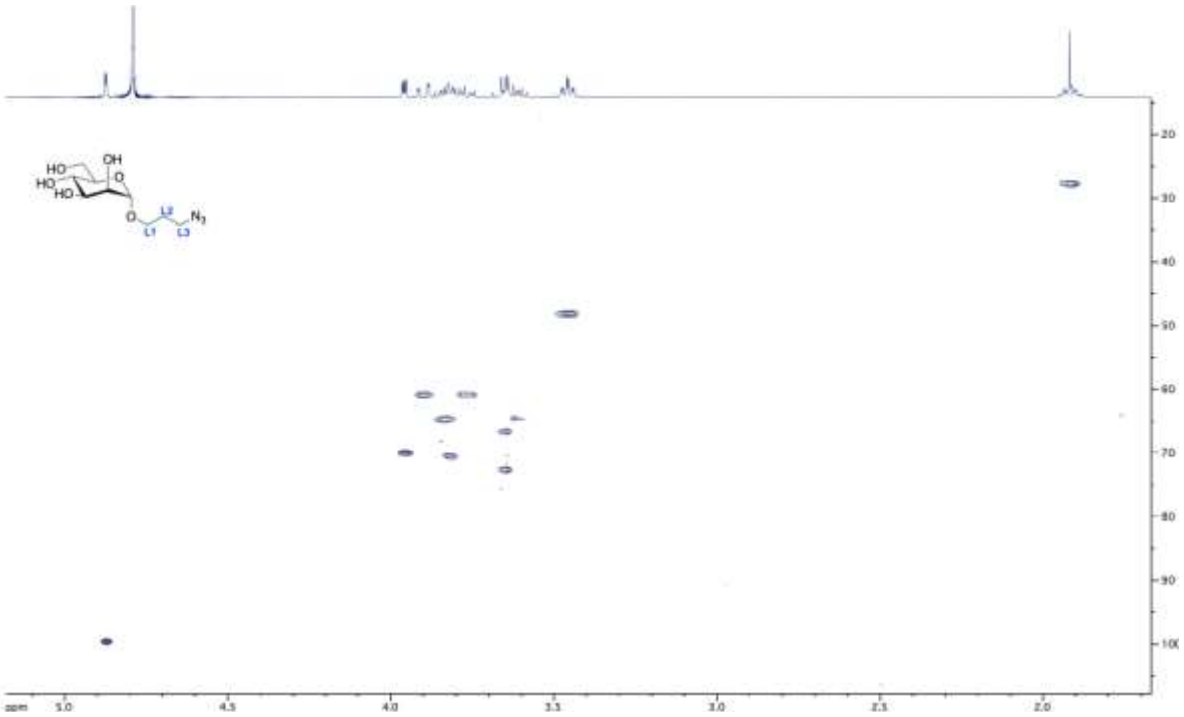

Figure S9. HSQC NMR spectrum of 3-azidopropyl-α-D-mannopyranoside in D_2O.

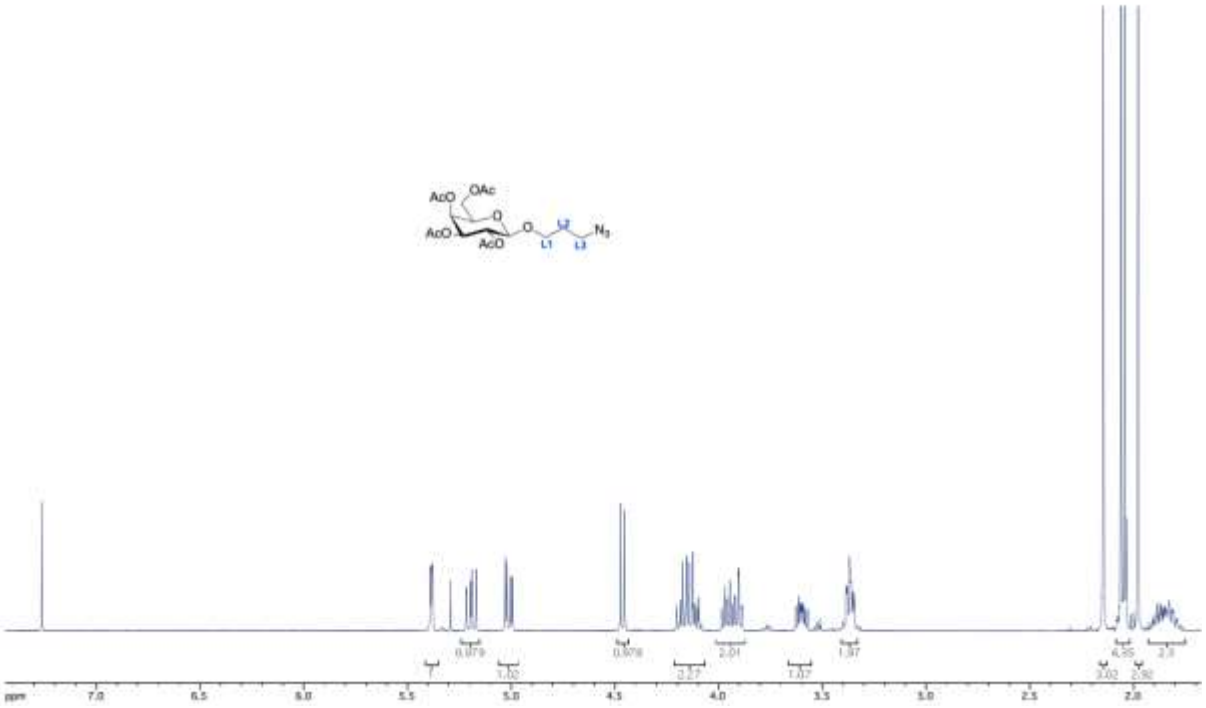

Figure S10. ^1H NMR spectrum of 3-azidopropyl (2,3,4,6-tetra-*O*-acetyl-β-D-galactopyranoside in $CDCl_3$.

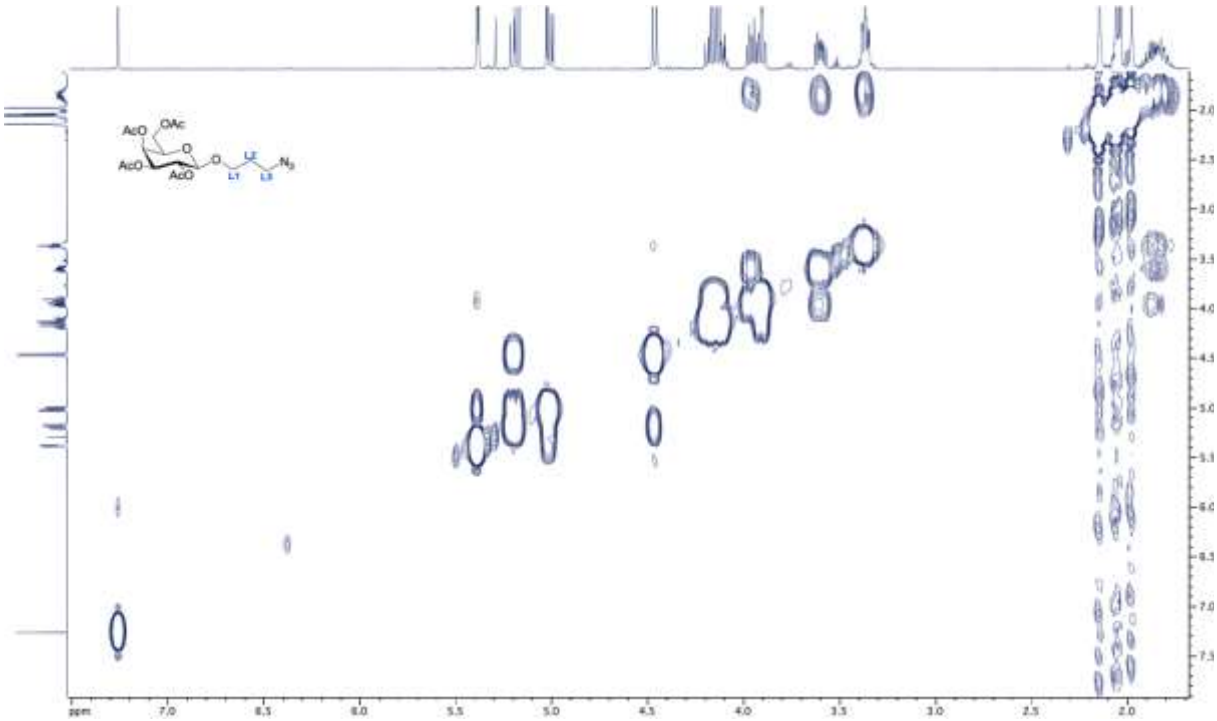

Figure S11. COSY NMR spectrum of 3-azidopropyl (2,3,4,6-tetra-*O*-acetyl-β-D-galactopyranoside in $CDCl_3$.

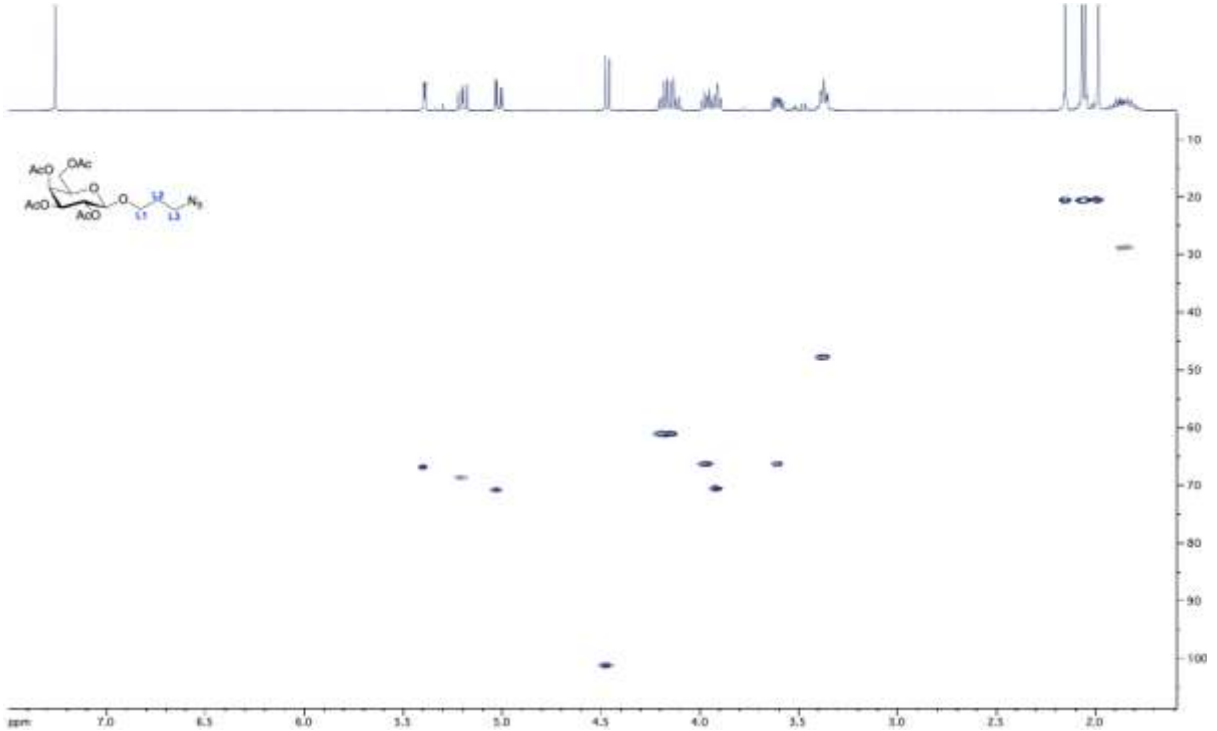

Figure S12. HSQC NMR spectrum of 3-azidopropyl (2,3,4,6-tetra-*O*-acetyl-β-D-galactopyranoside in $CDCl_3$.

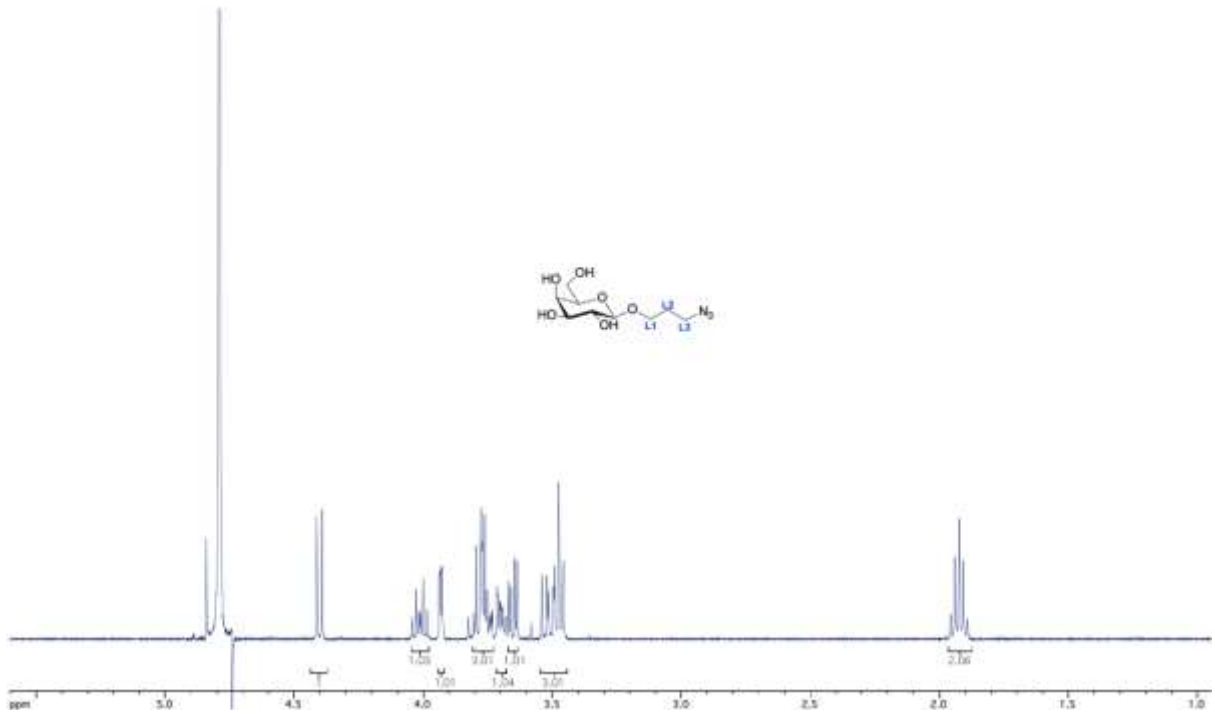

Figure S13. ^{1}H NMR spectrum of 3-azidopropyl-β-D-galactopyranoside in D_2O.

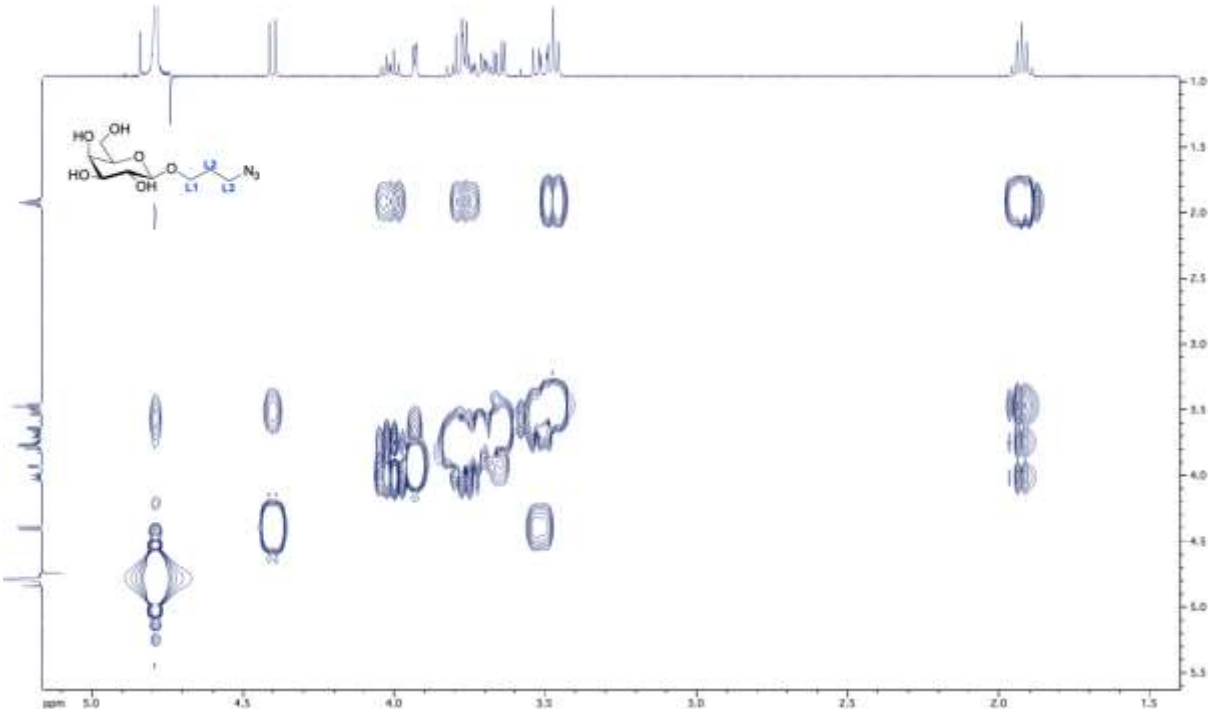

Figure S14. COSY NMR spectrum of 3-azidopropyl-β-D-galactopyranoside in D_2O.

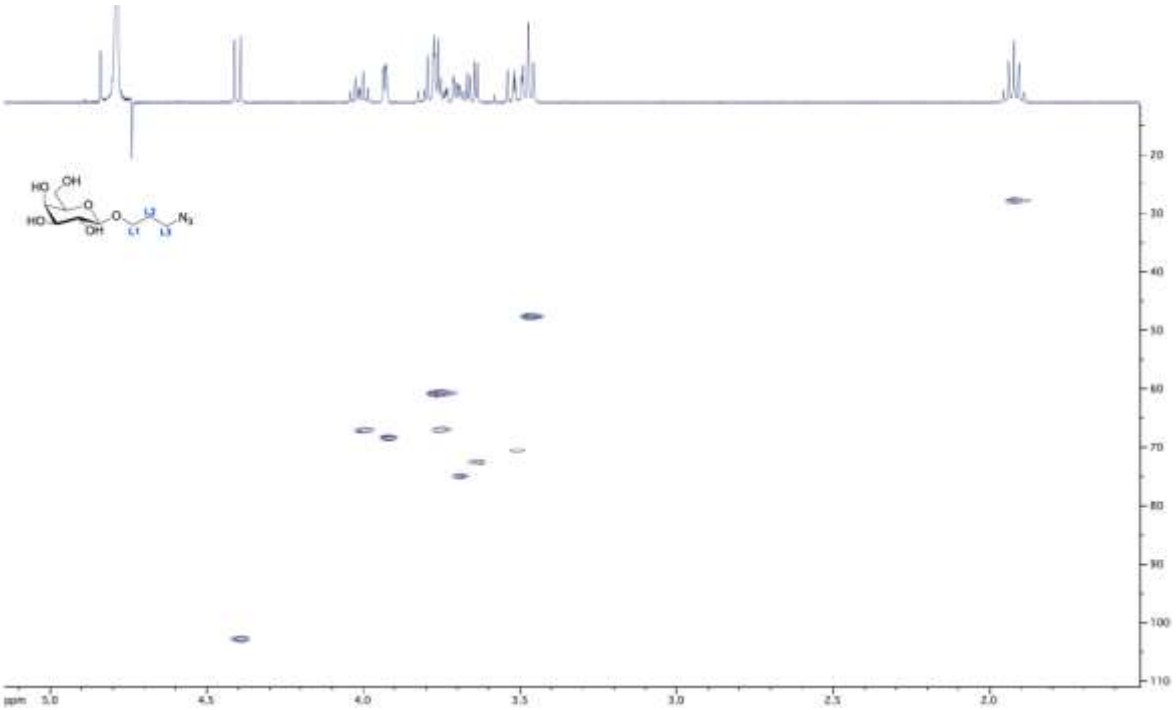

Figure S15. HSQC NMR spectrum of compound 3-azidopropyl-β-D-galactopyranoside in D_2O.

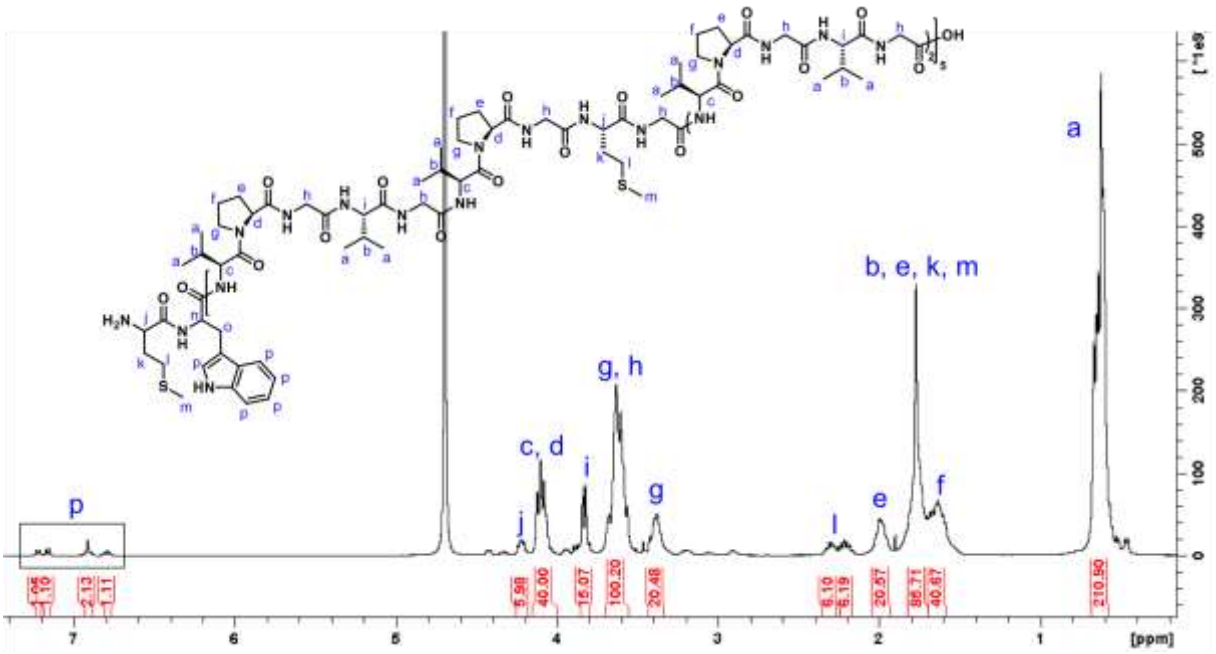

Figure S16. ^{1}H NMR spectrum of ELP[M_1V_3-20] in D_2O.

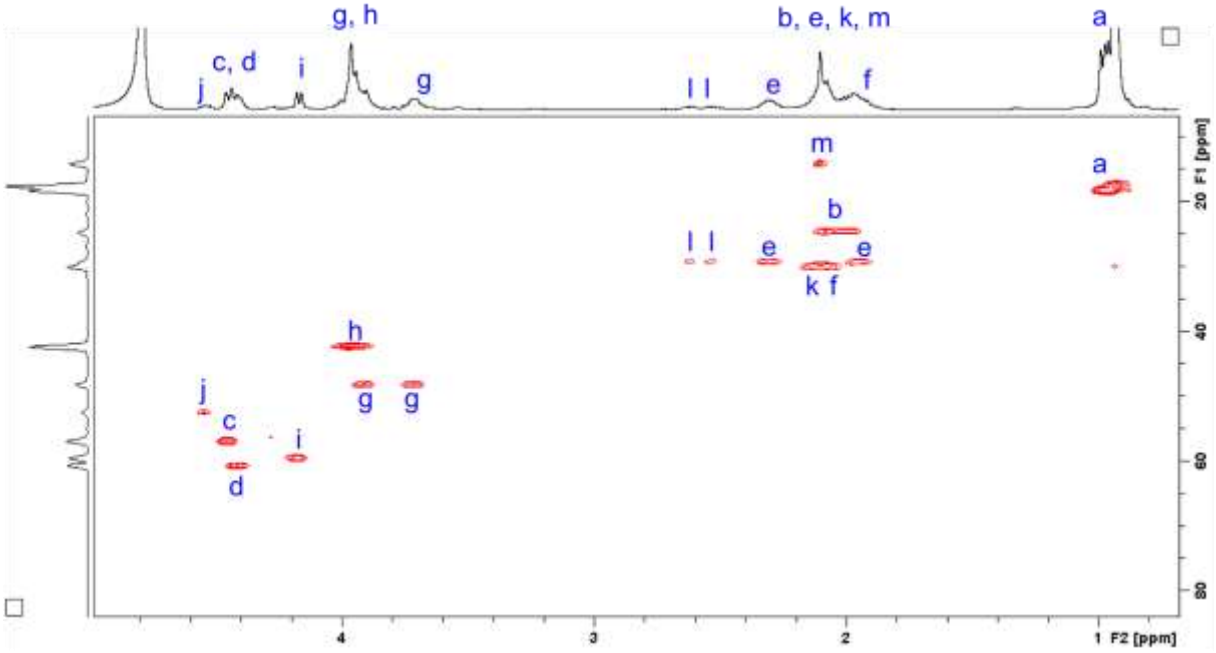

Figure S17. 2D NMR spectrum of ELP[M_1V_3-20] in D_2O, HSQC.

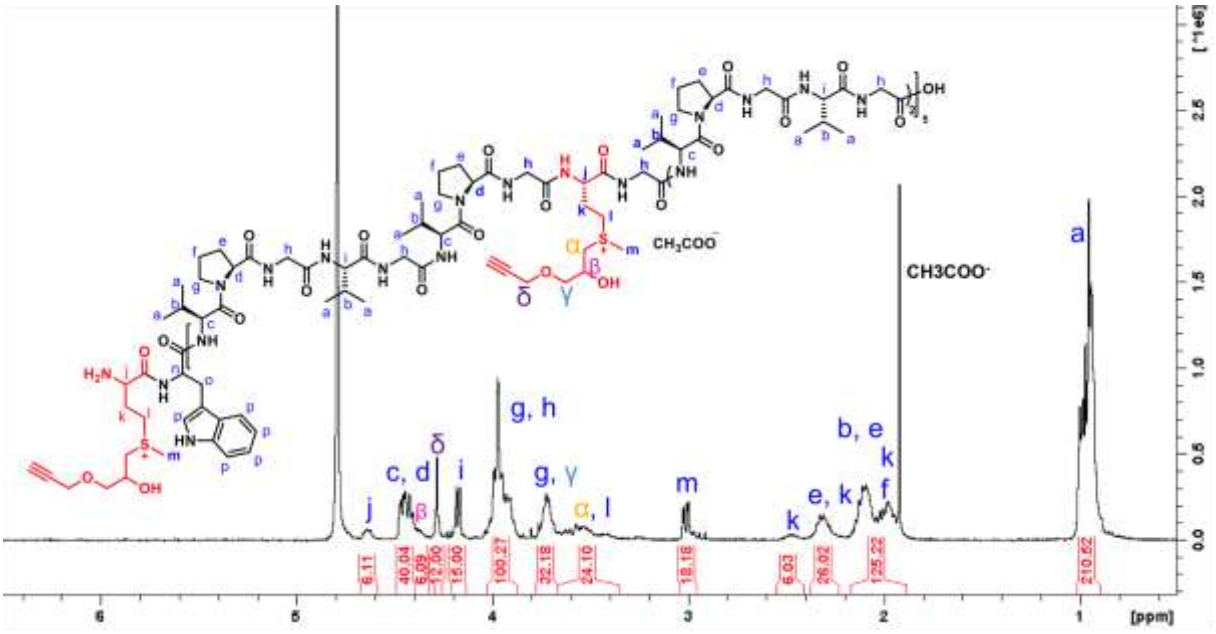

Figure S18. ^{1}H NMR spectrum of ELP[M(Alk)$_1$V$_3$-*20*], **<u>1</u>**, in D_2O.

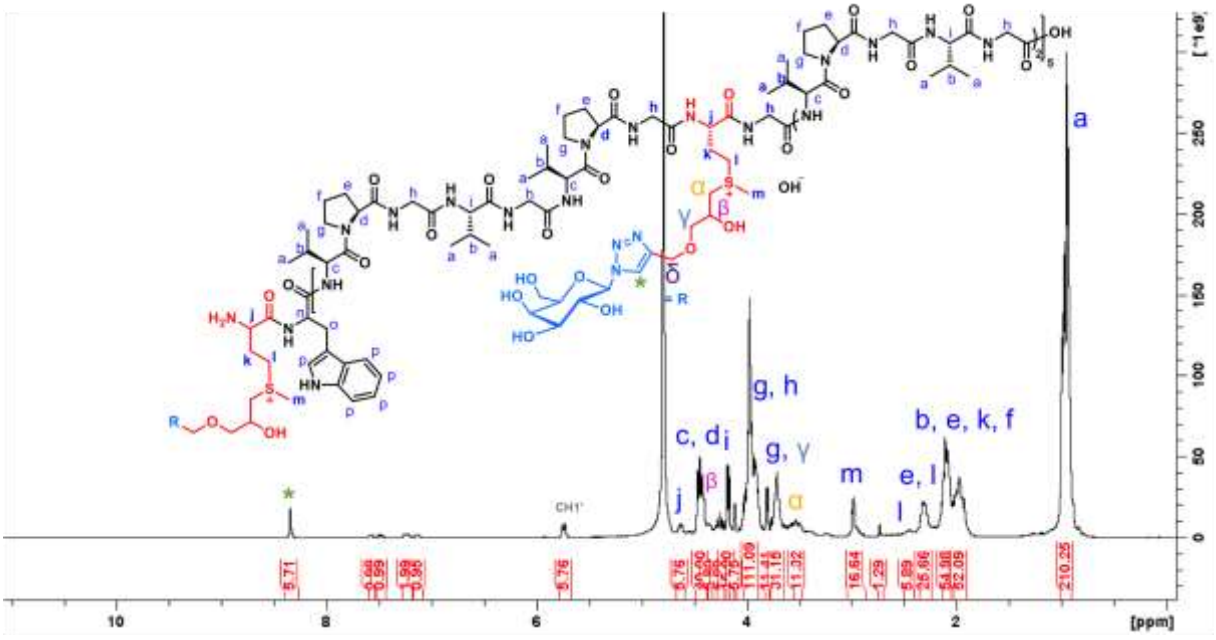

Figure S19. ^{1}H NMR spectrum of compound **<u>1a</u>** in D_2O.

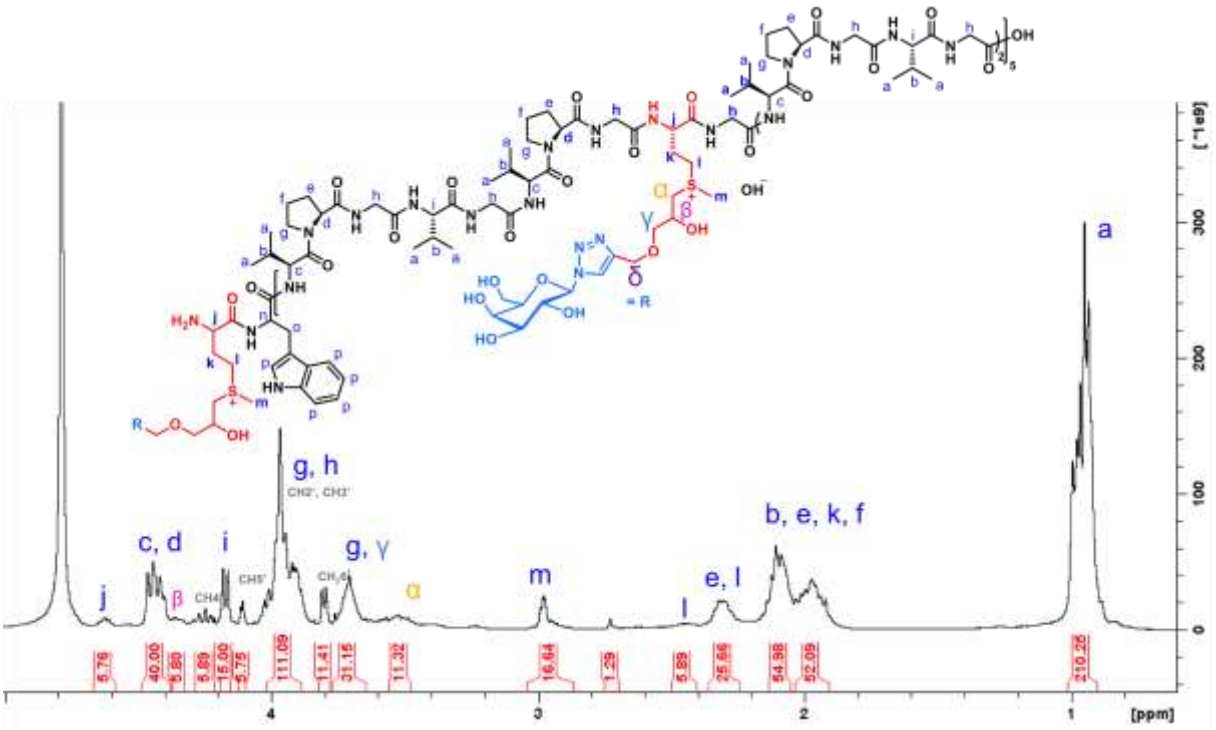

Figure S20. ^{1}H NMR spectrum of compound **1a** (zoom) in D_2O.

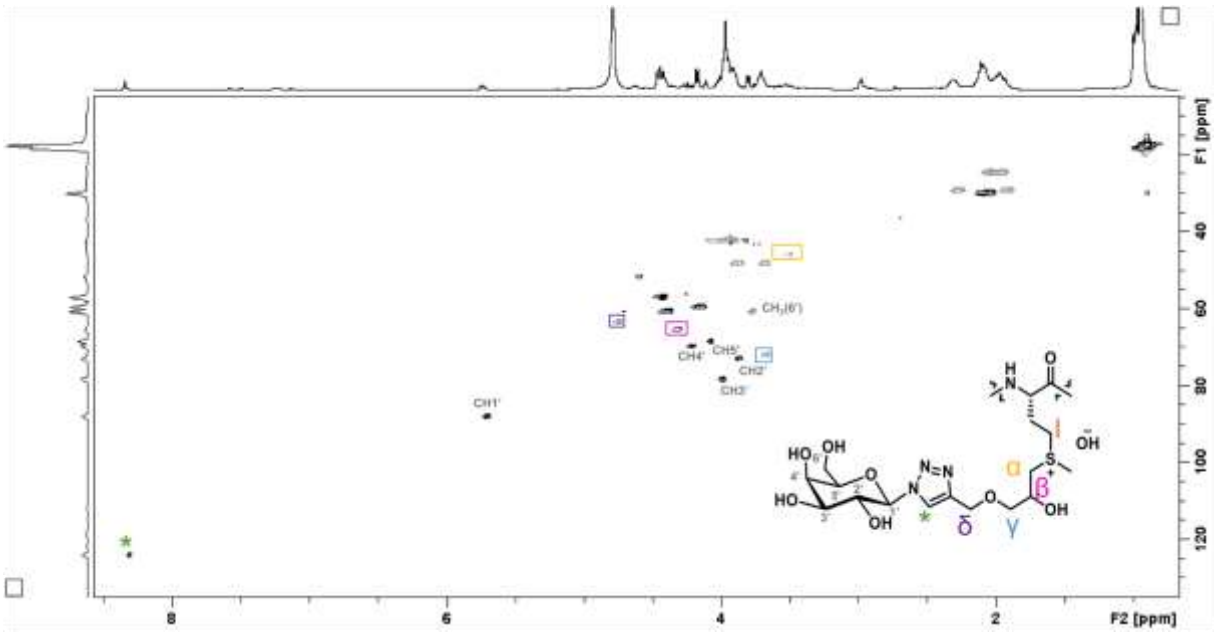

Figure S21. 2D NMR spectrum of compound **1a** in D_2O, HSQC.

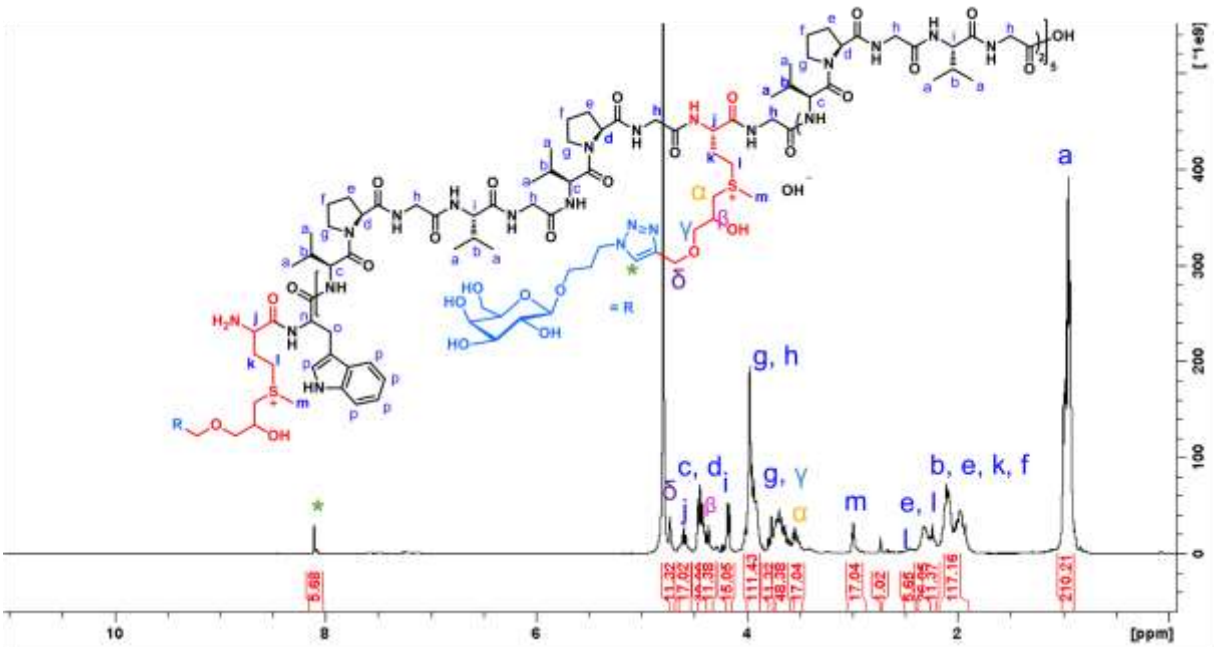

Figure S22. ^{1}H NMR spectrum of compound **<u>1b</u>** in D_2O.

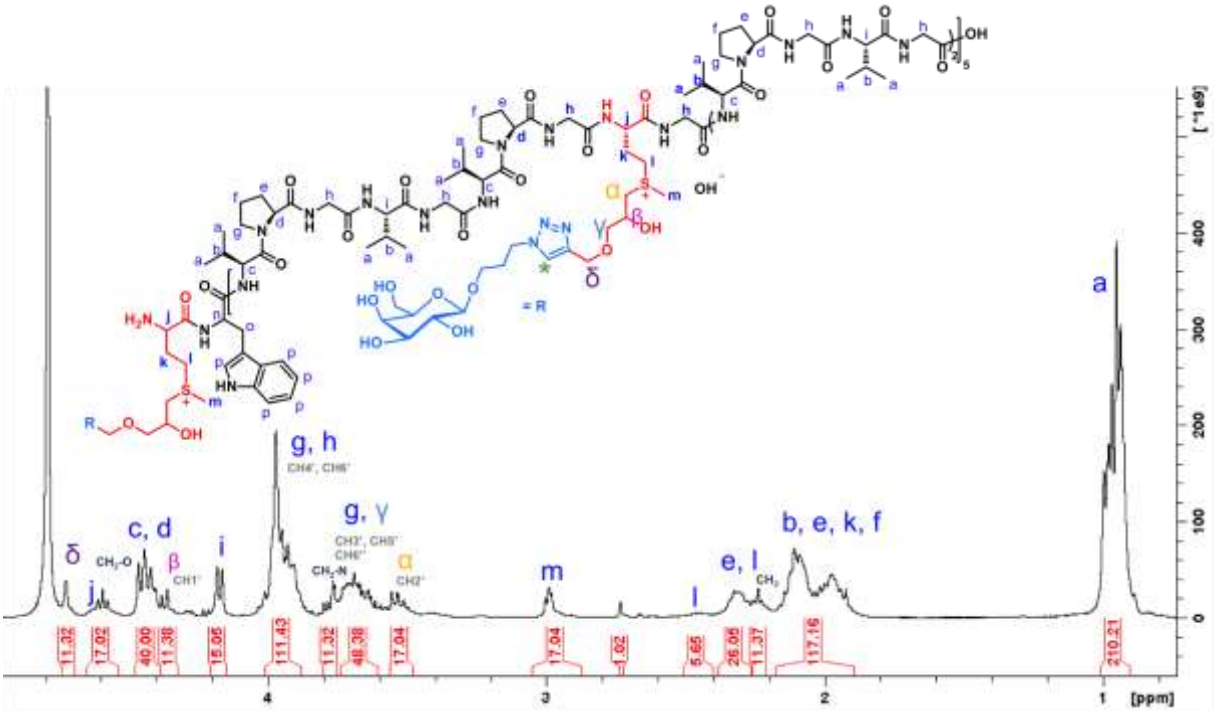

Figure S23. ^{1}H NMR spectrum of compound **<u>1b</u>** (zoom) in D_2O.

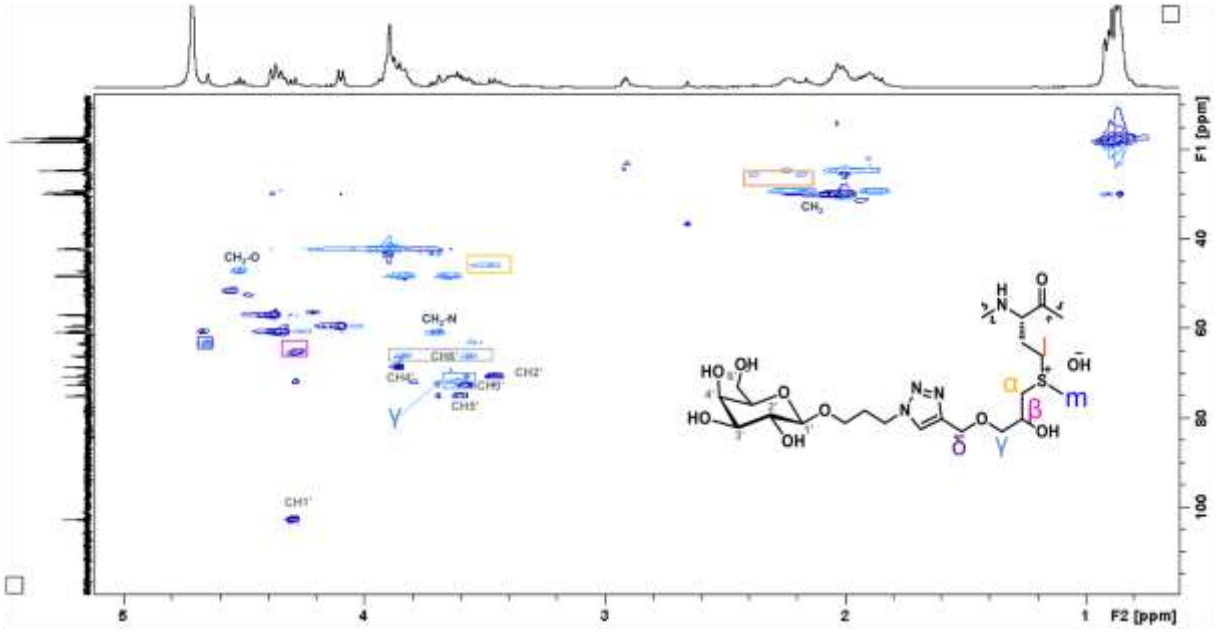

Figure S24. 2D NMR spectrum of compound **<u>1b</u>** in D_2O, HSQC.

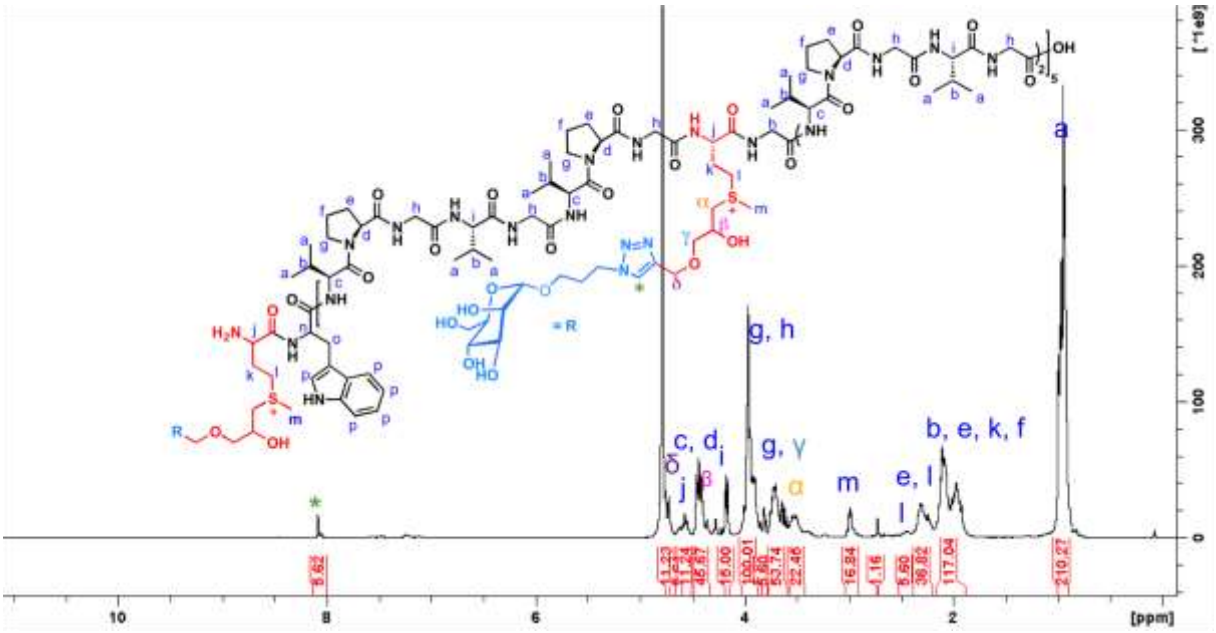

Figure S25. ^{1}H NMR spectrum of compound **<u>1c</u>** in D_2O.

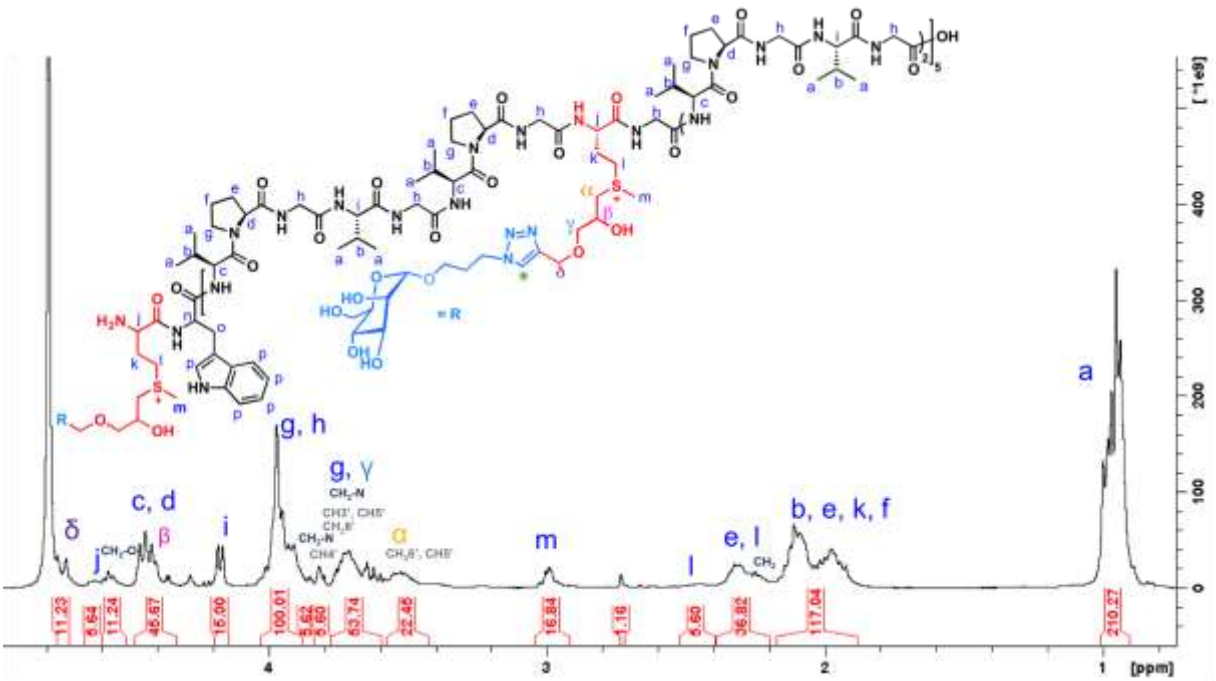

Figure S26. ^{1}H NMR spectrum of compound **1c** (zoom) in D_2O.

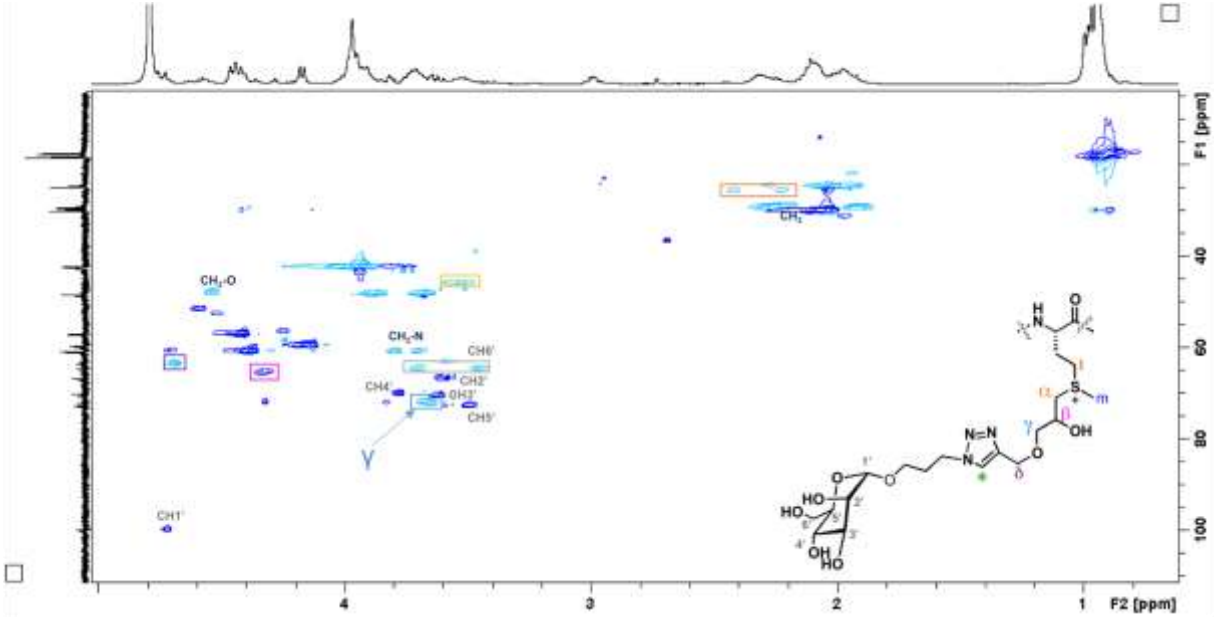

Figure S27. 2D NMR spectrum of compound **1c** in D_2O, HSQC.

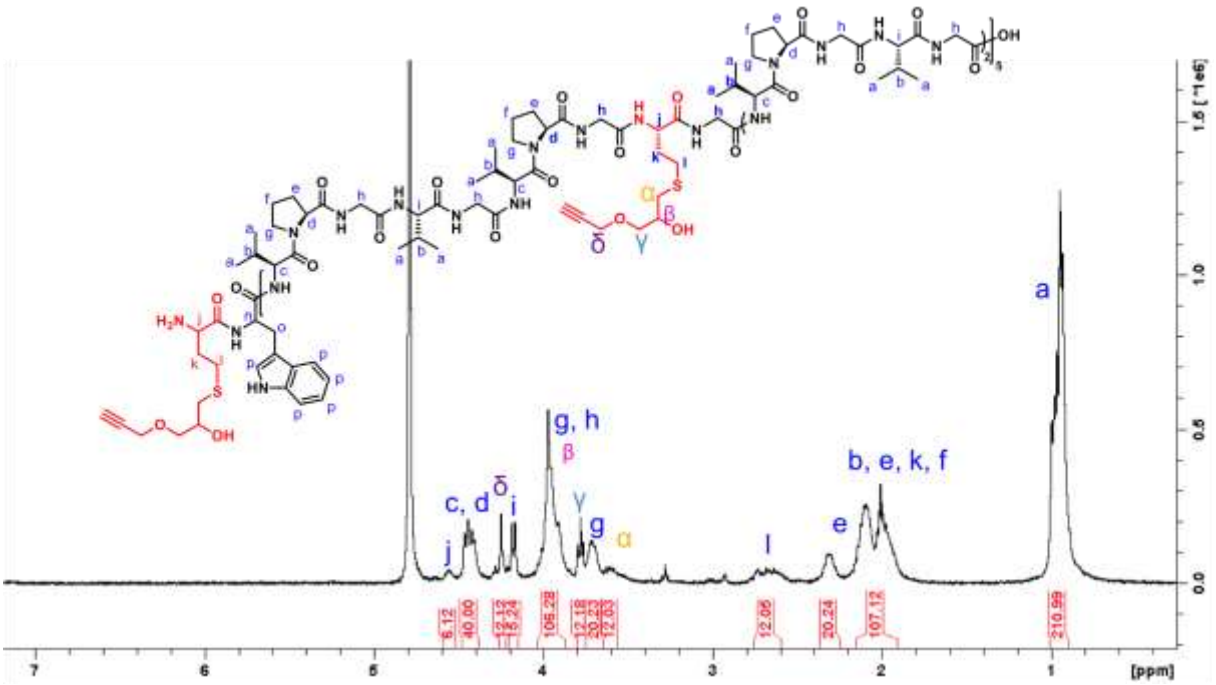

Figure S28. ^{1}H NMR spectrum of ELP[M(*Dem*Alk)$_1$V$_3$-*20*], **3**, in D_2O.

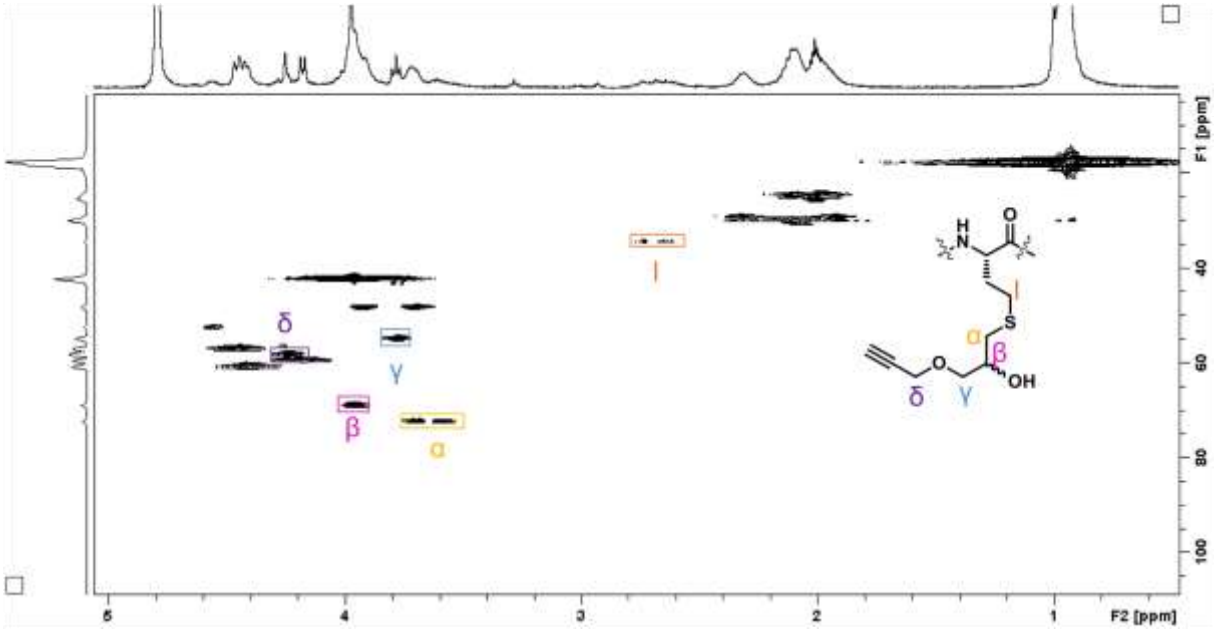

Figure S29. 2D NMR spectrum of ELP[M(*Dem*Alk)$_1$V$_3$-*20*], **3**, in D_2O, HSQC.

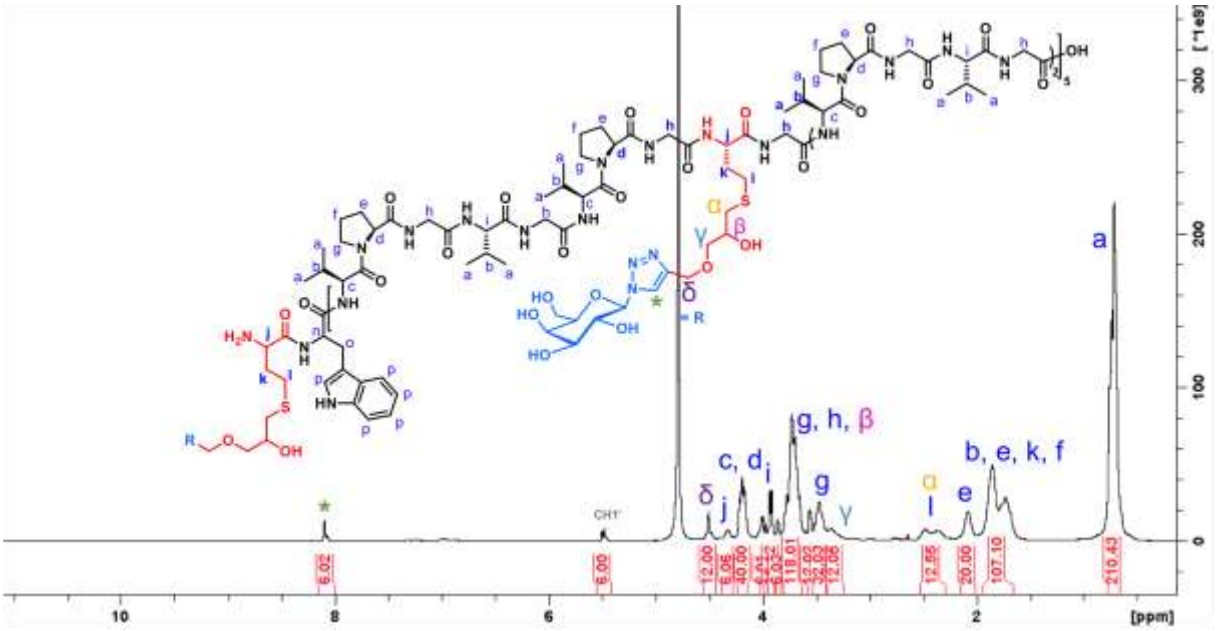

Figure S30. ^{1}H NMR spectrum of compound **3a** in D_2O.

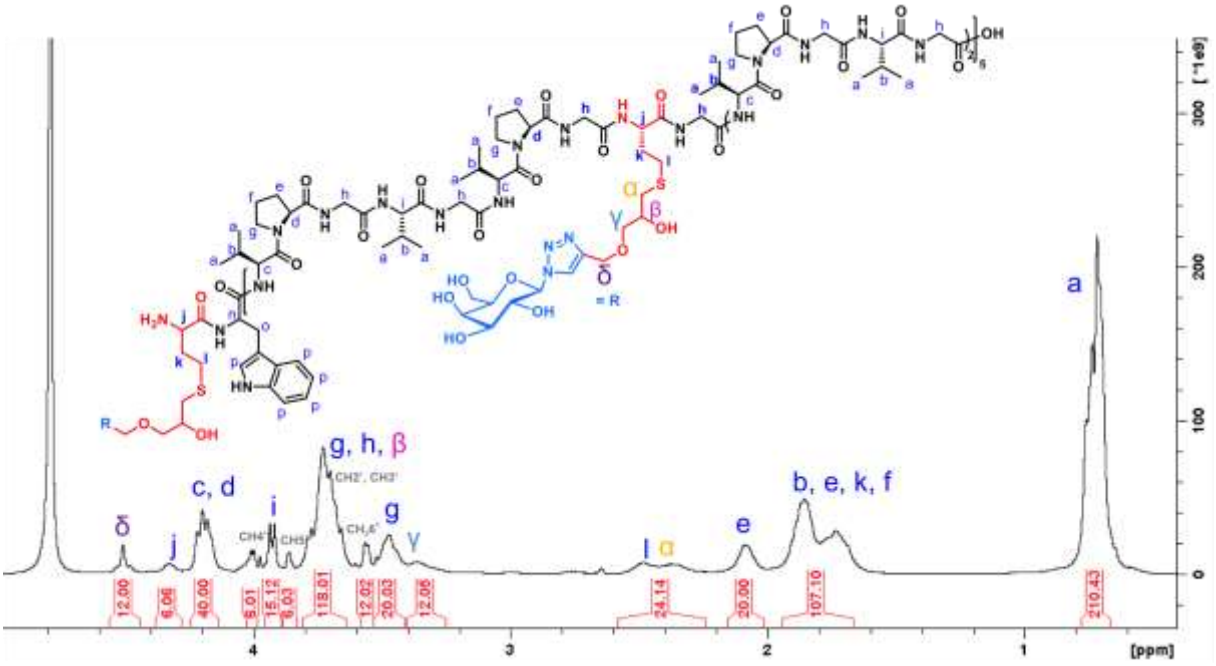

Figure S31. ^{1}H NMR spectrum of compound **3a** (zoom) in D_2O.

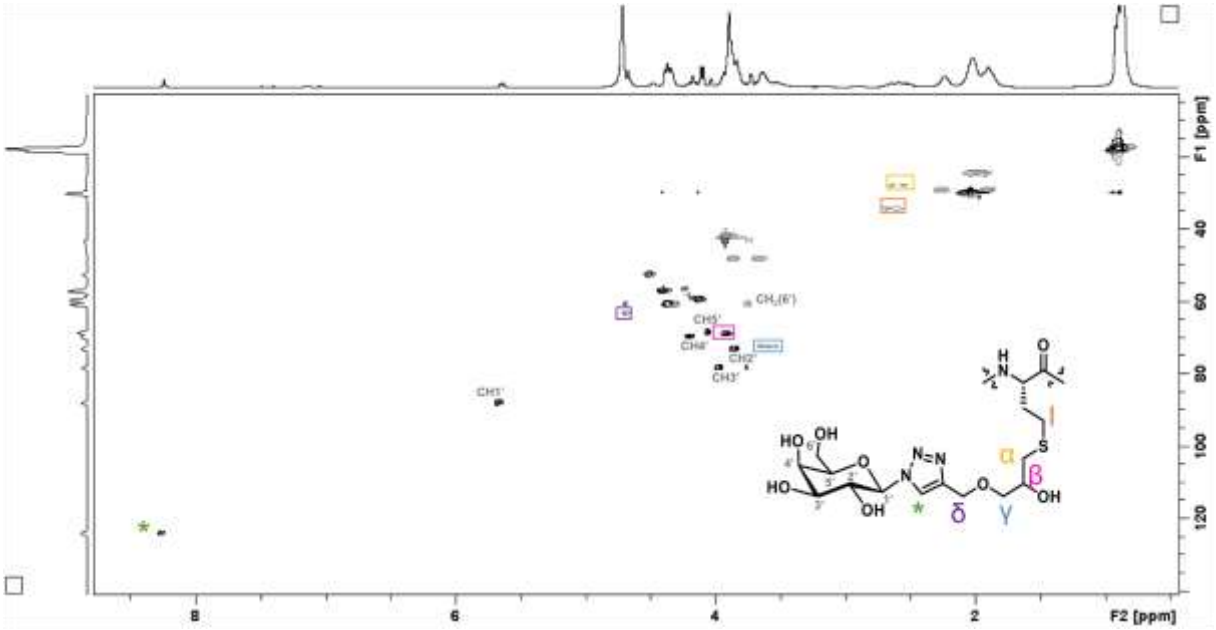

Figure S32. 2D NMR spectrum of compound **3a** in D_2O, HSQC.

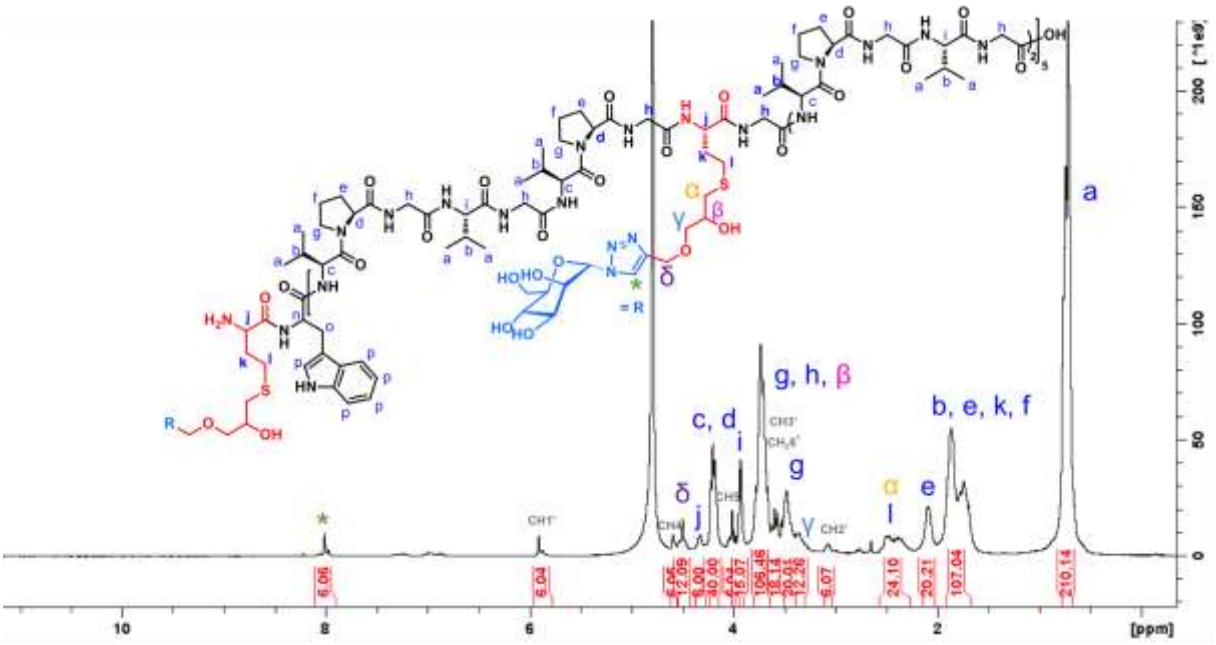

Figure S33. ^{1}H NMR spectrum of compound **3b** in D_2O.

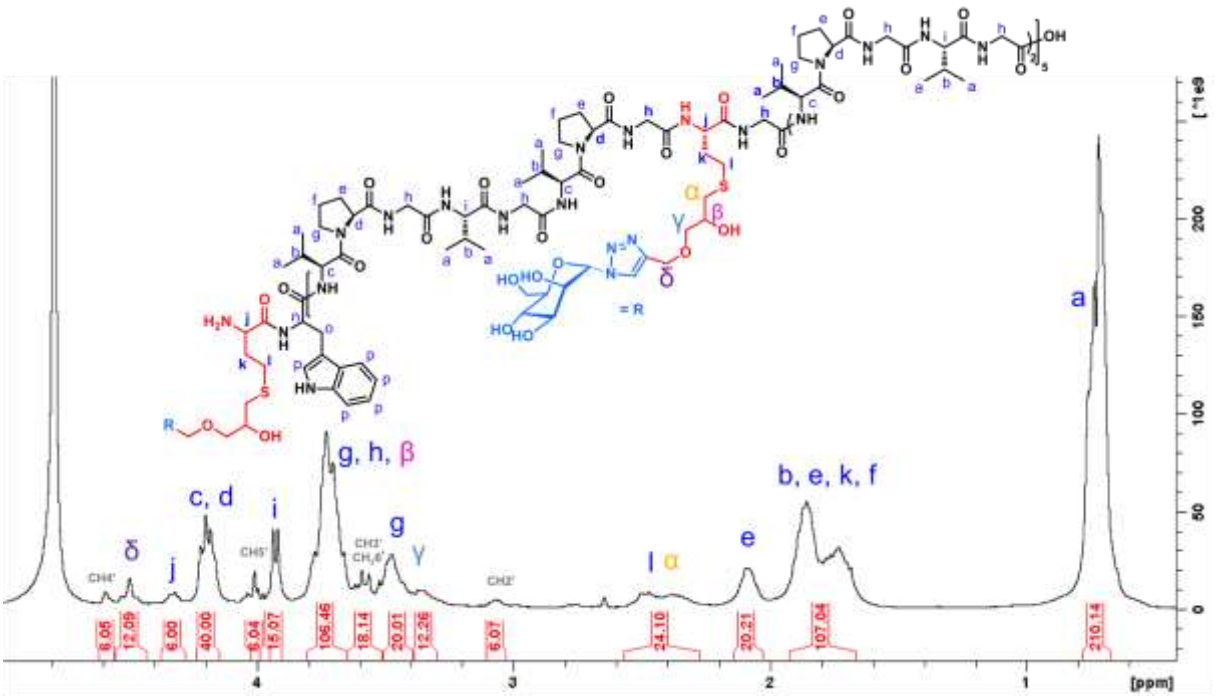

Figure S34. ^{1}H NMR spectrum of compound **3b** (zoom) in D_2O.

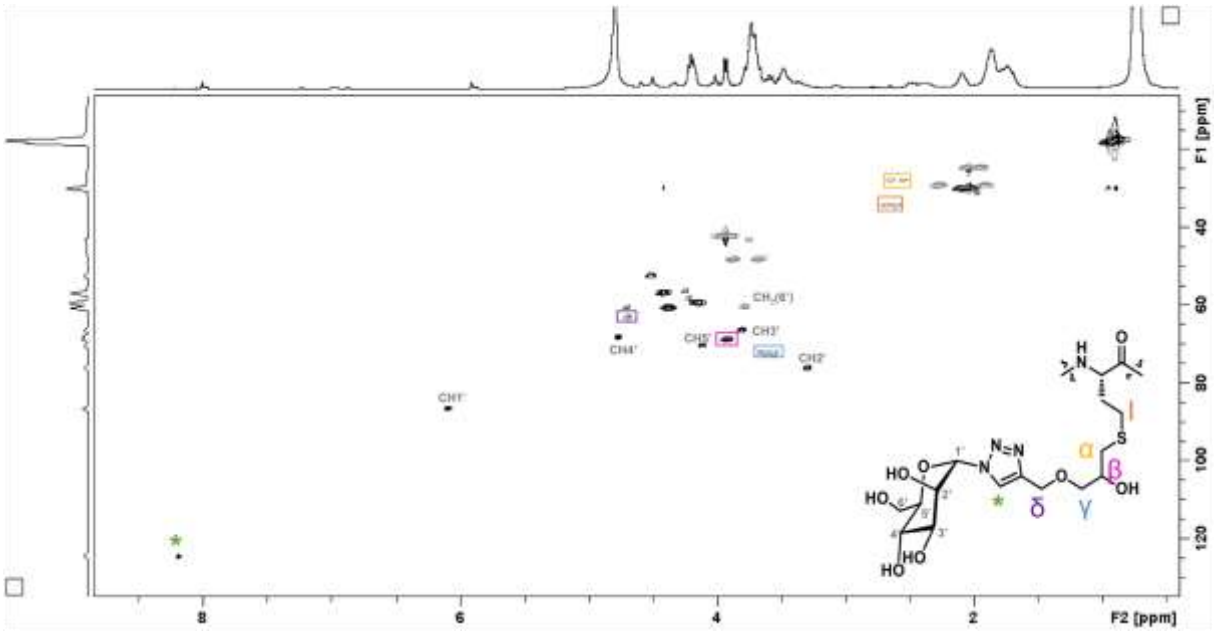

Figure S35. 2D NMR spectrum of compound **3b** in D_2O, HSQC.

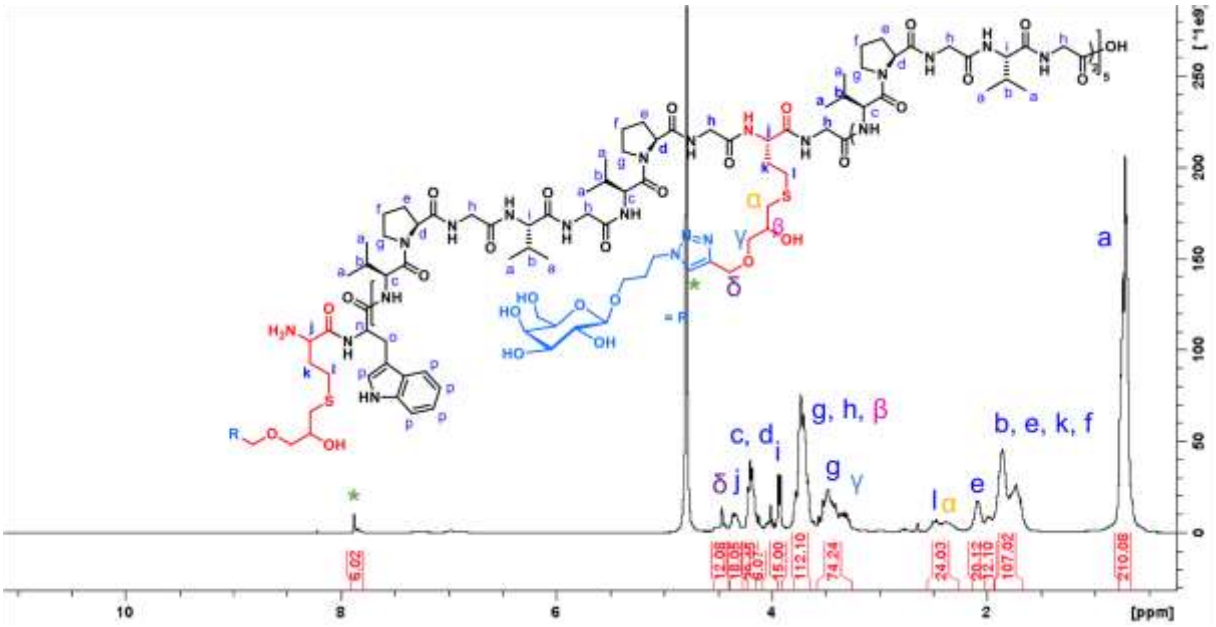

Figure S36. ^{1}H NMR spectrum of compound **3c** in D_2O.

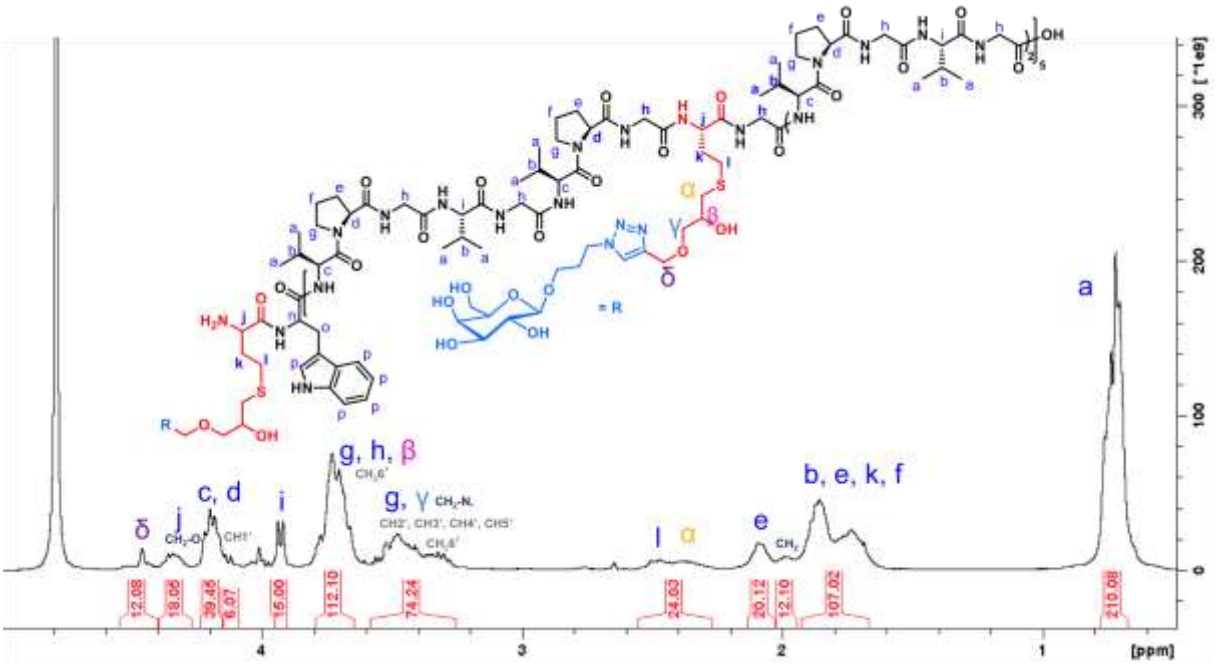

Figure S37. ^{1}H NMR spectrum of compound **3c** (zoom) in D_2O.

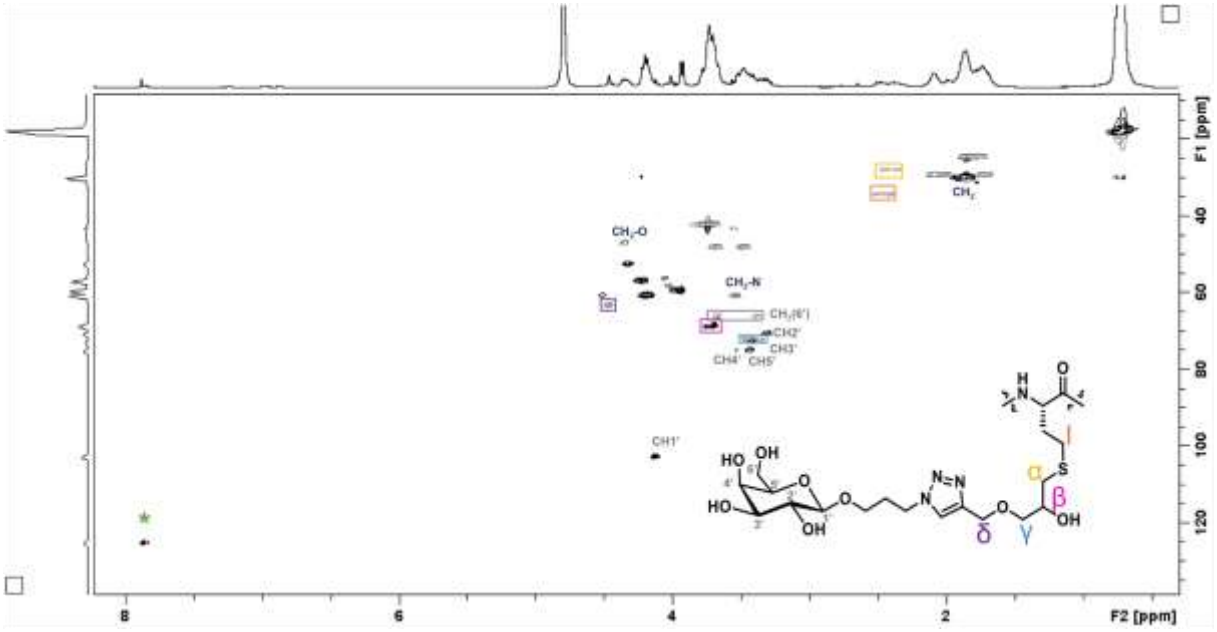

Figure S38. 2D NMR spectrum of compound **3c** in D_2O, HSQC.

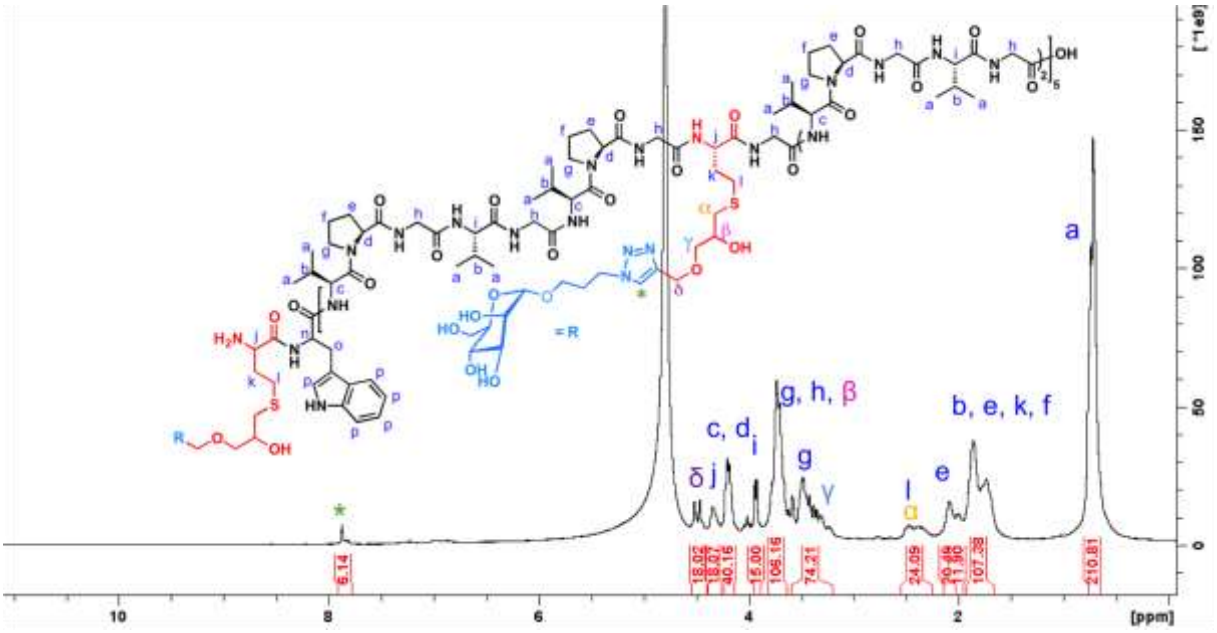

Figure S39. ^{1}H NMR spectrum of compound **3d** in D_2O.

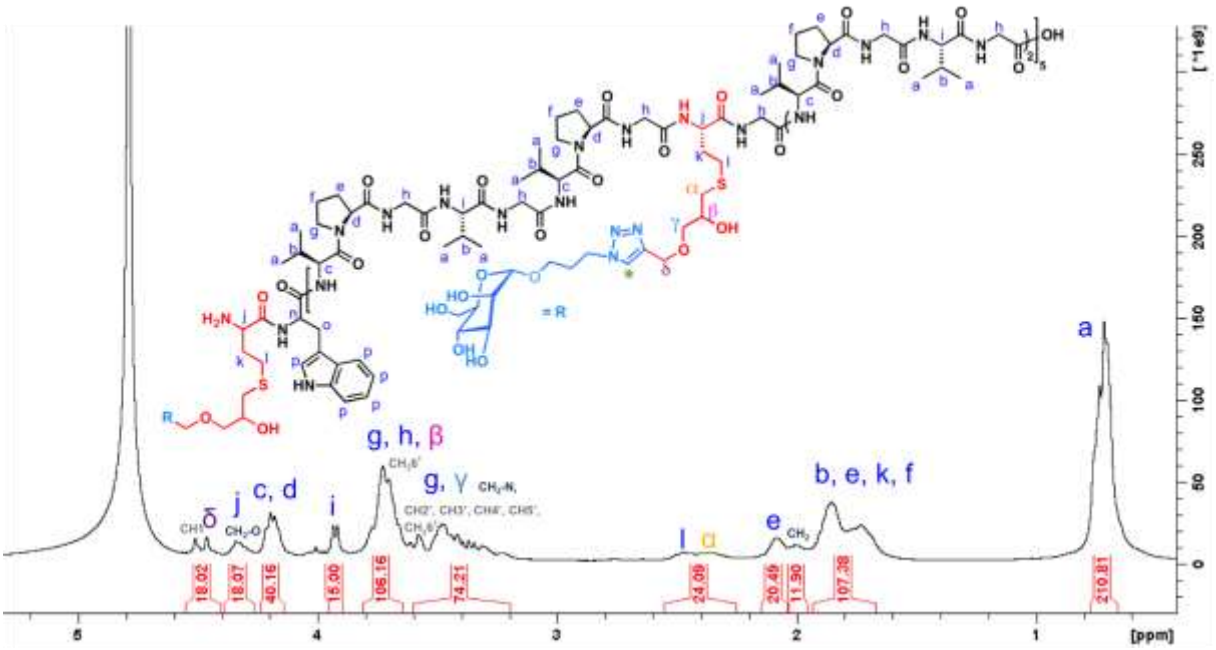

Figure S40. ^{1}H NMR spectrum of compound **3d** (zoom) in D_2O.

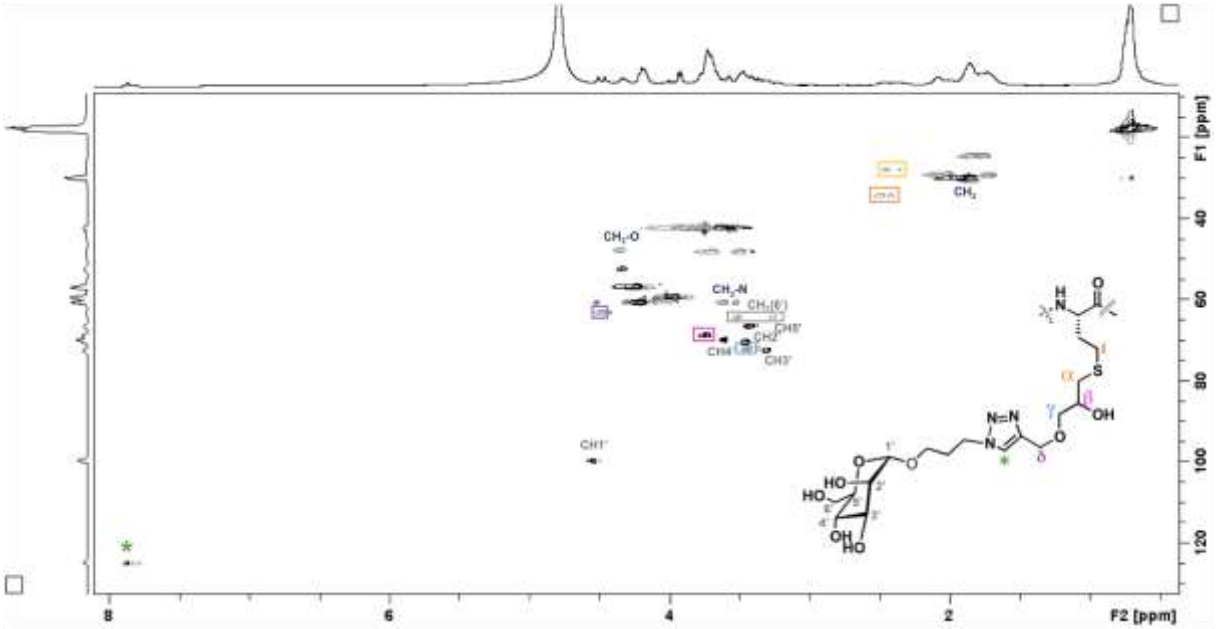

Figure S41. 2D NMR spectrum of compound **3d** in D_2O, HSQC.

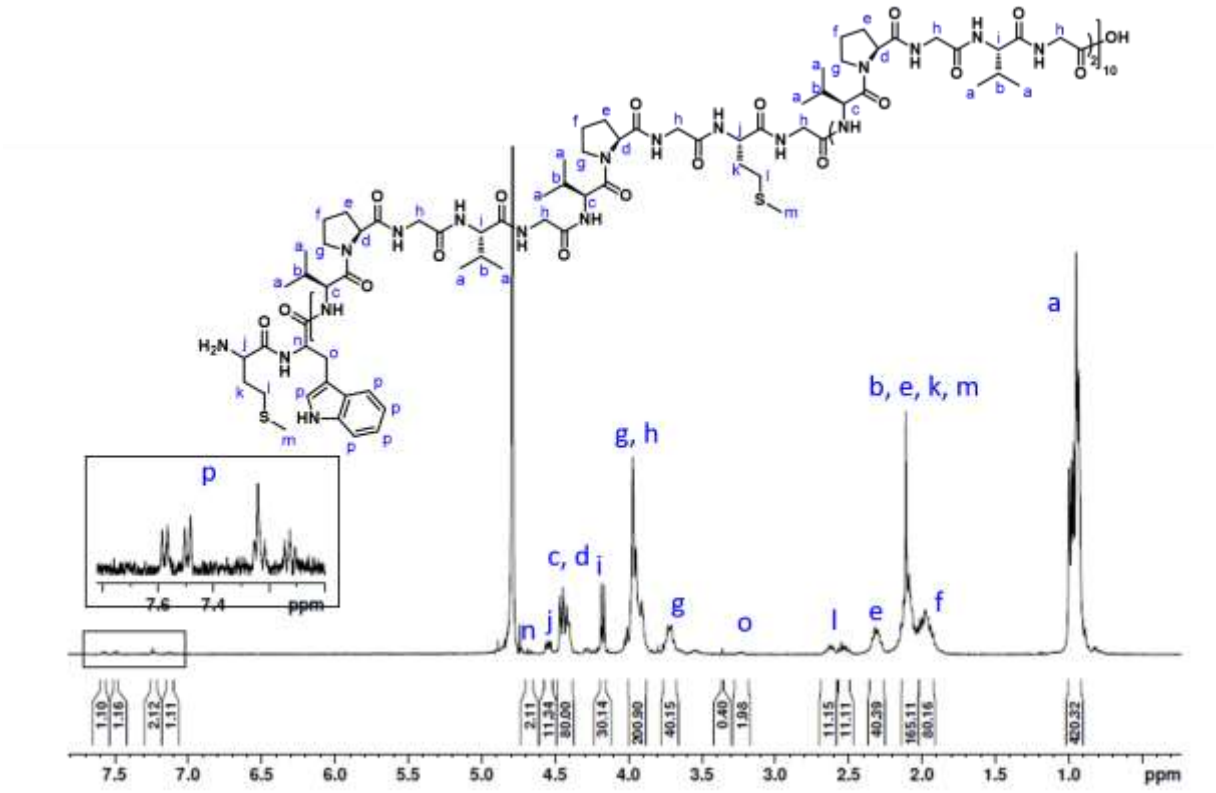

Figure S42. ^{1}H NMR spectrum of ELP[M_1V_3-40] in D_2O.

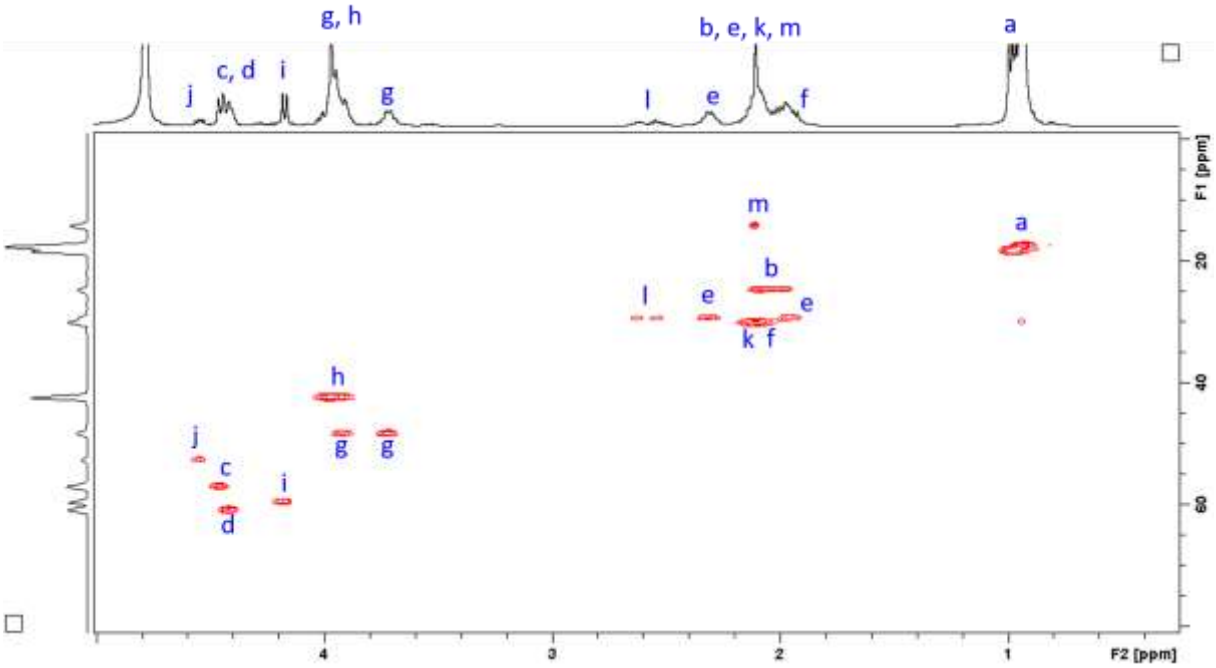

Figure S43. 2D NMR spectrum of ELP[M_1V_3-40] in D_2O, HSQC.

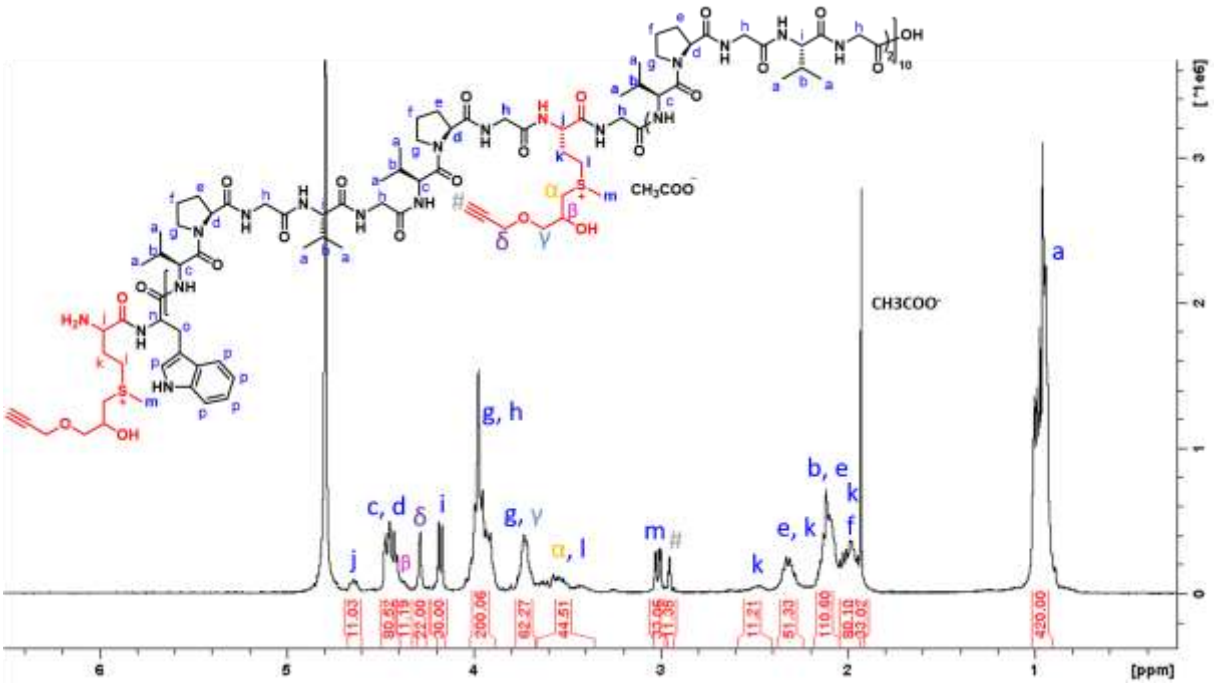

Figure S44. ^{1}H NMR spectrum of ELP[M(Alk)$_1$V$_3$-*40*], **2**, in D_2O.

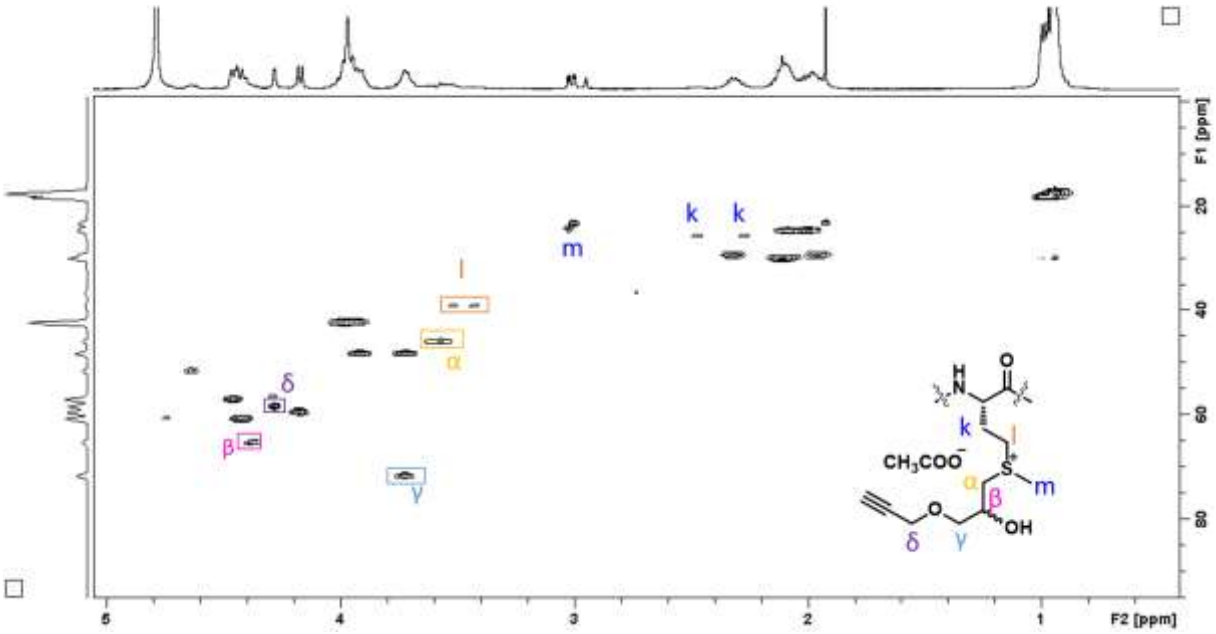

Figure S45. 2D NMR spectrum of ELP[M(Alk)$_1$V$_3$-*40*], **2**, in D_2O, HSQC.

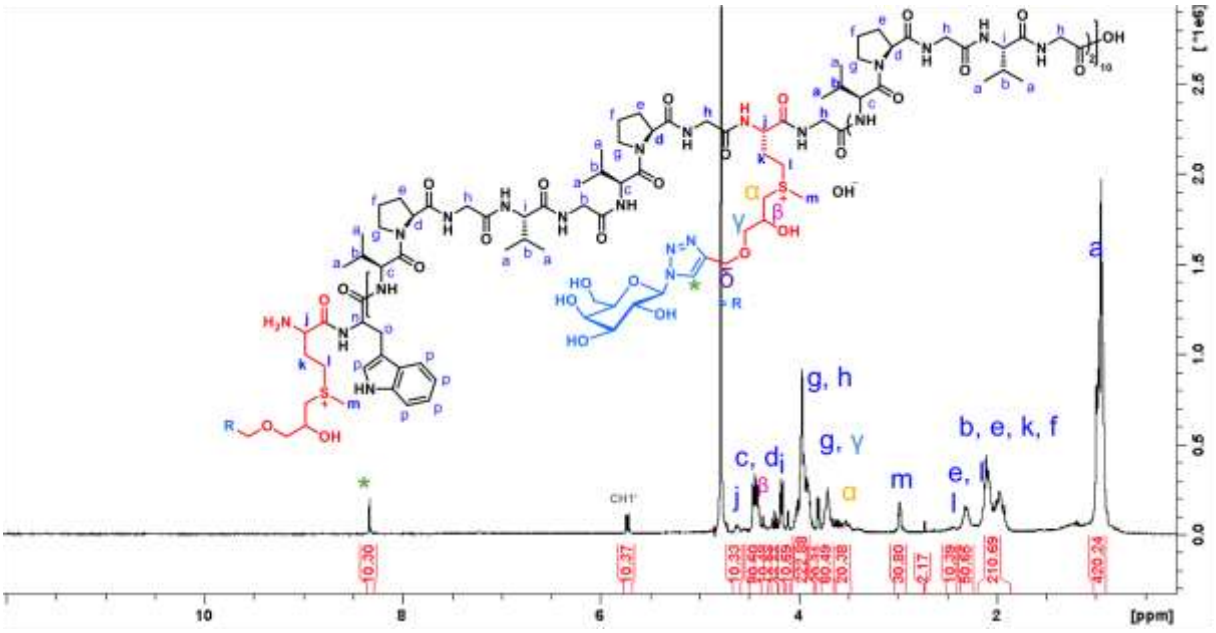

Figure S46. ^{1}H NMR spectrum of compound **2a** in D_2O.

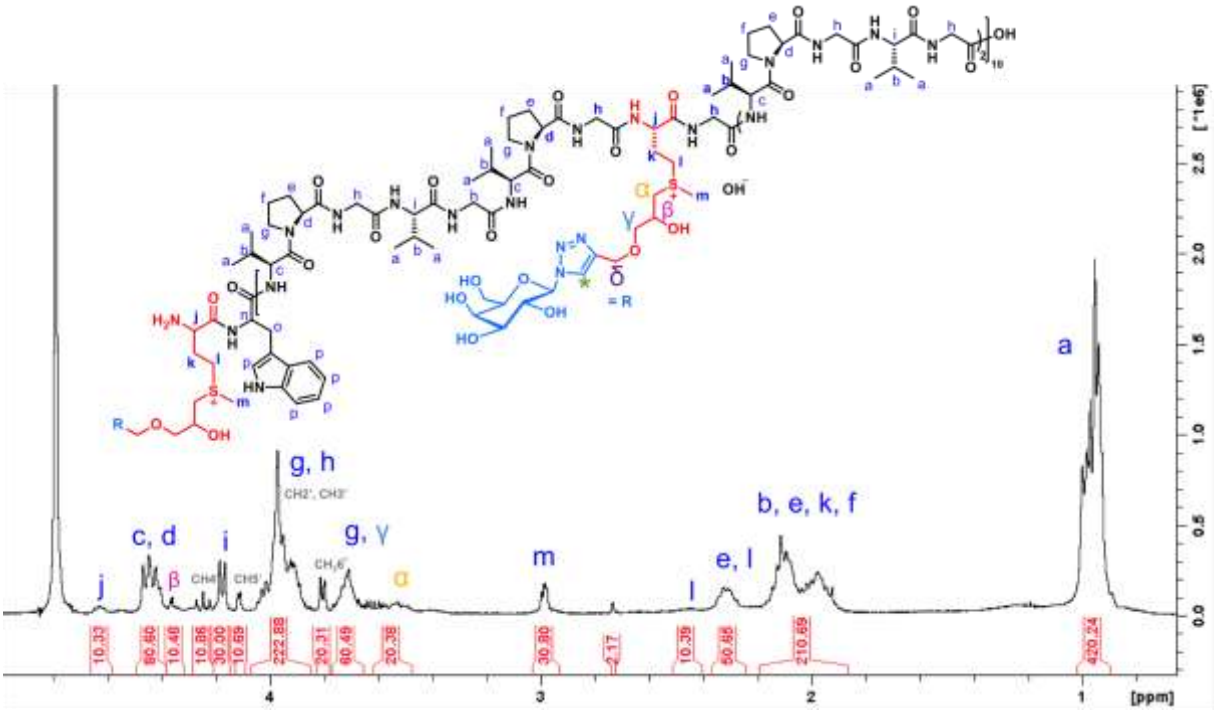

Figure S47. ^{1}H NMR spectrum of compound **2a** (zoom) in D_2O.

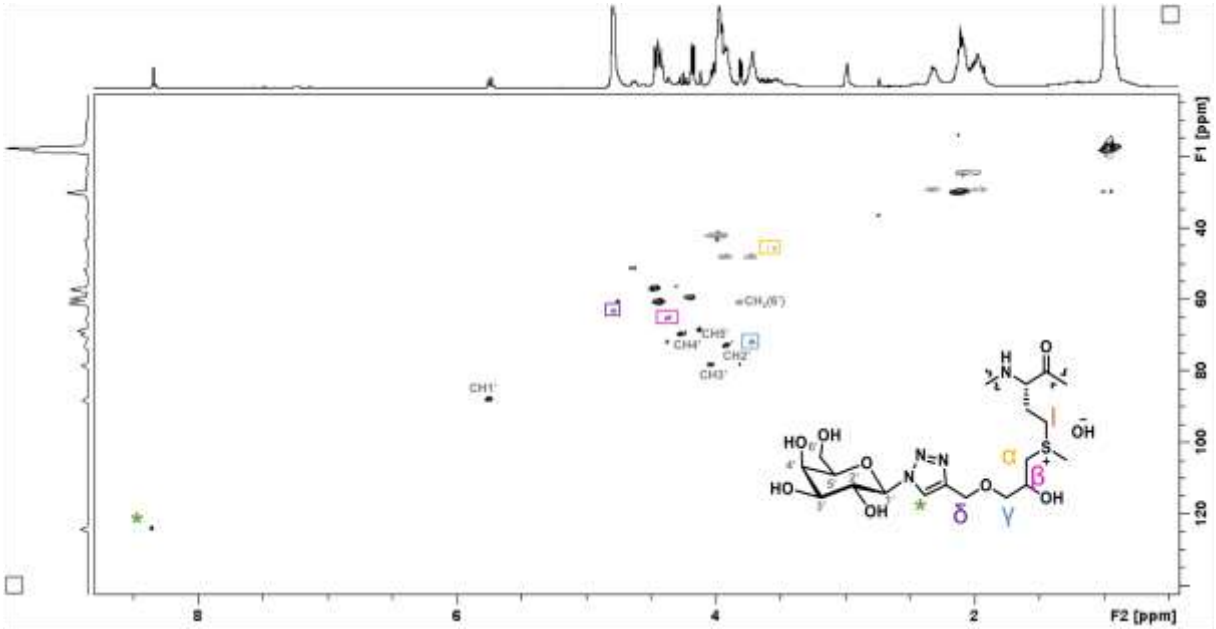

Figure S48. 2D NMR spectrum of compound **2a** in D_2O, HSQC.

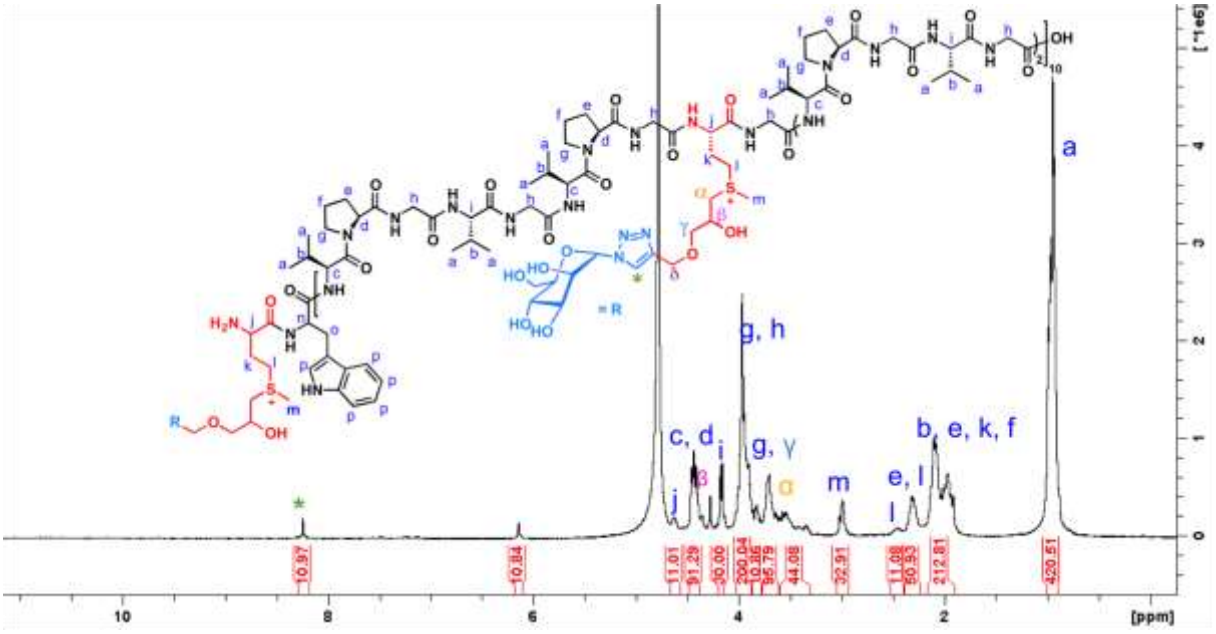

Figure S49. ^1H NMR spectrum of compound **2b** in D_2O.

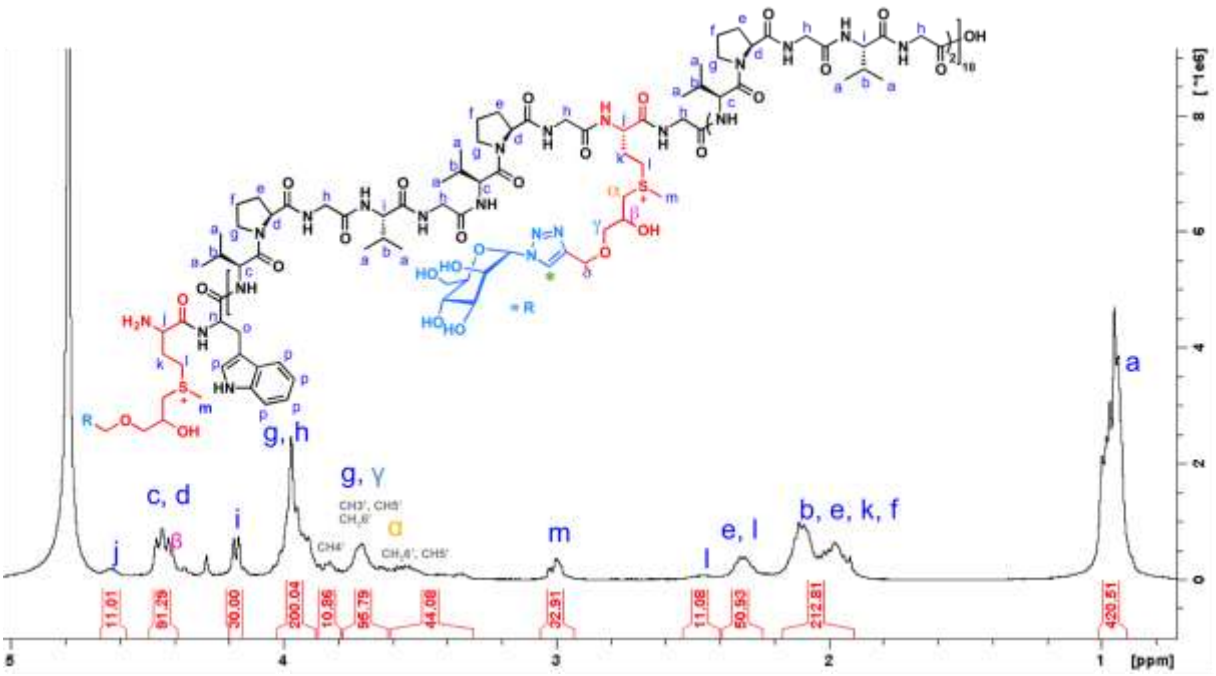

Figure S50. ^{1}H NMR spectrum of compound **2b** (zoom) in D_2O.

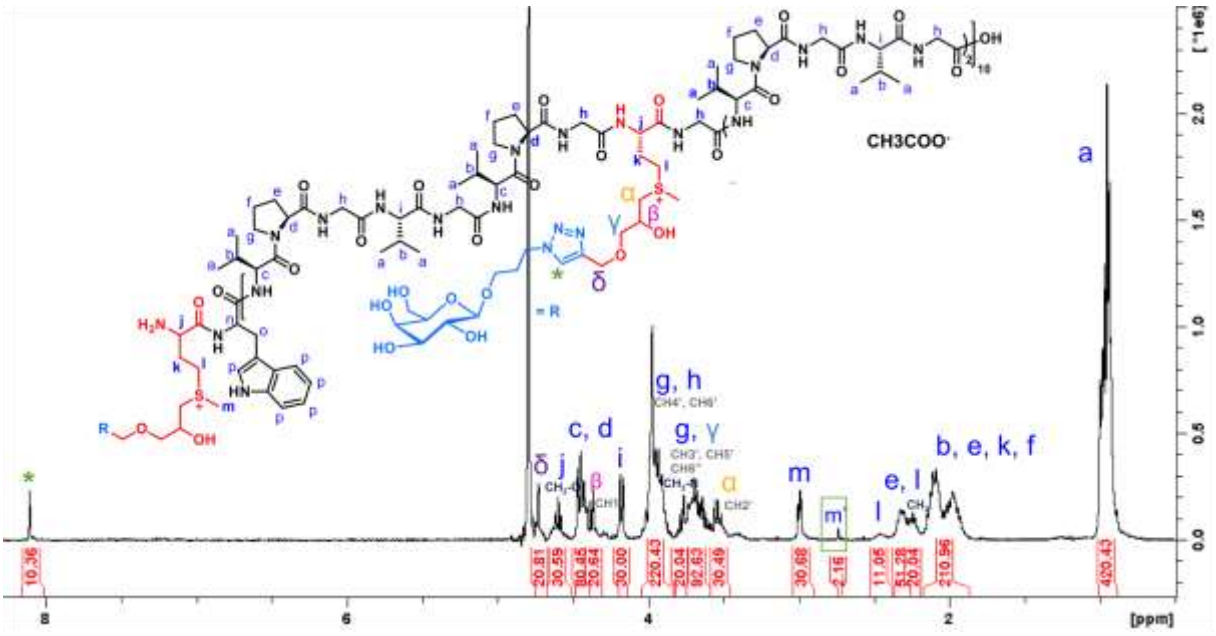

Figure S51. ^{1}H NMR spectrum of compound **2c** in D_2O.

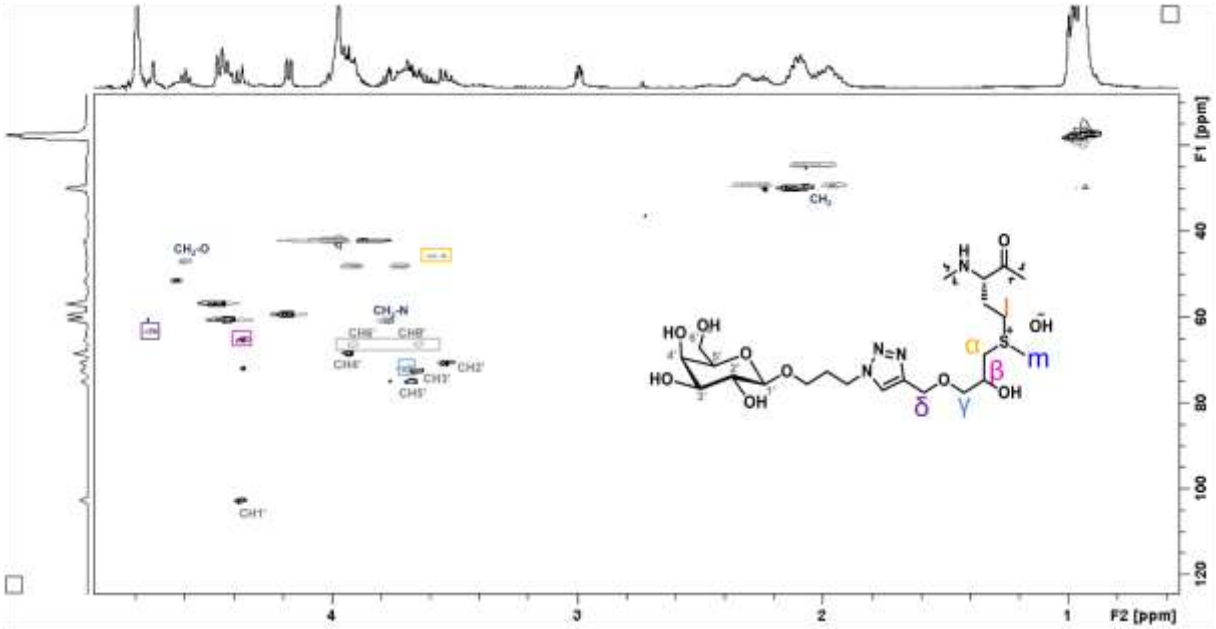

Figure S52. 2D NMR spectrum of compound **<u>2c</u>** in D_2O, HSQC.

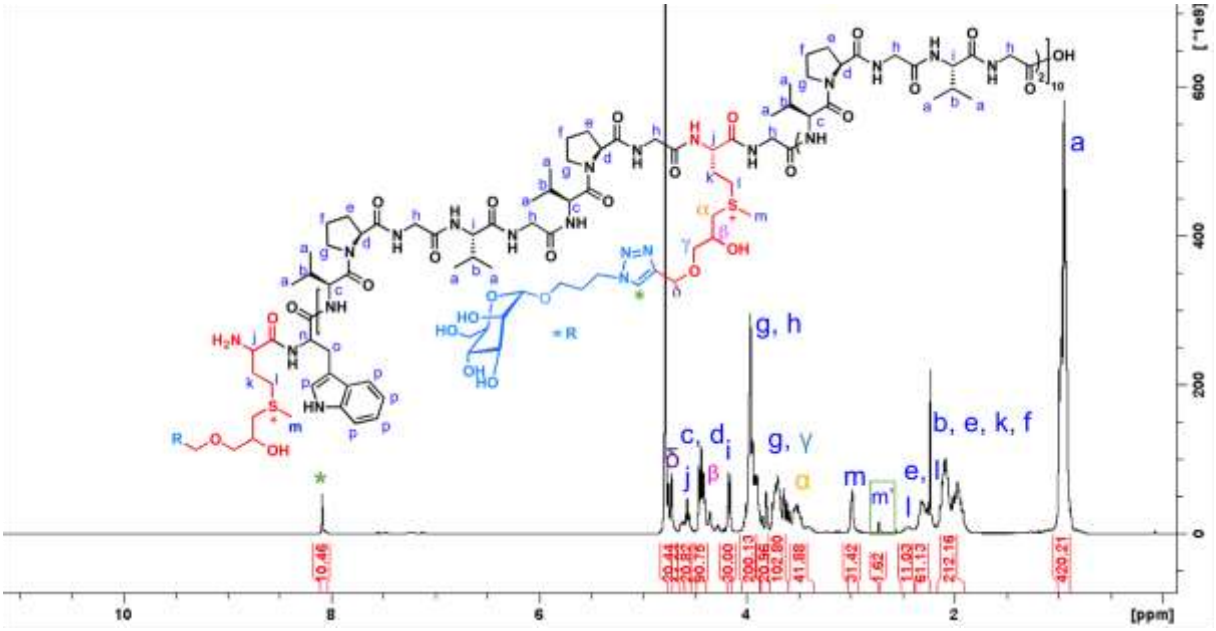

Figure S53. ^1H NMR spectrum of compound **<u>2d</u>** in D_2O.

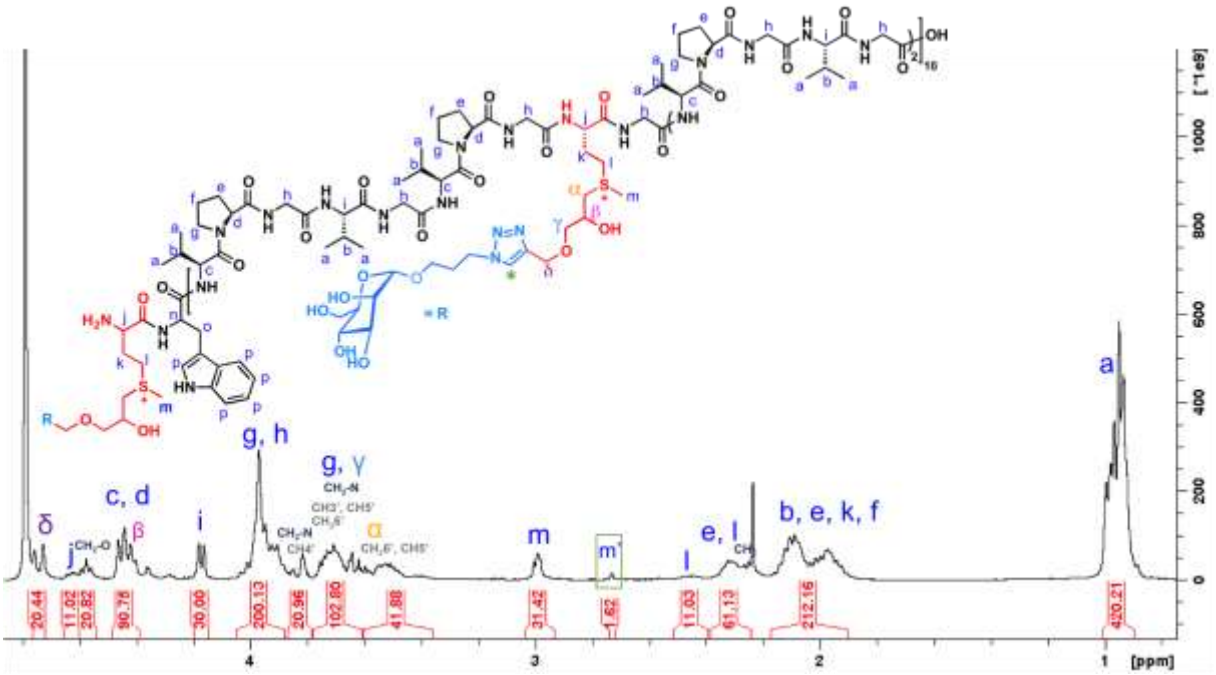

Figure S54. ^{1}H NMR spectrum of compound **2d** (zoom) in D_2O.

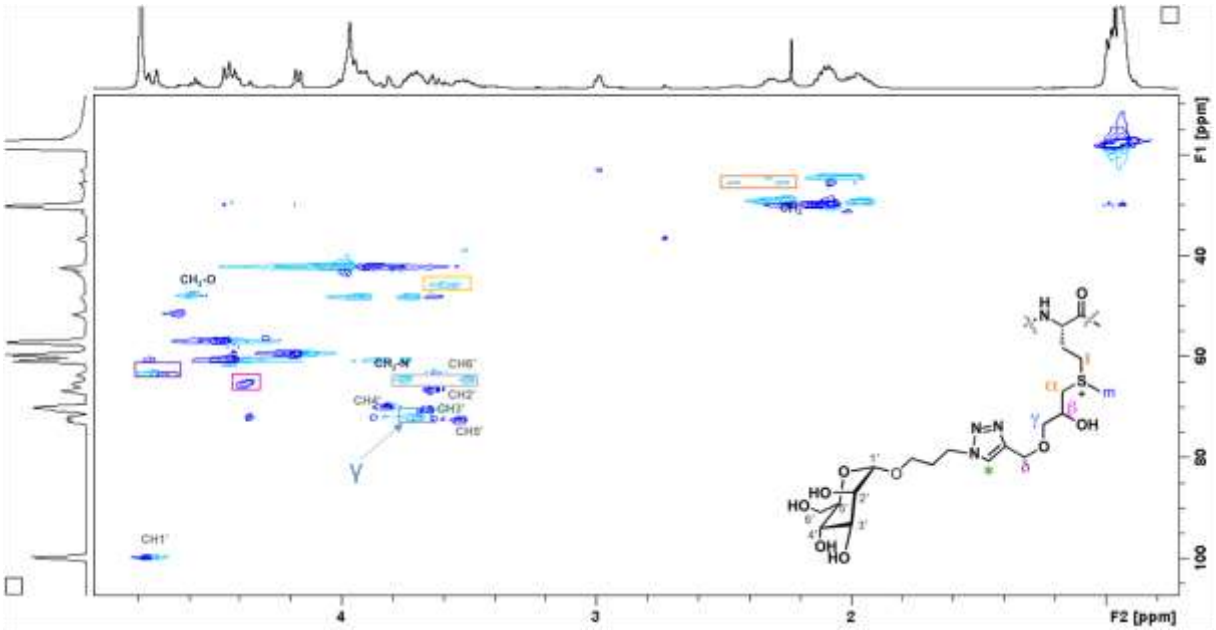

Figure S55. 2D NMR spectrum of compound **2d** in D_2O, HSQC.

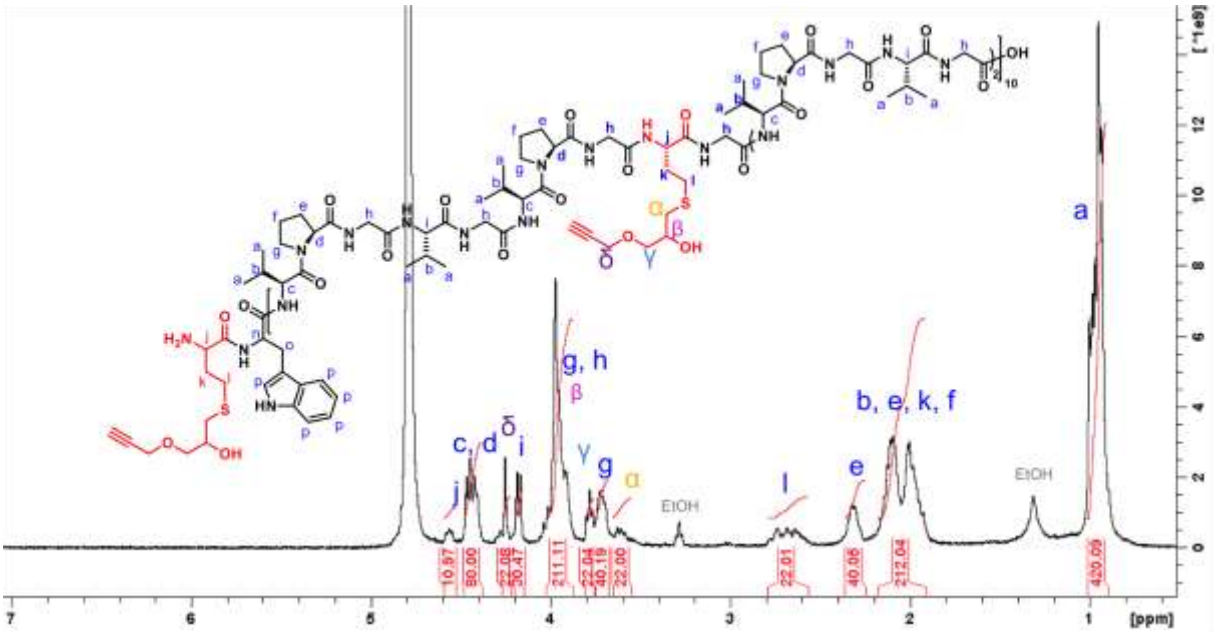

Figure S56. ^{1}H NMR spectrum of ELP[M(*Dem*Alk)$_1$V$_3$-*20*], **4**, in D_2O.

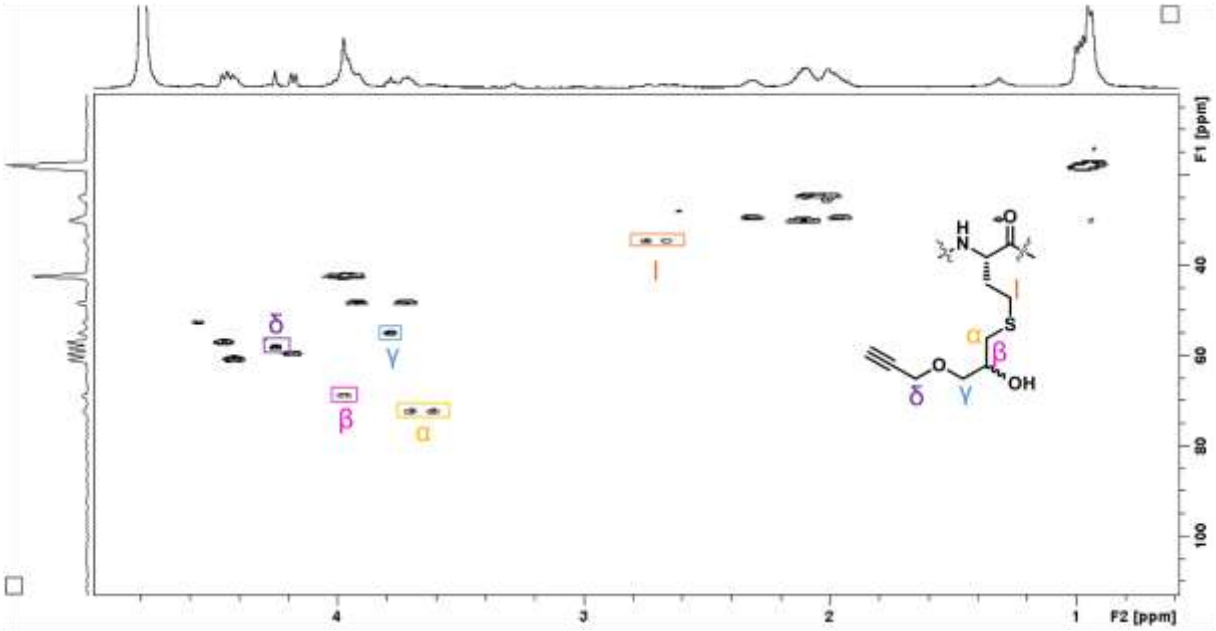

Figure S57. 2D NMR spectrum of ELP[M(*Dem*Alk)$_1$V$_3$-*20*], **4**, in D_2O, HSQC.

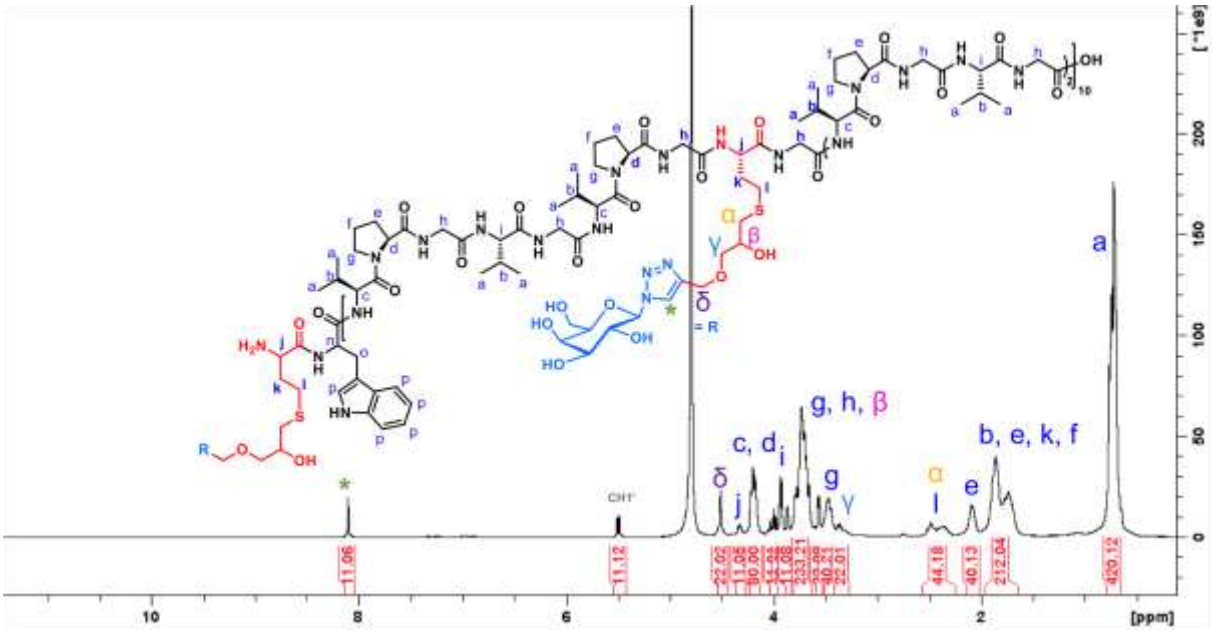

Figure S58. ^{1}H NMR spectrum of compound **4a** in D_2O.

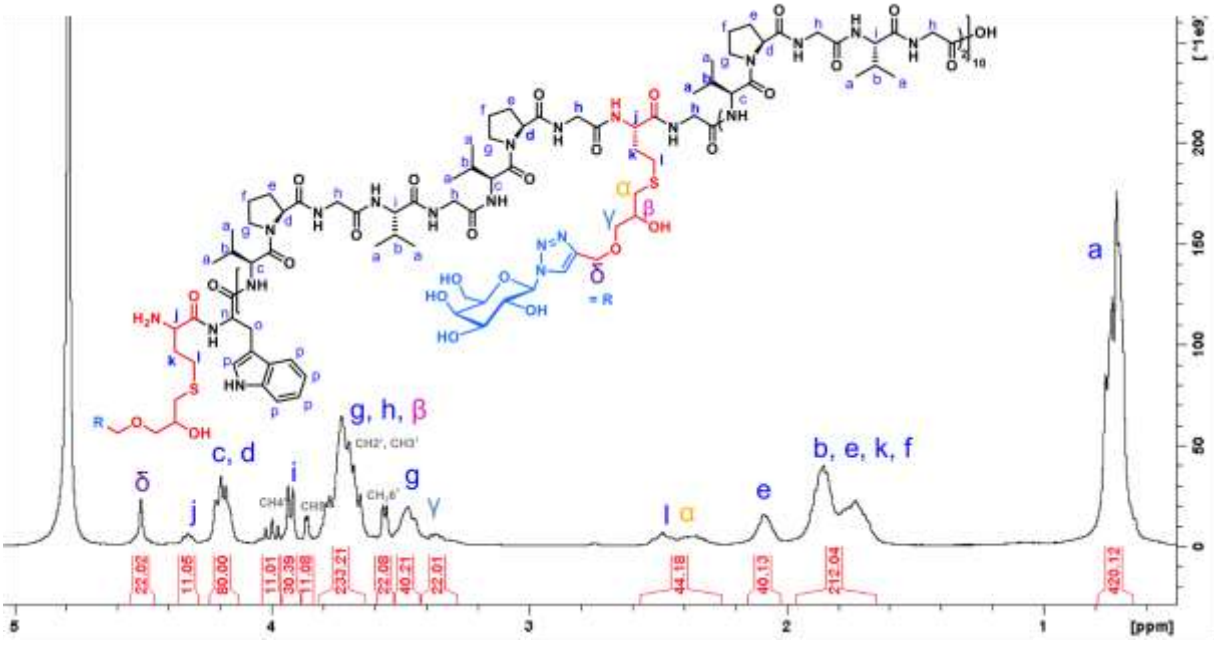

Figure S59. ^{1}H NMR spectrum of compound **4a** (zoom) in D_2O.

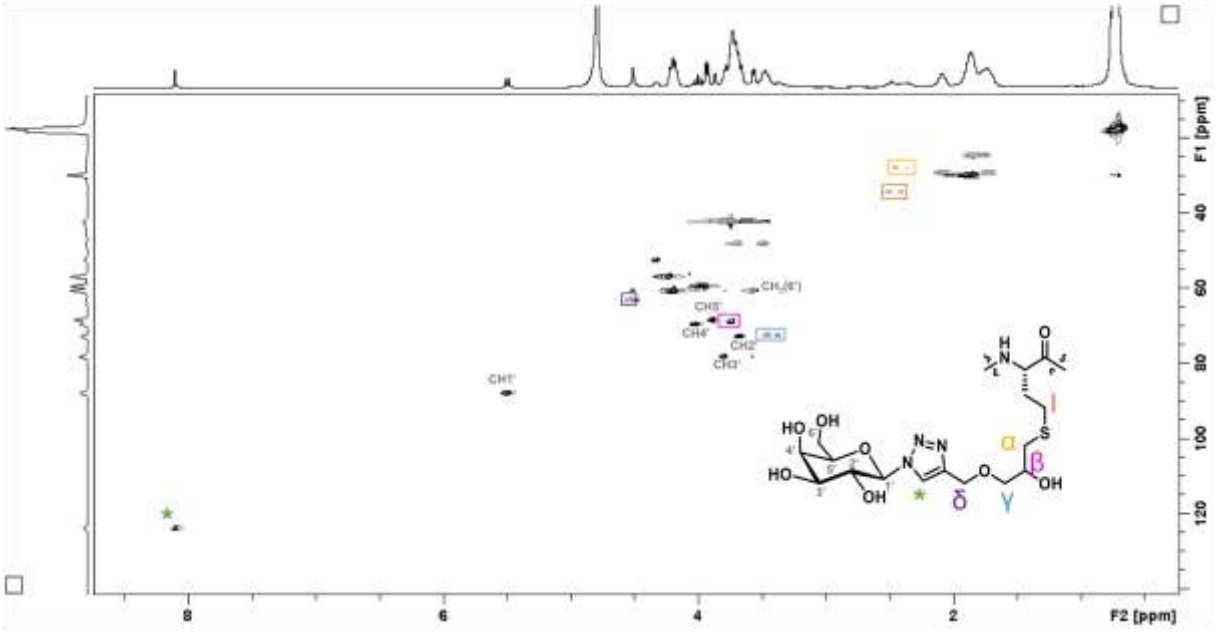

Figure S60. 2D NMR spectrum of compound **<u>4a</u>** in D_2O, HSQC.

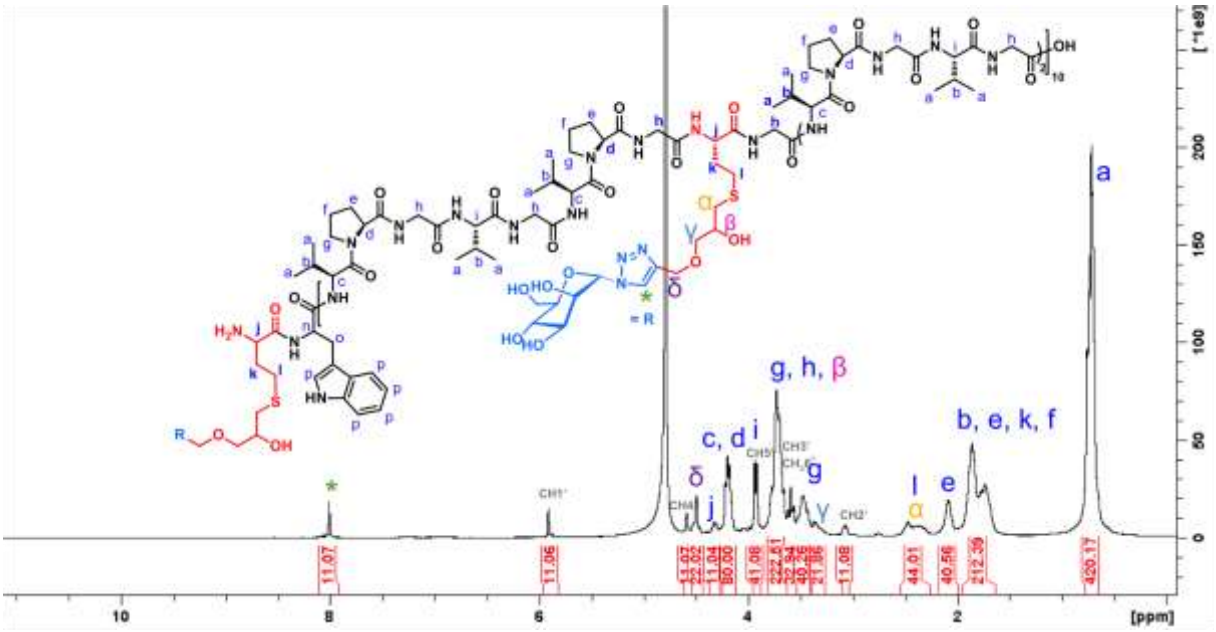

Figure S61. ^1H NMR spectrum of compound **<u>4b</u>** in D_2O.

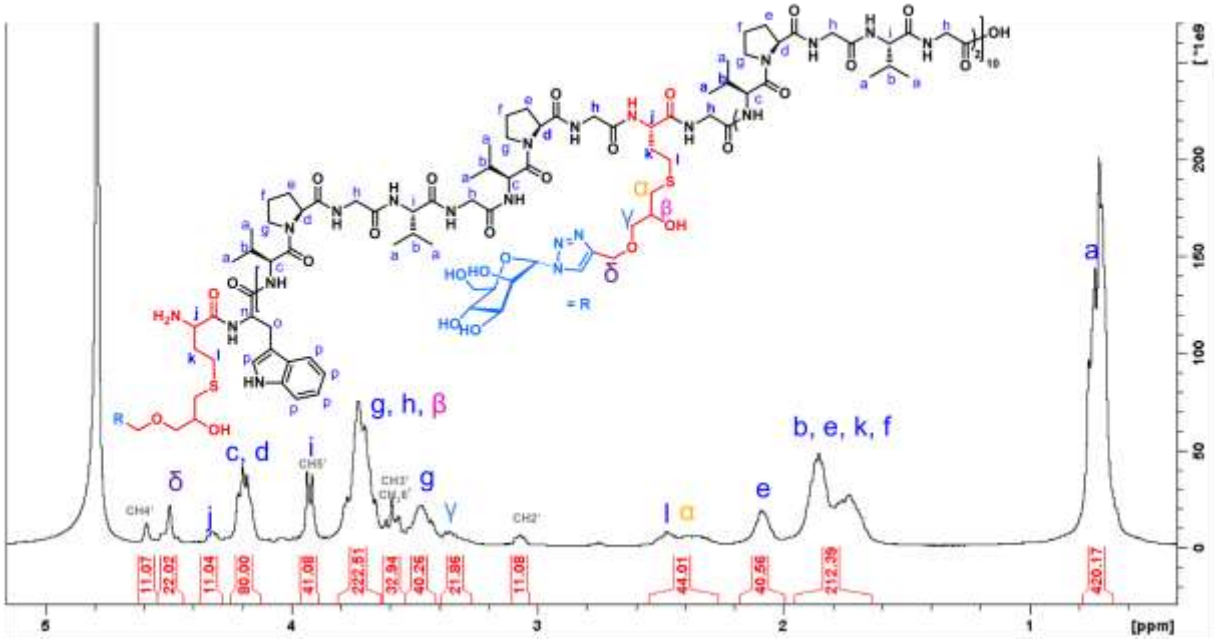

Figure S62. ^{1}H NMR spectrum of compound **4b** (zoom) in D_2O.

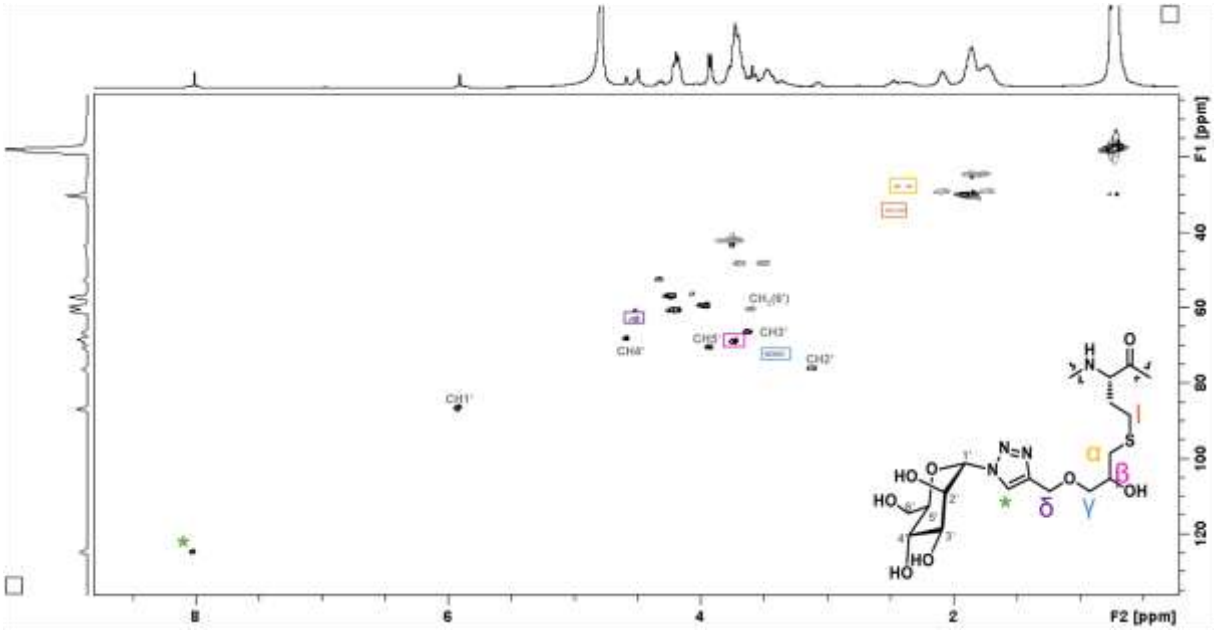

Figure S63. 2D NMR spectrum of compound **4b** in D_2O, HSQC.

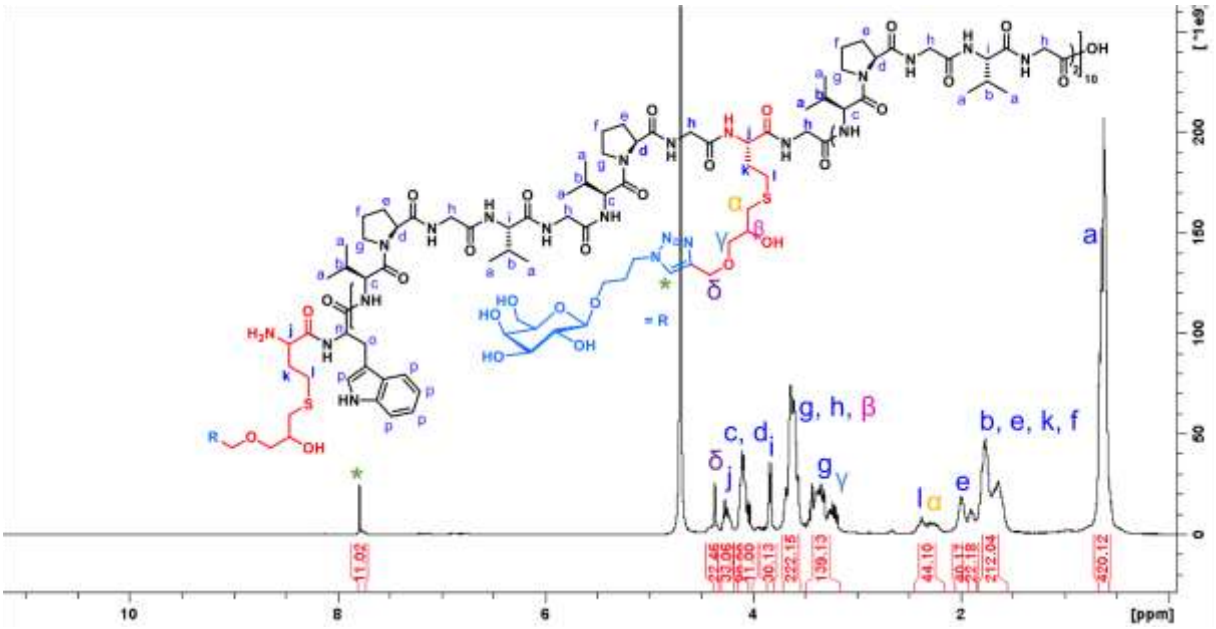

Figure S64. ^{1}H NMR spectrum of compound **<u>4c</u>** in D_2O.

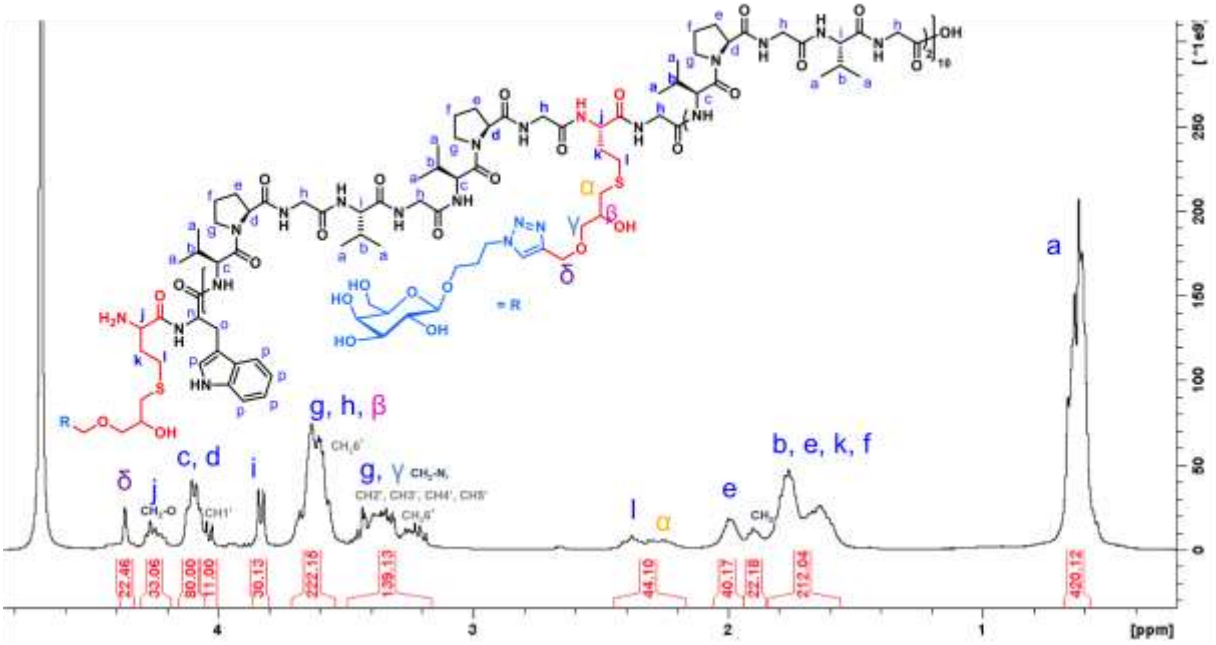

Figure S65. ^{1}H NMR spectrum of compound **<u>4c</u>** (zoom) in D_2O.

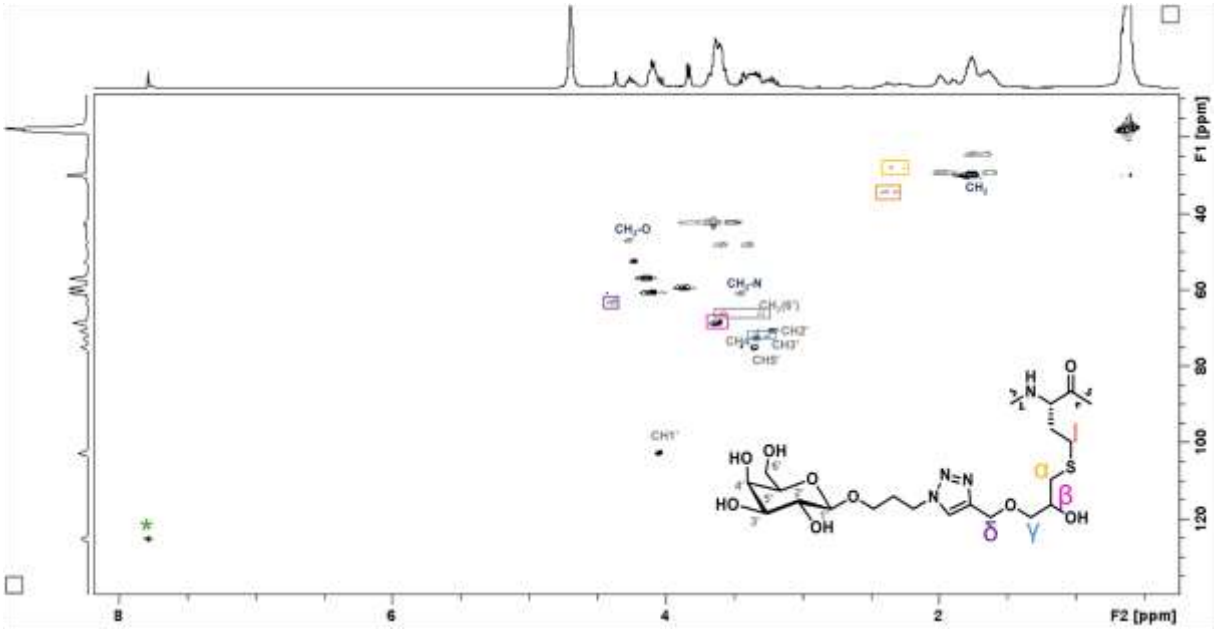

Figure S66. 2D NMR spectrum of compound **4c** in D_2O, HSQC.

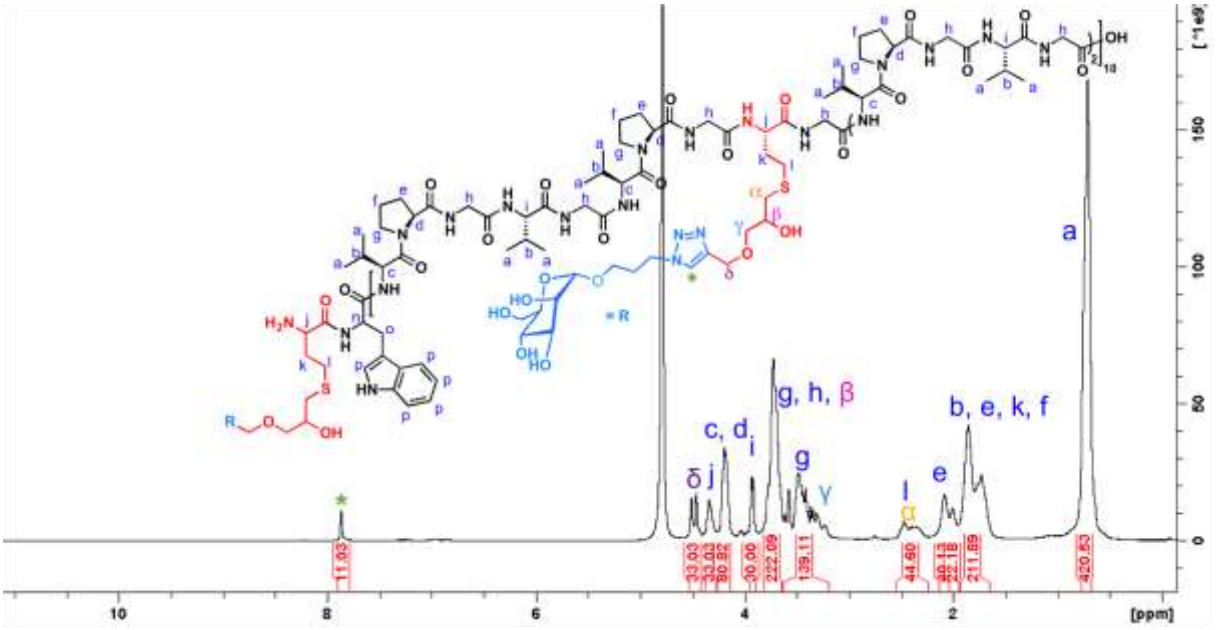

Figure S67. ^{1}H NMR spectrum of compound **4d** in D_2O.

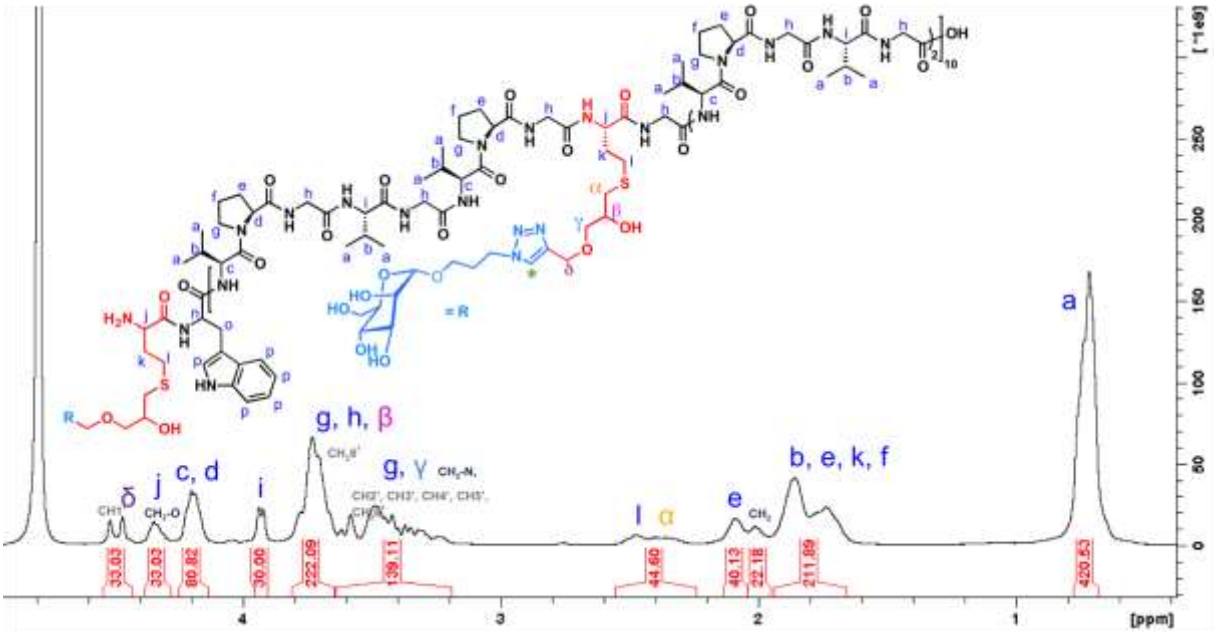

Figure S68. ^{1}H NMR spectrum of compound **4d** (zoom) in D_2O.

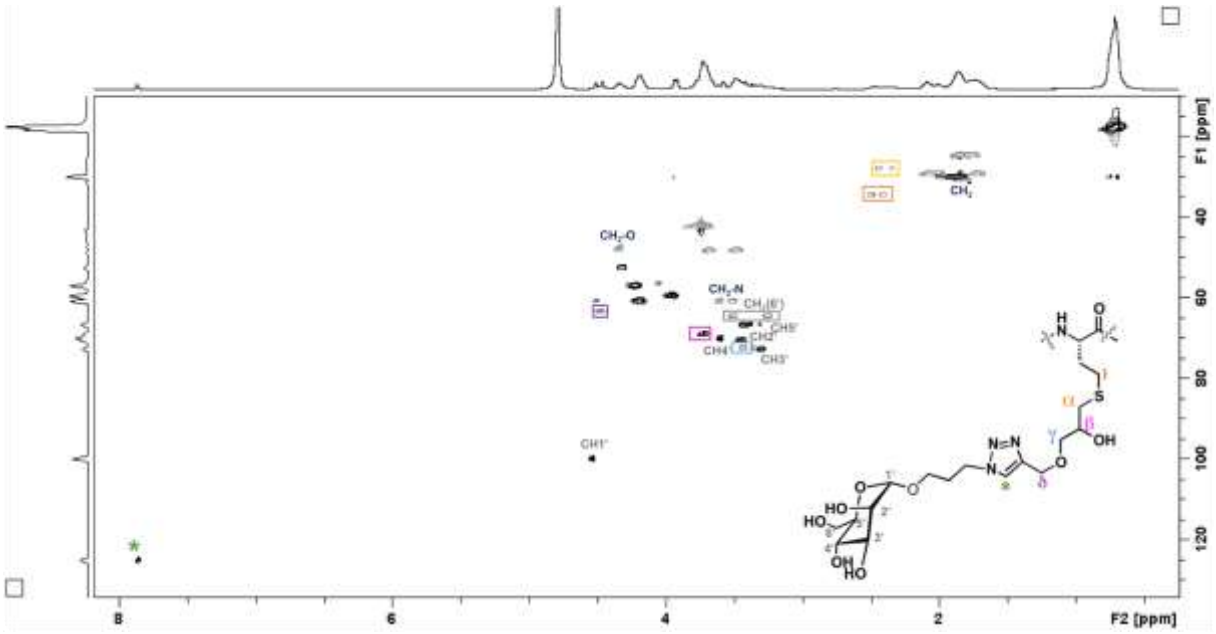

Figure S69. 2D NMR spectrum of compound **4d** in D_2O, HSQC.

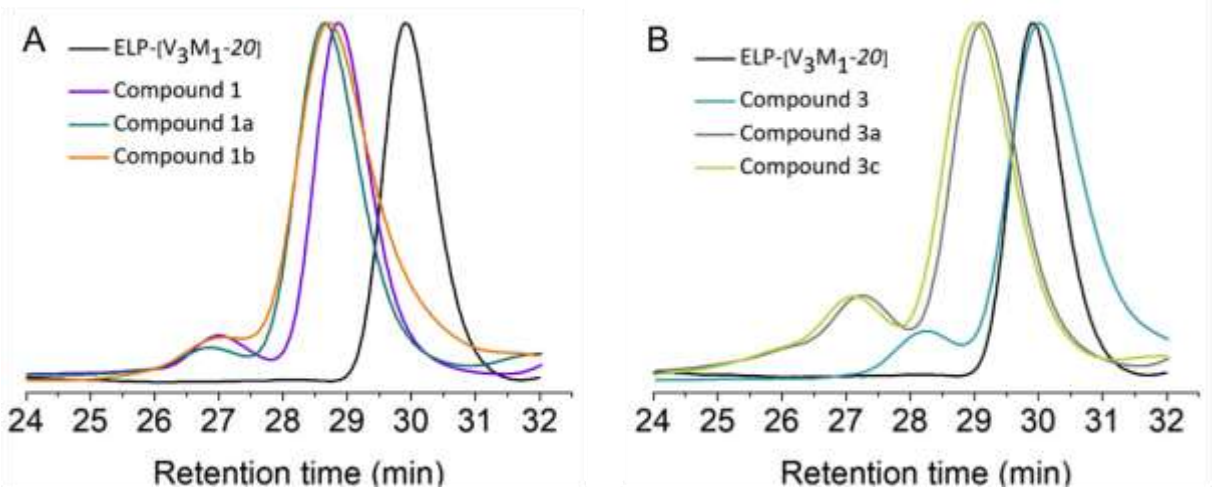

Figure S70. Size exclusion chromatography traces of ELP-[M_1V_3-*20*] for comparison with those of (A) compounds **1**, **1a**, **1b**, and (B) compounds **3**, **3a**, **3c** in AcOH/Ammonium Acetate/ACN (RI detection).

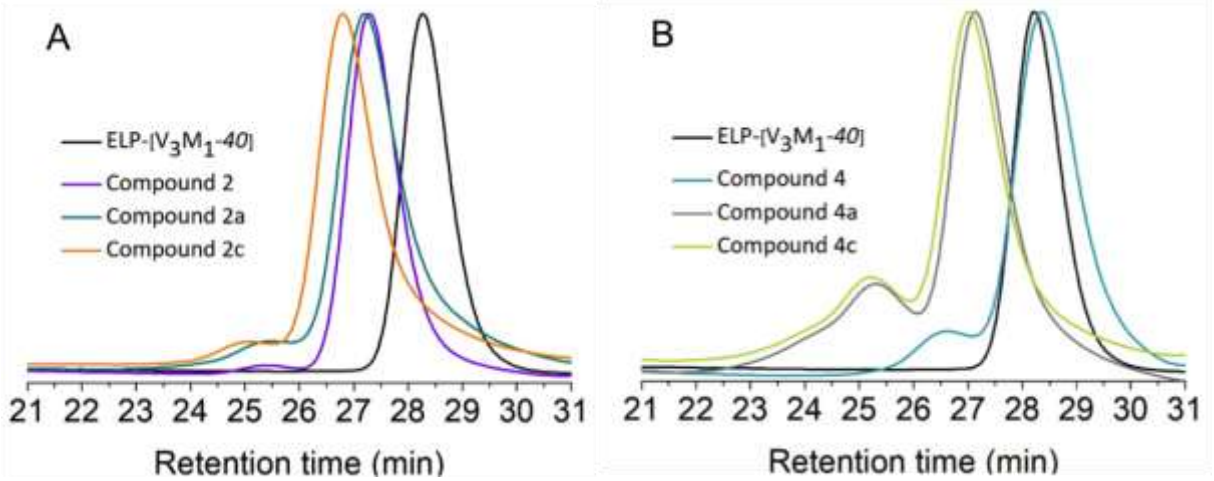

Figure S71. Size exclusion chromatography traces of ELP-[M_1V_3-*40*] for comparison with those of (A) compounds **2**, **2a**, **2c** and (B) compound **4**, **4a**, **4c** in AcOH/Ammonium Acetate/ACN (RI detection).

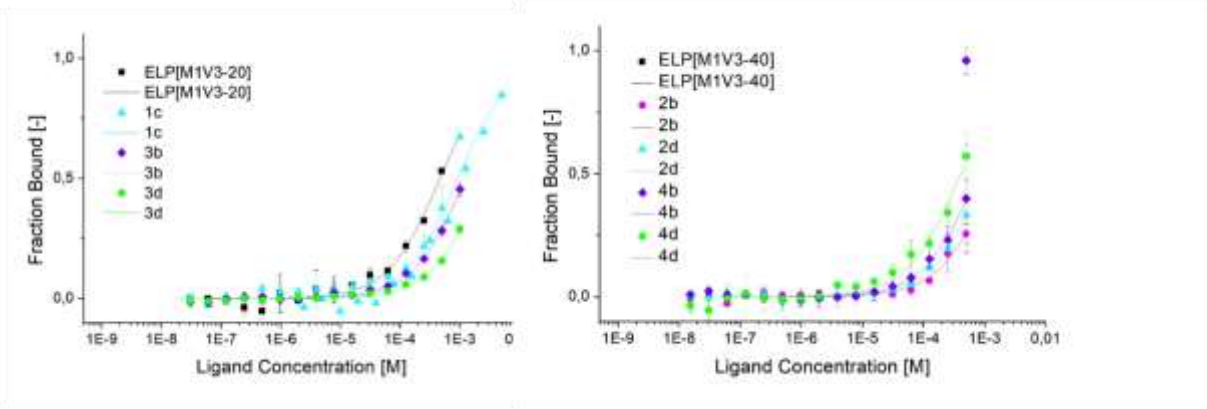

Figure S72. Thermophoretic analysis of interactions between lectin RCA_{120} and control ligands (mannose derivatives) in Tris buffer at 22°C.

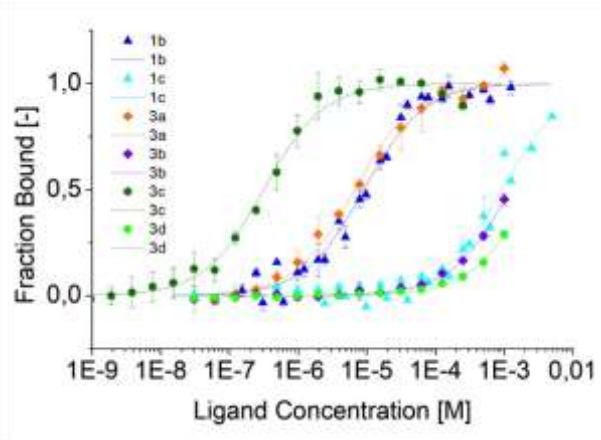

Figure S73. Thermophoretic analysis of interactions between lectin RCA_{120} and ligands **1b**, **3a** and **3c** as compared to control ligands **1c**, **3b** and **3d** in Tris buffer at 22°C.